ABSTRACT

Title of Document: TRACING CONTINENTALWEATHERING USING LITHIUM AND MAGNESIUM ISOTOPES: INSIGHTS FROM THE CHEMICAL WEATHERING OF COLUMBIA RIVER BASALTS AND MASS BALANCE MODELING

Xiao-Ming Liu, Ph.D., 2013

Directed By: Professors Roberta L. Rudnick & William F. McDonough, Department of Geology

Chemical weathering is an important mechanism that changes the mass and composition of the continental crust and regulates the global CO_2 cycle over geological time scales. Basalt, in particular, is the main building block of the juvenile continental crust, and it is estimated that basalt weathering currently accounts for more than 30% of global CO_2 consumption due to silicate weathering. Here I explore Li and Mg isotopes as tracers of chemical weathering. The primary objective of this dissertation is to understand Li and Mg isotopic fractionation mechanisms during

chemical weathering of basalts by analyzing Li and Mg isotopic compositions in weathering-related reservoirs. In addition, I perform mass balance modeling of Li to place constraints on the amount of continental crust that has been removed by chemical weathering. The samples include different flows of the fresh Columbia River Basalts (CRBs), drill cores through bauxites developed on the basalts, eolian dust, streams and ground waters draining only/mainly the CRBs.

The results show that: 1) leaching, secondary mineral formation, and eolian addition are the main processes controlling Li and its isotopic composition in weathered basalt, 2) gibbsite in the basalt regolith generates large Mg isotopic fractionation and δ^{26}Mg is also influenced by eolian addition, 3) the variations of δ^{7}Li in streams are likely to reflect weathering intensity, with lower δ^{7}Li corresponding to higher chemical weathering intensity, and 4) the mass of juvenile continental crust lost due to chemical weathering is at least 15% of the original crustal mass. Collectively, the results imply that: 1) chemical weathering may decrease the magnitude of the Nb anomaly of the bulk continental crust, 2) chemical weathering produces isotopically light Mg in water, leaving behind an isotopically heavy regolith and driving the bulk continental crust composition to heavier values, 3) Li and Mg isotopes have the potential to be useful in tracing continental chemical weathering, 4) chemical weathering played a significant role in changing the bulk continental crustal composition from basaltic to andesitic.

TRACING CONTINENTAL WEATHERING USING LITHIUM AND MAGNESIUM ISOTOPES: INSIGHTS FROM THE CHEMICAL WEATHERING OF COLUMBIA RIVER BASALTS AND MASS BALANCE MODELING

By

Xiao-Ming Liu

Dissertation submitted to the Faculty of the Graduate School of the
University of Maryland, College Park, in partial fulfillment
of the requirements for the degree of
Doctor of Philosophy
2013

Advisory Committee:
Professor Roberta L. Rudnick, Chair
Professor William F. McDonough
Professor Michael N. Evans
Professor Cin-Ty A. Lee
Professor Neil V. Blough

Preface

A portion of the work reported in this dissertation was previously published, submitted or in preparation for peer-reviewed journal articles. Some samples analyzed in this thesis are from my collaborators, provided either as powders or rock specimens. Therefore, this thesis reflects not only my own work, but also the contributions of my collaborators, as well as reviewers and editors.

Dedication

This dissertation is dedicated to my parents, who provide consistent inspiration and love.

Nothing in life is to be feared, it is only to be understood. Now is the time to understand more, so that we may fear less.

--Marie Curie

Acknowledgements

I want to thank many people for years of support during my PhD work. First of all, I thank my advisors: Roberta Rudnick and Bill McDonough. They taught me everything about being a good scientist, from attitude and ethics of research to details, such as English and analytical techniques. Most importantly, Roberta is always there to support me whenever I have a problem and is very tolerant when I mess things up. Bill taught me a great deal on how to work smart not just hard and be a better critical thinker. Both Roberta and Bill have the ability to think big and act careful, which always amazed me and keep amazing me.

I want to thank Cin-Ty Lee for inspiration that helped to generate Chapter five of my dissertation (my personal favorite chapter) and Mike Evans for helpful suggestions and discussion during the progress of my research; and thanks to both Cin-Ty and Mike for serving on my PhD examination committee. I appreciate Professor Neil Blough for agreeing to be on my committee as the Dean's representative.

I want to thank my coauthor Fangzhen Teng for letting me use his lab for Mg isotope studies and discussion on the Mg manuscripts. Also, I appreciate his generous and insightful advice. I thank Michael Cummings for providing precious drill core samples and insightful comments on the manuscripts.

I would like to acknowledge various people for their support in the lab: Richard Ash for his help in the ICP-MS lab, and Igor Puchtel for his help in the clean lab. I would like to thank Kangjun Huang, Yan Hu and Yan Xiao for help and friendship during the Mg isotope studies at the University of Arkansas. I would like

to thank Peter Zavalij for the assistance with XRD analyses and Stan Mertzman for performing the XRF analysis. I am grateful to Shuiwang Duan and Tammy Newcomer for their help with water ion chromatography analyses.

I also thank a number of people for help with field work: Steve Riedel for sampling help and providing some basalt samples, Terry Tolan for guidance with both weathering profiles and groundwater sampling. I would like to thank Marshall Gannett, Steve Hinkle, Mike Free, and Christie Galen for their assistance during field sampling.

I am grateful to the help of Geology faculty and staff members, who made my life joyful at Maryland! Especially, thanks to Rich Walker, Sujay Kaushal, Sash Hier-Majumder, Aaron Martin, Karen Prestegaard, Sarah Penniston-Dorland, and Philip Piccoli for providing helpful comments and suggestions, as well as Sandy Romeo, Jeanne Martin, Michelle Montero, Dorothy Brown, Joanna Patterson, and Todd Karwoski for their great support.

I would like to thank various postdocs and graduate colleagues that overlapped with me at Maryland, who provided tremendous help academically and personally: Madalyn Blondes, James Day, Richard Gaschnig, Audrey Ougier-Simonin, Mathieu Touboul, Yongbo Peng and Zoltan Zajacz. I would specially thank the “sporty gang” in the department that helped me stay healthy physically and mentally: Nick Gava, Yu Huang, Jingao Liu, and Lin Qiu. I appreciate the fun conversions with various graduate colleagues, especially Dana Borg, Caitlin Brown, Huan Cui, Julia Gorman, Jill Gribbin, Harry Lisabeth, N & M Sharps, Ming Tang, Tommy Tamarkin, Brain Tattitch, Lisa Walsh, Emily Worsham and Nanping Wu.

Table of Contents

List of Tables

List of Figures

Chapter 1: Introduction

Chemical weathering regulates the global climate and shapes the Earth's surface. Over geological time scales, atmospheric CO_2 levels are mainly controlled by the balance between CO_2 addition from volcanoes and CO_2 consumption from chemical weathering of silicate rocks (Berner, 1990; Berner et al., 1983; Kump et al., 2000). Weathering of basalts plays an important role in this system. For example, basalt weathering accounts for 30 - 35% of global CO_2 consumption due to silicate weathering, whereas basalts represent only ~ 8% of aerially exposed silicate rocks on Earth (Dessert et al., 2003; Gaillardet et al., 1999). Chemical weathering of basalts is also important in the formation of economic iron and aluminum deposits, such as laterites and bauxites. Finally, chemical weathering of basalts contributes to soil fertility, which is of great importance to agriculture and, consequently, humankind (White and Brantley, 1995).

During chemical weathering of the continents, soluble elements (e.g., Na, Ca, Mg and Li) are dissolved and transported to the oceans via rivers and/or groundwater, while insoluble elements, such as Si and Al, remain in the continental regolith. Ultimately, these soluble components may be recycled into the mantle by subduction (e.g., Mg and Ca) or may re-enter continental crust via arc magmatism (e.g., Na). Therefore, chemical weathering may be an important process that controls the mass and compositional evolution of the continental crust. It is well established that the average composition of the continental crust is intermediate or "andesitic", if described in terms of an igneous rock type (SiO_2 = 57 ~ 64 wt. %) (Rudnick and Gao, 2003b and references therein). However, the magmas that generate the present-day

continental crust are dominantly basalt (Rudnick, 1995 and references therein). This discrepancy has been referred to as the "Crust Composition Paradox" (Rollinson, 2008). Various hypotheses have been proposed to solve this paradox, including stripping of Mg through chemical weathering (Albarède, 1998; Anderson, 1982; Lee et al., 2008), removal of mafic/ultramafic lower crust through foundering/delamination (Arndt and Goldstein, 1989; Jull and Kelemen, 2001; Kay and Kay, 1993), subduction of continental crust followed by "relamination" of buoyant, felsic crust (Hacker et al., 2011), or direct addition of tonalites to the crust through slab melting in a hotter Archean Earth (e.g., Martin, 1986; Rollinson, 2008; Rudnick, 1995). However, before the present study, only one attempt has been made to quantify the influence of chemical weathering on the mass and composition of the continental crust (Lee et al., 2008).

With the advent of MC-ICP-MS methodology, new tracers of chemical weathering have been developed that employ non-traditional stable isotopes, such as Li, Mg, Si, and Fe isotopes (e.g., Bergquist and Boyle, 2006; Fantle and DePaolo, 2004; Georg et al., 2007; Huh et al., 1998; Pistiner and Henderson, 2003; Pogge von Strandmann et al., 2006; 2008; 2012; Teng et al., 2010a). By comparison to other systems, the behavior of lithium and magnesium isotopes during weathering is relatively simple.

Lithium has two stable isotopes, ^{7}Li and ^{6}Li, with abundances of 92.41% and 7.59% (Coplen et al., 2002), respectively, and 17% mass difference. Thus, ^{7}Li and ^{6}Li have great potential for mass-dependent fractionation. Lithium has many advantages as a potential geochemical tracer of weathering. Lithium is a water-soluble trace

element, but neither primary basalt dissolution nor metamorphic dehydration appears to fractionate Li isotopes (Marschall et al., 2007; Pistiner and Henderson, 2003; Qiu et al., 2009; Teng et al., 2007a; Wimpenny et al., 2010a). Nevertheless, Li isotopes have been shown to fractionate significantly during continental weathering, which is likely due to equilibrium partitioning between secondary minerals and water (e.g., Huh et al., 1998; Pistiner and Henderson, 2003; Teng et al., 2004; Vigier et al., 2008; Williams and Hervig, 2005). Lithium has only one redox state (+1 charge), and is thus insensitive to changes in oxygen fugacity (cf., Fe, Mo, etc.). Also, Li is not a nutrient; therefore, biological processes do not directly influence its elemental and isotopic behaviors. Moreover, large isotopic shifts have been observed in both natural and experimental settings (Pistiner and Henderson, 2003). For instance, chemical weathering could result in the enrichment of ^{7}Li in fluid and ^{6}Li enrichment in the residual rocks and/or soil (e.g., Rudnick et al., 2004). Therefore, the Li isotope system provides a relatively simple geochemical tool to assess continental weathering.

Magnesium has three stable isotopes, ^{26}Mg, ^{25}Mg and ^{24}Mg, with abundances of 78.99%, 10.00% and 11.00% (Coplen et al., 2002), respectively, and up to 8% mass difference. The magnesium isotopic system has multiple advantages as a potential geochemical tracer for chemical weathering and related processes. Magnesium is one of the most abundant elements in the continental crust (e.g., Rudnick and Gao, 2003b; Taylor and McLennan, 1995), and it is water-soluble, preferentially released into the ocean during continental weathering. Also, Mg has only one redox state (+2 charge) and is thus insensitive to changes in oxygen fugacity, (cf., Fe, Cu, Mo, etc.). In addition, no significant Mg isotopic fractionation

has been observed during igneous differentiation (e.g., Teng et al., 2010b; Teng et al., 2007b). Most importantly, Mg isotopes have been shown to fractionate significantly during continental weathering in both soils and rivers, as well as in mineral dissolution and precipitation experiments (e.g., Brenot et al., 2008; Huang et al., 2012; Pogge von Strandmann et al., 2008; 2012; Teng et al., 2010a; Tipper et al., 2012a; 2006a, 2008; 2006b; 2012b; Wimpenny et al., 2011; 2010a). In contrast to Li, Mg is a nutrient during biological activities, and Mg isotopes fractionate during the uptake into chlorophyll and into higher plants (Black et al., 2006; Bolou-Bi et al., 2010; Ra and Kitagawa, 2007). Therefore, biological activity may have large impact on the isotopic composition of fresh waters (Bolou-Bi et al., 2010). Previous investigations of Mg isotope behavior in weathering reveal the complexity of Mg isotope fractionation mechanisms, and there is no consensus on either the direction or mechanisms of Mg isotope fractionation during chemical weathering.

The mass removed from the continents and what remains behind during weathering can be addressed through the study of rivers and rock weathering profiles in the same region. These two data sets then can be combined to provide a quantitative mass balance of the weathering flux. An ideal place in which to carry out such a study is the Columbia River Basalts in the Pacific NW of the Unite States, one of the best-preserved and well-studied continental flood basalt provinces on Earth. Erupted from dike systems in eastern Oregon and western Idaho ~15 million years ago, the basalts flowed over 200,000 km^2 and extend 500 km westward to the Pacific Ocean. Also, CRB occur on both west and east sides of the Cascades, therefore, the rain shadow effect of the Cascades produces wet weathering conditions in the west

and dry in the east. Consequently, basalts that have experienced various degrees of weathering can be investigated. In addition, the great Missoula floods (15,000 to 13,000 years ago) washed away sediments and soils that were developed on the CRB, leaving a relatively fresh basaltic surface which can be compared to their weathered counterparts and directly linked with the present riverine flux. Moreover, the stratigraphy of the CRB is well-characterized and chemical compositions of the CRB flows are remarkably uniform (Reidel et al., 1989 and references therein), which enables us to constrain the chemical composition of the parent basalts prior to weathering.

The following four chapters are presented as four independent papers that have either already been published, have been submitted for publication, or will be. The following three chapters (2, 3 and 4) examine chemical weathering of the Columbia River Basalts using lithium and magnesium isotopes in fresh basalts, soils, river and ground waters, as well as possible eolian components. Chapter 5 quantifies the mass loss during continental weathering using lithium isotopes. The final chapter 6 summarizes the dissertation.

Chapter two examines the mineralogical, chemical, and Li and Nd isotopic compositions of two drill cores through bauxites developed on the Miocene Columbia River Basalts in order to document the chemical changes associated with basalt weathering and provide insights into the processes involved. The profiles show strong Li depletion relative to fresh basalt, with Li concentrations increasing systematically towards the surface in the quartz-bearing samples. The δ^7Li values decrease systematically towards the surface, reaching values that are up to ~7‰ lower than

those of the fresh basalt. The systematic enrichment of Li and quartz at the top of both profiles, coupled with the very low δ^7Li at the surface (down to ~-5‰) indicate that additional processes, such as addition of an eolian component, accompanied by secondary mineral formation, likely occurred. This work has been submitted as an article entitled "Tracing Chemical Weathering of Basalts Using Lithium Isotopes: A Case Study from the Columbia River Basalts" *to Geochimica et Cosmochimica Acta*, with the authorship Liu, Rudnick, McDonough, and Cummings.

Chapter three investigates the behavior of magnesium isotopes during intense weathering of basalts by analyses of the same drill core bauxites studied in Chapter three. The δ^{26}Mg values in bauxites are extremely high (up to +1.8) relative to the fresh basalts. Moreover, δ^{26}Mg values are positively correlated with the gibbsite contents, suggesting gibbsite controls the very heavy δ^{26}Mg values in bauxites. The results clearly show that chemical weathering produces isotopically light Mg in water, leaving an isotopically heavy regolith on the continental crust. This work will be submitted as an article entitled "Massive magnesium isotopic fractionation produced by basalt weathering" with the authorship Liu, Teng, Rudnick, McDonough, and Cummings.

Chapter four examines Li isotopic behavior and fractionation mechanisms during chemical weathering by investigating streams and ground waters occurring in the flood basalts. I found large δ^7Li variations (up to 20‰) in the streams that drain only basalts, suggesting catchment lithology alone is not the primary factor controlling riverine Li isotopic composition. The main finding of this study is that δ^7Li and Li/Na are potentially sensitive tracers of weathering intensity. Chemical

weathering intensity correlates neither with climate nor distance to the coast. Instead, the Li isotopic composition of rivers may be controlled by formation and destruction of secondary minerals at various stages of chemical weathering. This work is in preparation for publication as an article entitled "Li isotopes as chemical weathering intensity tracers in streams and ground waters draining basalts" with the authorship Liu, Rudnick, and McDonough.

Chapter five quantitatively constrains the mass evolution of the continental crust using a mass balance model for lithium inputs and outputs from the continental crust. The results suggest that over the Earth's history, the mass of continental crust that has been lost due to chemical weathering is at least 15% of the original mass of the juvenile continental crust, and may be as high as 60%, with a best estimate of approximately 45%. Therefore, the results suggest that chemical weathering and subsequent subduction of soluble elements have major impacts on both the mass and the compositional evolution of the continental crust. This work has been published as an article entitled "Constraints on continental crustal mass loss via chemical weathering using lithium and its isotopes" *in Proceedings of the National Academy of Sciences of the United States of America* by Liu and Rudnick.

Conclusions and future directions are presented in Chapter 6.

Chapter 2: Tracing chemical weathering of basalts using lithium isotopes: drill cores from the Columbia River Basalts

Abstract

The mineralogical, chemical, and Li and Nd isotopic compositions of two drill cores through bauxites developed on the Miocene Columbia River Basalts were analyzed in order to document the chemical changes associated with basalt weathering and provide insights into the processes involved. X-Ray diffraction (XRD) analyses of the bauxites reveal a mineralogy of gibbsite, hematite, +/- kaolinite, halloysite, goethite and maghemite. Quartz occurs near the tops of the cores and its abundance decreases progressively with depth; no quartz is observed below five meters depth in either core. Significant depletion of most major and trace elements, including "mobile" and some "immobile" elements, are observed. In both profiles, Li is strongly depleted relative to fresh basalt, with Li concentrations increasing systematically towards the surface in the quartz-bearing samples. By contrast, δ^7Li values decrease systematically towards the surface, reaching values that are up to ~7‰ lower than those of the fresh basalt. While Li was likely lost from the bauxites through leaching, which may have little impact on its isotopic composition, the isotopically light Li in the profiles suggests Li uptake onto secondary minerals, which can produce large isotopic fractionations. Moreover, the systematic enrichment of Li and quartz, as well as the less radiogenic Nd isotopic composition at the tops of both profiles suggests addition of an eolian component to the soils. The low δ^7Li of samples showing the greatest eolian addition (-4) suggests that this component may

also have been affected by leaching and secondary mineral precipitation, which lowered its δ^7Li. Our results demonstrate that lithium isotopes are sensitive tracers of chemical weathering, particularly in extreme weathering settings, and are consistent with the hypothesis that chemical weathering played an important role in controlling the mass and composition of the continental crust. In particular, because Nb is less mobile relative to the rare earth elements, chemical weathering may lessen the negative Nb anomaly in the continental crust.

1. Introduction

Chemical weathering regulates the global climate and shapes the Earth's surface. Over geological time scales, atmospheric CO_2 levels are controlled by the balance between CO_2 additions from volcanoes and CO_2 consumption from chemical weathering of silicate rocks (Berner, 1990; Berner et al., 1983; Kump et al., 2000). Weathering of basalts plays an inordinately important role in this system. For example, basalt weathering accounts for 30 - 35% of global CO_2 consumption due to silicate weathering, while basalts represent only ~ 8% of aerially exposed silicate rocks on Earth (Dessert et al., 2003; Gaillardet et al., 1999). Chemical weathering of basalt is also important in the formation of economic iron and aluminum deposits, such as laterites and bauxites. Finally, weathering of basalt contributes to soil fertility, which, in turn, is of great importance to agriculture (White and Brantley, 1995).

Chemical weathering may also have a profound influence on the average composition of the continental crust. It is well established that the current bulk continental crust is andesitic (SiO_2 = 57 ~ 64 wt.%) (Rudnick and Gao, 2003a and references therein). However, primary lavas at convergent margins, where much of

the continental crust is generated, are basaltic (SiO_2 = 45% - 55%) (Rudnick, 1995), and chemical weathering has been proposed to be one of the mechanisms that shifts the crustal composition from basaltic to andesitic composition (e.g., Albarède, 1998). Several recent studies attempt to quantify the continental mass loss due to chemical weathering. Lee et al. (2008) used mass balance of soluble elements, Mg and Li and concluded that more than 20% of continental mass was lost by weathering. By contrast, Liu and Rudnick (2011) employed a Li isotopic mass balance approach to show that chemical weathering is responsible for at least 15% of continental mass loss over Earth's history, and possibly much greater. Both studies indicate that chemical weathering and subsequent subduction of soluble elements can have a major impact on both the mass and the compositional evolution of the continental crust. Therefore, it is useful to develop tracers for chemical weathering of juvenile continental crustal material.

With the advent of MC-ICP-MS methodology, new tracers of chemical weathering have been developed that employ non-traditional stable isotopes, such as Li, Mg, Si, and Fe isotopes (e.g., Bergquist and Boyle, 2006; Fantle and DePaolo, 2004; Georg et al., 2007; Huh et al., 1998; Pistiner and Henderson, 2003; Pogge von Strandmann et al., 2006; Pogge von Strandmann et al., 2008; Pogge von Strandmann et al., 2012; Teng et al., 2010a). By comparison to other systems, the behavior of lithium isotopes during weathering is relatively well studied.

Lithium has two stable isotopes, ^{7}Li and ^{6}Li, with abundances of approximately 92.41% and 7.59% (Coplen et al., 2002), respectively, and ~17% mass difference. Thus, lithium isotopes have great mass-dependent fractionation potential.

Lithium has a few advantages as a potential geochemical tracer of weathering: first, lithium is a water-soluble trace element, but neither primary basalt dissolution nor metamorphic dehydration appears to fractionate Li isotopes (Marschall et al., 2007; Pistiner and Henderson, 2003; Qiu et al., 2009; Teng et al., 2007a; Wimpenny et al., 2010a). Nevertheless, Li isotopes have been shown to fractionate significantly during continental weathering, which is likely due to equilibrium partitioning between secondary minerals and water (e.g., Huh et al., 1998; Pistiner and Henderson, 2003; Teng et al., 2004; Vigier et al., 2008; Williams and Hervig, 2005). Li has only one redox state (+1 charge), and is thus insensitive to changes in oxygen fugacity (cf., Fe, Mo etc). Also, Li is not a nutrient, so biological processes do not directly influence its elemental and isotopic behaviors. Large isotopic shifts have been observed in both natural and experimental settings (Pistiner and Henderson, 2003). For instance, chemical weathering could result in the enrichment of heavy Li isotope in fluid and light Li isotope enrichment in the residual rocks and/or soil (e.g., Rudnick et al., 2004). Therefore, the Li isotope system provides a relatively simple geochemical tool to assess continental weathering.

Previous investigations of Li isotopes in weathering profiles/products developed on basalts (or their intrusive equivalents) found differing influences related to weathering and associated secondary mineralogy, deposition of marine aerosol and eolian dust, and diffusion. Pistiner and Henderson (2003) found large lithium isotopic fractionation associated with the formation of certain secondary minerals during weathering, such as gibbsite (+14‰), but little Li isotopic fractionation associated with formation of some other secondary minerals, such as smectite. Li isotopic

fractionation is also observed in soil profiles developed on Hawaiian basalts, where the influence of marine aerosols on Li isotope behavior could be important (Huh et al., 2004). Analysis of a weathering profile developed on the Deccan Traps further confirmed that secondary mineral formation plays an important role in determining lithium isotopic distributions during weathering (Kisakürek et al., 2004). However, Kisakurek et al. (2004) suggest that the negative correlation observed between Li concentrations and δ^7Li may have been caused by addition of eolian dust to the top of the profile, in addition to Rayleigh fractionation associated with Li removal. Finally, Rayleigh fractionation of Li isotopes may be overprinted by kinetic fractionation associated with diffusion across a paleo water table, such as that reported in a saprolite profile developed on a diabase dike (Rudnick et al., 2004; Teng et al., 2010a).

In general, ^{6}Li partitions preferentially into secondary minerals formed during chemical weathering of silicate rocks (e.g., clays and hydroxides), while ^{7}Li partitions into the associated water. The amount of fractionation depends on the type of secondary minerals formed, which may, in turn, reflect the weathering intensity experienced by the rocks. However, the lithium isotopic composition of the regolith may also be influenced by the addition of eolian dust, marine aerosol in the coastal regions, and even kinetic fractionation, if Li diffuses through water saturated soil. All of these factors could complicate our understanding of the behavior of Li during chemical weathering (e.g., Huh et al., 2004; Kisakürek et al., 2004; Rudnick et al., 2004; Teng et al., 2010a).

The aim of this study is to enhance our understanding of the behavior of Li isotopes during weathering, especially under high-intensity chemical weathering conditions. In addition, we provide insights into chemical weathering processes that occur in basalts using the mineralogy, major and trace elements and Li and Nd isotopic tracers. We aim to address the following main questions: 1) How do lithium and its isotopes behave during extreme weathering of basalts? 2) What are the mechanism(s) and factors that control lithium isotopic behavior? 3) What insights can elements and lithium isotopes offer to chemical weathering, especially extreme weathering of basalts? 4) Is lithium isotopic behavior predictable for basalt weathering? 5) What are the implications of this study for tracing continental weathering?

2. Geological settings, climate and samples

The Columbia River Basalts (CRBs) erupted in the Miocene (between 17 Ma to 6 Ma, with the greatest volume erupting between 16.6 ~ 15.3 Ma) in the US Pacific Northwest, covering large portions of southern Washington, northeast Oregon and western Idaho (Fig. 1; Hooper, 1997; Tolan et al., 1989). Distribution of individual flows in the CRBs has been recognized based on field relationships, geochemistry and paleomagnetic properties (e.g., Hooper, 1997; Reidel et al., 1989).

The CRBs crop out both east and west of the Cascade Mountain Range. The Cascades developed progressively since the Late Eocene, with topography increasing more or less steadily since the Late Oligocene (Kohn et al., 2002 and references therein). This topographic increase created two different climate zones that affected the CRBs via the rain shadow effect: the wet-western and dry-eastern regions.

Regions west of Cascades have high mean annual precipitation (MAP) (1500-2000 mm), whereas annual precipitation east of Cascades is less than 300 mm (Kohn et al., 2002; Takeuchi et al., 2010). The origin of bauxites is still controversial (e.g., Bogatyrev et al., 2009; Schellmann, 1994), though they typically form on basalts subjected to extreme weathering conditions. The bauxites studied here in the two drill cores formed on CRBs occurring on the western, wet side of the Cascades (Figure 1) (see Section 4.1).

The present-day mean annual temperature (MAT) and MAP in the study area (Figure 1) are ~11 ^{o}C and ~1100 mm, respectively, according to the Western Regional Climate Center (http://www.wrcc.dri.edu). Geological and paleofloral evidence suggests that in the middle to late Miocene, around the time that the CRBs erupted, climate in the inland Pacific Northwest was warmer and wetter than today (Takeuchi et al., 2010). For example, oxygen isotope evidence suggests that central Oregon had an estimated MAT of 18 ^{o}C at 15–16 Ma and ~15 ^{o}C at 10–11 Ma and 7–8 Ma; the MAT then decreased to 13 ^{o}C by 3.2 Ma and finally dropped to its current ~10 ^{o}C (Kohn et al., 2002).

The bauxite units were developed on two different CRB flows and sampled via drill cores: the Sentinel Bluffs Member of the Grande Ronde Basalt in Columbia County, Washington (hereafter referred to as the "Columbia drill core"), and the

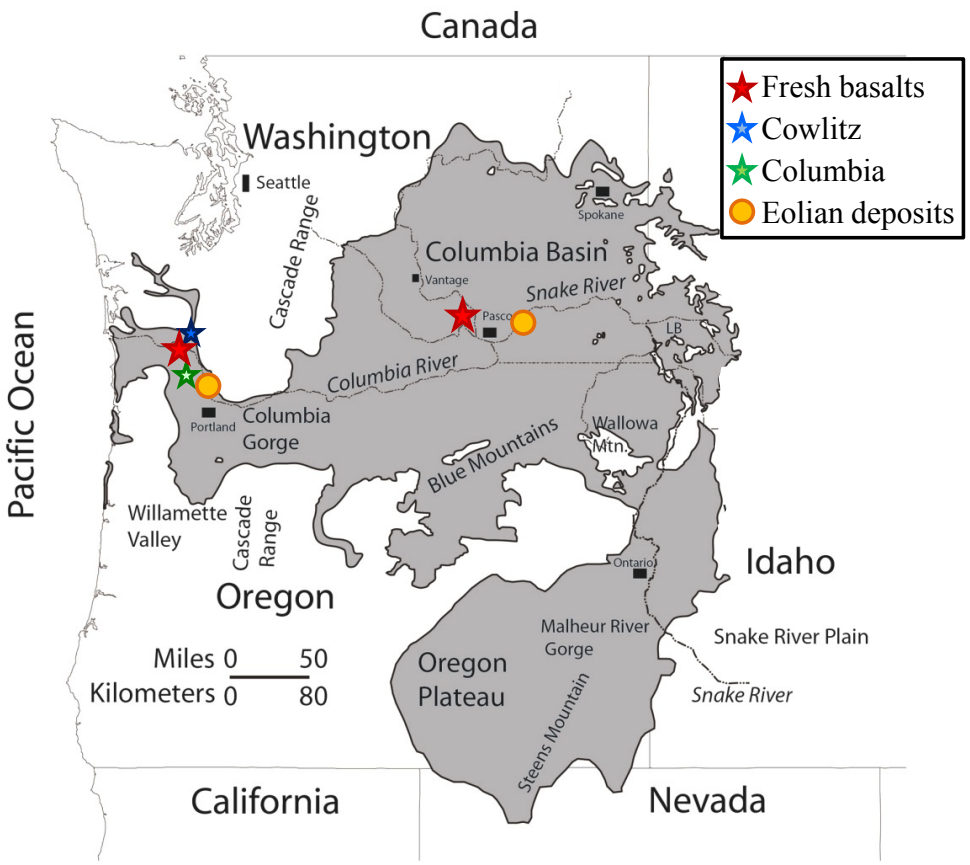

Figure 1. Map showing the distribution of the Columbia River Basalts (gray) and the location of samples investigated here.
The base map is courtesy of Steve Riedel.

Pomona Member of the Saddle Mountains Basalt in Cowlitz County, Oregon (hereafter referred to as the "Cowlitz drill core"). Seven bauxite samples were taken from the Columbia drill core, which penetrated to 7.9 m in depth. Ten bauxite samples were taken from the 9.1 m deep Cowlitz drill core. Fresh basalt was not penetrated in either of these two profiles (Fassio, 1990), and so a number of samples of unweathered portions of the same flows were sampled elsewhere in order to characterize the original composition of these basalts prior to weathering and evaluate heterogeneity within the flows: ten samples were taken from the Sentinel Bluffs basalts and 17 samples were taken from fresh Pomona basalts (see Table 1 for latitude and longitude of the sampling sites). Two of the ten Sentinel Bluffs basalts were sampled from outcrops west of the Cascades, and eight were taken from drill cores in the Pasco Basin of eastern Washington; one of the fresh Pomona basalts was sampled from an outcrop in western Washington and the rest were sampled from a roadcut in the Pasco Basin of eastern Washington.

Finally, two samples of recent eolian deposits were collected from west and east of the Cascade Mountains in order to determine the composition of possible sources of eolian dust to the weathering profiles. The Portland Hills silt (PHS-1) was collected from excavation in a housing construction site in the Portland Hills, whereas the Palous formation (Palous-1), perhaps as old as 2 Ma (Busacca, 1989) was taken from a road cut along Highway 12 near Starbuck, eastern Washington (see Table 1).

Table 1. Major (in wt. %) and trace (in ppm) element concentrations of fresh basalts and eolian deposits.

Sample #	WC-6	WC-7	WC-8	WC-9	WC-10	WC-12	WC-13	WC-14	WC-15	WC-16	WC-17	WC-18	WC-19	WC-20	WC-21	WC-22	Pomona-1
	Pomona basalt																
Logitude (°)	*-119.39644*																*-123.23352*
Latitude (°)	*46.58776*																*46.18477*
SiO2	51.51	50.85	50.56	51.14	50.49	51.08	50.56	51.55	51.01	49.70	51.26	51.30	51.18	51.21	51.40	50.61	51.71
TiO2	1.73	1.61	1.61	1.85	1.80	1.75	1.69	1.75	1.65	1.68	1.72	1.65	1.65	1.62	1.69	1.62	1.64
Al2O3	14.89	14.91	14.78	14.47	15.17	14.78	15.30	14.87	14.90	15.04	14.79	14.76	14.92	14.51	15.06	14.72	14.70
Fe2O3T	11.87	11.52	12.16	12.46	12.64	12.40	12.01	12.76	12.32	12.49	12.06	11.50	11.87	11.83	11.46	12.17	11.68
MnO	0.21	0.16	0.17	0.21	0.17	0.17	0.18	0.16	0.17	0.18	0.18	0.16	0.17	0.17	0.16	0.17	0.18
MgO	6.10	6.37	6.76	6.02	6.35	6.36	6.50	5.62	6.53	6.89	6.57	6.63	6.47	6.50	6.54	6.59	6.74
CaO	11.00	11.13	11.23	10.95	10.84	10.86	11.12	10.44	10.87	11.04	10.71	10.86	10.94	10.73	11.00	11.34	10.54
Na2O	2.28	2.35	2.36	2.30	2.15	2.36	2.30	2.39	2.29	2.33	2.27	2.25	2.28	2.25	2.32	2.33	2.45
K2O	0.42	0.40	0.41	0.64	0.39	0.40	0.33	0.49	0.37	0.39	0.53	0.50	0.44	0.47	0.46	0.47	0.57
P2O5	0.28	0.25	0.25	0.30	0.27	0.27	0.27	0.29	0.24	0.25	0.26	0.24	0.25	0.23	0.25	0.23	0.23
LOI	1.95	2.23	1.86	1.97	2.71	2.79	3.01	3.40	1.54	1.34	2.68	2.20	2.58	2.33	2.04	2.77	0.97
Total	100.29	99.55	100.29	100.34	100.27	100.43	100.26	100.32	100.35	99.99	100.35	99.85	100.17	99.52	100.34	100.25	100.44
CIA	0.38	0.38	0.37	0.37	0.39	0.38	0.39	0.39	0.38	0.38	0.38	0.38	0.38	0.38	0.38	0.37	0.38
Rb	10.8	9.2	12.5	14.9	8.7	6.8	5.8	6.5	6.4	11.0	12.1	11.9	11.0	11.1	11.3	12.3	11.3
Sr	256	244	229	239	248	247	247	245	244	240	244	248	246	237	246	250	228
Y	39.7	26.0	28.2	28.9	33.3	26.8	25.3	29.4	26.5	30.0	28.0	26.4	25.6	26.4	27.0	29.9	27.4
Zr	138	131	126	151	139	138	129	139	126	129	139	134	135	130	139	120	130
V	303	283	265	302	300	289	283	279	287	308	284	280	284	279	299	279	281
Ni	42	51	54	42	46	47	51	46	46	51	46	45	45	49	44	57	47
Cr	115	129	121	96	131	130	119	120	118	122	101	109	117	105	115	120	98
Nb	10.6	10.3	10.2	11.6	10.6	10.5	9.6	10.3	10.2	11.1	10.1	9.9	10.1	9.7	10.9	11.1	9.0
Ga	16.8	16.9	15.3	16.6	17.2	16.7	17.4	17.0	16.8	15.8	17.1	17.5	17.0	17.1	17.3	18.2	17.5
Cu	49	56	52	59	39	58	60	59	53	46	56	54	50	59	59	57	55
Zn	87	86	81	88	84	90	87	86	85	84	90	86	84	97	92	83	87
Co	43	44	47	43	43	45	42	45	43	48	44	42	41	45	42	48	42
Ba	238	192	201	266	170	231	219	245	243	243	224	200	100	214	197	512	251
La	31	15	18	19	24	14	16	18	16	15	17	18	14	15	16	17	16
Ce	46	37	33	38	44	34	38	34	33	34	37	31	32	31	33	33	35
U	1.5	<0.5	0.6	<0.5	1.2	<0.5	0.9	<0.5	<0.5	0.5	<0.5	1.0	1.1	<0.5	1.0	0.8	0.6
Th	3.1	<0.5	<0.5	3.6	6.2	1.2	4.7	0.8	2.9	<0.5	3.4	3.5	<0.5	4.8	<0.5	4.0	2.0
Sc	36	36	36	36	37	35	36	35	37	35	34	37	35	35	35	36	33
Pb	4	6	15	11	<1	<1	10	7	2	6	5	9	6	5	4	11	7

Table 1. Major (in wt. %) and trace (in ppm) element concentrations of fresh basalts and eolian deposits continued.

Sample #	SB-1	SB-2	2170+	2242+	2256.5+	2340+	2370+	2380+	2430+	2450+	PHS-1	Palous-1
	Sentinel Bluffs basalt										*eolian dust*	
Logitude (°)	*-123.08005*		*-119.39645*								*-122.79138*	*-117.93652*
Latitude (°)	*44.83813*		*46.58777*								*45.57083*	*46.39157*
SiO2	53.17	53.37	53.61	54.98	54.11	54.18	54.84	53.70	51.26	53.30	69.01	69.34
TiO2	1.82	1.97	1.75	1.70	1.64	1.81	1.72	1.75	1.92	1.78	1.01	0.80
Al2O3	14.39	14.12	14.73	14.19	14.13	13.99	14.19	14.03	14.62	13.99	14.81	14.15
Fe2O3T	12.70	12.92	11.09	10.95	11.02	11.35	11.27	11.35	11.79	11.67	6.50	5.03
MnO	0.20	0.20	0.19	0.20	0.20	0.18	0.19	0.20	0.21	0.19	0.10	0.09
MgO	4.91	4.66	4.87	5.19	4.93	4.33	4.91	4.80	5.14	4.94	1.39	1.77
CaO	9.05	8.62	9.09	8.43	8.73	8.30	8.44	8.60	9.38	8.92	2.26	3.57
Na2O	2.81	3.03	2.90	3.24	3.01	3.08	3.20	3.03	2.88	2.91	2.30	2.38
K2O	1.05	1.18	0.88	1.19	1.06	1.22	1.09	1.18	1.11	0.97	1.91	2.14
P2O5	0.28	0.33	0.29	0.29	0.27	0.37	0.32	0.32	0.30	0.28	0.18	0.17
LOI	1.17	0.12	-	-	-	-	-	-	-	-	7.48	7.24
Total	100.38	100.40	99.40	100.35	99.10	98.81	100.17	98.95	98.61	98.95	99.47	99.44
CIA	0.39	0.39	0.40	0.39	0.39	0.39	0.39	0.39	0.39	0.39	0.866	0.835
Rb	20.9	24.2	21	20	29	33	24	33	18	31	60.5	70.3
Sr	320	316	318	307	302	309	306	309	322	309	325	350
Y	28.6	29.4	33	32	33	37	32	33	36	33	30.2	29.5
Zr	148	163	159	150	153	165	151	154	157	149	319	287
V	329	342	319	324	300	301	306	302	343	319	133	96
Ni	23	21	13	11	12	8	8	10	18	14	38	36
Cr	63	45	56	51	53	43	50	49	56	57	90	89
Nb	8.4	11.0	10.3	12.3	10.9	12.7	13.0	11.9	12.6	11.8	15.5	16.6
Ga	19.0	19.1	20	21	19	21	22	24	19	21	17.9	16.9
Cu	42	48	21	30	26	25	21	24	29	31	32	30
Zn	98	104	113	116	106	117	115	109	114	109	71	68
Co	40	42	-	-	-	-	-	-	-	-	22	16
Ba	400	504	407	426	515	706	521	539	316	454	712	761
La	17	16	34	29	10	17	14	21	10	11	33	34
Ce	38	39	29	42	46	49	31	52	46	30	73	78
U	0.6	0.7	-	-	-	-	-	-	-	-	3.0	3.0
Th	0.7	5.2	0	4	5	5	3	7	4	7	11.2	9.7
Sc	31	32	37	42	36	33	36	38	32	35	18	15
Pb	13	5	4	7	6	7	5	7	7	8	12	3

+ indicates data from unpublished data of Steve Riedel.

3. Analytical methods

3.1 Major and trace elements

Major and trace elements analysis was carried out by X-Ray Fluorescence analysis (XRF) at Franklin and Marshall College. Precision can best be evaluated by analyzing multiple preparations of the same sample for both major and trace elements and accuracy can best be evaluated by analyzing known geochemical rock standards under the same exact analytical conditions as the samples. Such data are reported at the website: http://www.fandm.edu/earth-and-environment/precision-and-accuracy. In addition, since some of the mobile major elements, such as Mg, Na, and K, have very low concentrations in the drill core samples, the precision of major and trace elements are evaluated here by repeat analyses of one sample with a typical bauxite chemical composition. Most major and trace elements have better than 10% (2σ) precision, except for Na_2O and K_2O as well as those trace elements that have low concentrations (<10ppm) (see Table A.1). According to repeat analyses of BHVO-2 standard (n=10, http://www.fandm.edu/earth-and-environment/precision-and-accuracy), the accuracy for most major elements is better than 2% (2σ), except for K_2O (2σ = 2.7%); and the accuracy of trace elements are mostly better than 10% (2σ) except for those at lower concentrations (<10 ppm), such as U, Th and Pb.

3.2 Mineral identification and preparation

X-Ray Diffraction (XRD) analysis was performed at the X-Ray Crystallographic center of the University of Maryland. The powder x-ray patterns were measured on a Bruker D8 Advance powder diffractometer equipped with a

LynxEye PSD detector, Soller slits, and a Ni beta-filter using CuKα radiation from a sealed tube. Mineral phases were identified by peak matching analysis and the proportions of mineral phases were determined semi-quantitatively using the combination of spectra and major element analyses. We first identify major mineral phases in each bauxite sample and classify the mineral phases into three main categories: Al-, Fe-, and Si-dominanted minerals. Using relative abundances of minerals in a single category (Al, Fe or Si-bearing) and their molecular weight, we calculate the percentage of each mineral phase combined with major element data from the XRF analysis. The approach gives a semi-quantitative mineral percentage estimate in each bauxite sample.

3.3 Lithium isotope analyses

The method of lithium isotope analysis used here was previously described in Liu et al. (2010b) and follows from that originally described by Moriguti and Nakamura (1998b). All preparation and analyses were performed at the Geochemical Lab of the University of Maryland. A brief description of sample dissolution, column chemistry and instrumental analysis is provided below.

Fresh basalts were cut and then pulverized using an alumina jaw crusher after any weathered/altered surfaces of samples were sawn off. Bauxite samples were air-dried before pulverizing. For each sample, between 20 to 100 mg of rock powder was dissolved using a ~ 3:1(v/v) mixture of HF and HNO_3 in Savillex® screw-top beakers on a hot plate (T ≈ 90 ^{o}C), followed by twice HNO_3 and once HCl addition until all powder was dissolved and the final solution was clear. Final solutions in 4M HCl were then purified using four-step cation exchange columns (BioRad AG50W-x12,

200-400 mesh). The first two columns eliminate major cations in samples using 2.5M HCl and 0.15M HCl, respectively. The third column separates Na from Li using 30% ethanol in 0.5M HCl and the fourth column is a repeat of the third to further separate Na from final solution for instrumental analysis. Yields from the chromatography were determined to be greater than 95% (Marks et al., 2007). Finally, Li solutions (~ 50 ppb Li in ~2% HNO_3) were analyzed using a Nu Plasma Multi Collector-Inductively Coupled Plasma-Mass Spectrometer (MC-ICP-MS) employing a "dry" introduction system, either a CETAC Aridus or ESI Apex nebulizer. Background signals for ^7Li ($<10^{-4}$ V) were negligible compared to the typical sample signals (1-3 V). Standard bracketing, using L-SVEC (Flesch et al., 1973), was performed for all analyses. The Li concentration is determined to within 10% (1σ). The Li isotopic composition is reported as δ^7Li, where $\delta^7Li_{sample} = [(^7Li/^6Li)_{sample}/(^7Li/^6Li)_{standard}-1]\times1000$, where the standard used is a lithium carbonate, L-SVEC. The external precision of δ^7Li, based on 2σ of duplicate runs of pure Li standard solutions, is ≤±1.0‰. For example, repeat analyses of two pure Li solutions, analyzed during the course of this study (08/2010 to 09/2011) yield the following results: IRMM-016 (Qi et al., 1997) $\delta^7Li = 0.0 \pm 0.8$‰ (2 σ, n = 15); and the in-house standard, UMD-1, a purified Li solution from Alfa Aesar®, gives $\delta^7Li = +54.5 \pm 1.0$‰ (2 σ, n = 12). In addition, several USGS rock standards were run repeatedly (Table A.2). BHVO-1 yielded δ^7Li of 4.7 ± 1.1 (n= 5) cf. 4.0 to 5.6 in the literature (GeoReM database: http://georem.mpch-mainz.gwdg.de/), AGV-1 yielded δ^7Li of 4.6 ± 0.8 (n = 2) cf. 4.6 and 6.7 for AGV-1 in Liu et al. (2010b) and Magna et al. (2004), respectively; and

BCR-2 yielded δ^7Li of 2.7 ± 1.3 (n = 2) cf. 2.6 to 4.6 in the literature (GeoReM database).

3.4 Neodymium isotope analyses

Neodymium isotope analyses were performed in the Geochemistry Laboratory of the University of Maryland. The dissolution procedure is the same as that used for Li isotope analyses. After complete dissolution, final solutions were purified using two-step cation exchange columns (BioRad AG50W-x8, 100-200 mesh). The primary columns separate REEs using 4N HNO_3. The secondary columns separate Nd from the rest of the REE using 0.225M methyllactic acid. Finally, sample solutions were analyzed for Nd isotopes using the Nu Plasma MC-ICP-MS. The mass bias of Nd isotopes was corrected using $^{146}Nd/^{144}Nd$ of 0.7219. Repeated analyses of a Nd standard, AMES, gives an average $^{143}Nd/^{144}Nd$ of 0.512157±0.000036 (n=42). Each measured $^{143}Nd/^{144}Nd$ was then normalized using averaged $^{143}Nd/^{144}Nd$ of AMES within a given day and assuming an AMES standard value of 0.512138 (Aulbach et al., 2008). Several USGS standards were run repeatedly (Table A.3). BHVO-1 yields an average $^{143}Nd/^{144}Nd$ of 0.513029 ±0.000020 (n=2) and a single analysis of BCR-2 gives $^{143}Nd/^{144}Nd$ of 0.512651. The results are comparable to those in the GeoReM database, where the ranges of $^{143}Nd/^{144}Nd$ values are 0.512949 - 0.513048 and 0.512608 - 0.512656 for BHVO-1 and BCR-2, respectively.

4. Results

Major & trace elements, loss on ignition (LOI), and chemical index of alteration (CIA) in fresh basalts, bauxites and eolian deposits are reported in Tables 1 and 2. Major mineral phases in bauxites, and their calculated proportions are reported in Table 3. Lithium and neodymium concentrations and isotopic compositions in the fresh basalts, bauxites and eolian deposits are given in Table 4.

4.1 Mineralogy

X-Ray Diffraction (XRD) results confirm that all the basalt samples are fresh, as no secondary minerals were detected.

XRD results reveal that both of the drill core bauxites contain gibbsite, hematite, +/- halloysite, kaolinite, goethite, and maghemite; quartz occurs at the top of the drill cores and its abundance decreases progressively with depth. No quartz is observed below 5 m depth in either core. Mineralogy and calculated proportions of mineral phases in bauxites are summarized in Table 3.

4.2 Major and trace elements

Being extreme weathering products of the Columbia River Basalts, the drill cores are mainly composed of alumina and iron, with average alumina (Al_2O_3) of 47% and total iron oxide (Fe_2O_3) of 33%. Only samples from the top five meters of the drill cores have more than 10% SiO_2 (see Table 1). According to the definition of Retallack (2010), rocks with more than 45.5% by weight alumina and no more than

Table 2. Major (in wt. %) and trace (in ppm) element concentrations of drill core bauxites.

Sample #	9/3-1	9/3-2	9/3-3*	9/3-5	9/3-9	9/3-10	9/3-19	9/3-21	9/3-22	9/3-23	5/1-4	5/1-6*	5/1-8	5/1-10	5/1-12	5/1-14	5/1-15*
	Cowlitz drill core (Log: -122.77471°, Lat: 46.17463°)										*Columbia drill core (Log: -122.87639°, Lat: 45.75444°)*						
Depth(m)	2.13	2.44	2.74	3.35	4.88	5.79	6.25	7.62	8.23	9.14	2.74	3.96	4.57	5.49	6.71	7.32	7.92
SiO2	20.14	14.21	7.74	3.66	3.33	2.04	3.77	5.96	6.00	7.85	33.88	22.10	19.80	3.98	4.57	1.94	9.89
TiO2	4.59	5.67	4.28	3.50	4.27	5.75	4.65	5.01	5.04	4.68	3.35	3.23	6.46	10.78	8.54	10.02	7.02
Al2O3	39.70	49.81	35.34	63.02	63.96	57.09	61.82	56.71	56.04	57.31	42.92	33.82	38.58	31.48	36.17	50.55	28.62
Fe2O3T	34.60	29.40	31.24	28.85	27.68	34.13	28.91	31.47	31.98	29.29	18.90	23.86	33.83	52.71	49.45	36.62	36.89
MnO	0.04	0.04	0.17	0.02	0.05	0.07	0.05	0.05	0.05	0.05	0.06	0.17	0.03	0.03	0.03	0.09	0.19
MgO	0.19	0.18	0.15	0.14	0.15	0.15	0.15	0.15	0.16	0.16	0.25	0.21	0.19	0.12	0.12	0.20	0.20
CaO	0.06	0.06	-	0.04	0.04	0.04	0.04	0.04	0.05	0.04	0.12	0.04	0.07	0.05	0.05	0.04	-
Na2O	0.07	0.07	0.01	0.06	0.05	0.07	0.06	0.06	0.07	0.06	0.06	0.01	0.07	0.09	0.08	0.07	-
K2O	0.15	0.08	0.05	0.01	0.00	0.00	0.01	0.01	0.03	0.02	0.29	0.20	0.16	0.02	0.01	0.00	0.02
P2O5	0.23	0.27	0.34	0.49	0.33	0.44	0.39	0.40	0.45	0.41	0.26	0.35	0.61	0.77	0.76	0.63	0.51
LOI	17.15	20.34	20.11	25.24	25.13	23.62	24.43	23.60	23.78	23.32	17.34	16.67	15.91	13.82	17.34	21.31	15.77
Total	99.77	99.79	99.43	99.79	99.86	99.78	99.85	99.86	99.87	99.87	100.09	100.66	99.80	100.03	99.78	100.16	99.11
CIA	0.990	0.994	0.996	0.997	0.998	0.997	0.997	0.997	0.996	0.997	0.985		0.989	0.992	0.994	0.996	
Rb	18.1	11.6	-	5.4	4.4	3.4	3.1	4.9	4.8	4.8	52.4	-	18.0	4.1	3.7	3.6	-
Sr	14	11	-	4	5	5	4	4	6	6	24	-	17	9	7	4	-
Y	10.4	10.9	-	3.5	3.2	3.1	3.5	2.4	4.9	2.8	15.5	-	8.4	5.5	5.5	3.2	-
Zr	631	798	-	460	326	362	319	322	355	301	618	-	727	887	942	399	-
V	689	726	-	671	704	852	715	800	800	733	411	-	846	1416	1291	1222	-
Ni	42	30	-	26	24	24	27	33	28	29	52	-	34	18	17	19	-
Cr	365	281	260	300	281	293	303	326	306	288	168	-	174	234	234	116	-
Nb	61.7	90.3	50	30.8	28.6	40.9	34.7	35.7	35.3	33.5	58.2	56	81.1	139.7	83.5	53.5	45
Ga	57.3	57.6	90	35.5	37.8	34.4	32.8	32.5	34.9	31.8	49.1	83	62.1	72.4	53.7	38.1	55.0
Cu	69	62	-	41	41	50	52	66	65	66	78	-	64	58	62	39	-
Zn	51	36	-	34	66	81	74	81	81	80	55	-	44	33	42	112	-
Co	39	31	-	33	34	27	30	35	31	33	29	-	38	12	9	27	-
Ba	60	30	-	9	<3	<3	<3	<3	3	<3	237	-	39	<3	<3	<3	-
La	3	3	7	2	1	3	1	1	3	<1	10	18	3	25	8	16	4
Ce	8	9	-	10	7	10	5	5	11	12	15	-	8	65	20	43	-
U	10.3	11.8	7	4.1	6.6	1.0	0.7	1.5	<0.5	<0.5	9.4	7	9.7	9.8	4.9	6.4	3
Th	76.6	91.2	30	74.1	64.0	80.4	66.6	62.8	64.5	60.5	60.9	24	77.1	126	127.4	76.7	10
Sc	36	37	42	46	60	83	79	76	77	69	27	32	28	28	42	59	86
Pb	19	9	-	14	16	13	22	4	5	10	10	-	20	8	<1	<1	-

* indicates data from Fassio (1990).

Table 3. Mineral phases in bauxites.

Sample #	Gibbsite	Halloysite	Kaolinite	Hematite	Goethite	Maghemite	Quartz
Cowlitz County							
9/3-1	21	25	15	6	11	8	13
9/3-2	70	-	-	13	-	7	10
9/3-3	42	23	-	14	15	-	6
9/3-5	54	26	-	7	7	4	-
9/3-9	63	-	18	6	5	7	-
9/3-10	51	27	-	11	-	10	-
9/3-19	51	29	-	6	7	5	-
9/3-21	58	18	-	7	6	8	-
9/3-22	47	28	-	5	7	8	-
9/3-23	58	18	-	11	9	-	-
Columbia County							
5/1-4	23	16	26	6	7	-	22
5/1-6	22	15	25	10	10	-	17
5/1-8	24	15	23	24	0	-	14
5/1-10	27	27	-	19	24	-	-
5/1-12	20	17	21	17	20	-	-
5/1-14	48	25	-	8	9	8	-
5/1-15	25	16	30	7	6	8	-

Notes: Mineral abundances are shown in percentage (%), which is calculated from combined XRD spectrum and major element analyses. - indicate the mineral phase is not detected.

Table 4. Lithium and Nd concentrations and isotopic compositions in bauxites, parents, and eolian deposits.

Sample #	Depth (m)	[Li] (ppm)	Li/Nb	δ^7Li	Sm (ppm)	Nd (ppm)	^{143}Nd/^{144}Nd	ε_{Nd}
Cowlitz bauxites								
9/3-1(2)	2.13	21.7	0.35	-1.9	7.3	6.3	0.512100	-10.5
9/3-2(2)	2.44	14.5	0.16	-3.4	-	6.4	0.511983	-12.8
9/3-3(2)	2.74	8.7	0.18	-2.6	-	5.1	0.512128	-9.9
9/3-5	3.35	1.8	0.06	-3.4	0.4	1.3	0.512471	-3.3
9/3-5**		2.1		-1.4				
9/3-9	4.88	0.8	0.02	-1.2	0.3	1.1	0.512461	-3.5
9/3-10	5.79	0.4	0.01	-0.8	4.0	11.6	0.512413	-4.4
9/3-19	6.25	0.7	0.02	-1.1	2.1	12.0	0.512359	-5.4
9/3-21	7.62	1.3	0.03	-0.2	-	14.2	0.512389	-4.9
9/3-21*		1.2		-1.0				
9/3-22	8.23	1.5	0.04	-1.7	9.1	31.2	0.512385	-4.9
9/3-23	9.14	1.8	0.05	-3.2	-	18.29	0.512390	-4.8
Pomona basalts								
WC-6		4.5	0.42	0.2				
WC-7		3.3	0.32	-0.5				
WC-8		5.2	0.51	-0.9				
WC-9(2)		9.0	0.79	-0.9				
WC-9**		9.5		-0.8				
WC-10		3.7	0.35	1.4				
WC-12		5.6	0.53	-0.1				
WC-13(2)		6.1	0.64	0.6				
WC-14		5.1	0.49	0.8				
WC-15		5.1	0.50	-0.1				
WC-16		5.6	0.50	1.1				
WC-17		5.7	0.56	1.7				
WC-18		5.2	0.53	1.9				
WC-19		2.8	0.27	1.5				
WC-20		3.8	0.39	1.8				
WC-21		7.0	0.64	0.8				
WC-22		6.2	0.56	-0.6				
Pomona-1		6.0	0.67	0.9	4.8	20.1	0.512415	-4.4
Pomona-1*		4.8		1.3				
average		*5.5*		*0.5*				
1σ stdev		*1.7*		*1.0*				

Note: (#) number of mass spectrometry analyses; values are average of individual runs; * repeat column chemistry for the same sample solution; and ** redissolved and run through column chemistry from the same sample powder.

Table 4. Lithium and Nd concentrations and isotopic compositions in bauxites, parents, and eolian deposits continued.

Sample #	Depth (m)	[Li] (ppm)	Li/Nb	δ^7Li	Sm (ppm)	Nd (ppm)	^{143}Nd/^{144}Nd	ε_{Nd}
Columbia bauxites								
5/1-4(2)	2.74	35.4	0.61	-3.7	2.4	13.7	0.511900	-14.4
5/1-6(2)	3.96	23.0	0.41	-4.7	2.3	12.5	0.512019	-12.1
5/1-8(2)	4.57	19.0	0.23	-3.3	1.7	10.1	0.512100	-10.5
5/1-10	5.49	2.2	0.02	-2.8	0.9	3.5	0.512445	-3.8
5/1-10*		3.1		-1.6				
5/1-12	6.71	4.5	0.05	-2.8	7.4	2.9	0.512721	1.6
5/1-12**		3.9		-1.7				
5/1-14	7.32	1.6	0.04	-1.9	5.4	1.6	0.512583	-1.1
5/1-14*		3.1		-1.7				
5/1-15(2)	7.92	6.9	0.15	-0.3	0.7	2.5	0.512587	-1.0
5/1-15*		5.7		0.5				
Sentinel Bluffs basalts								
SB-1		8.7	0.95	-1.0	5.3	21.8	0.512634	-0.1
SB-1**		6.4		-0.5				
SB-2		9.3	0.85	2.8				
2170		14.4	1.40	3.6				
2170*		12.3		1.5				
2242		7.3	0.60	5.0				
2242**		10.0		6.0				
2256.5		8.8	0.81	-0.8				
2256.5**		11.5		-0.9				
2340		15.7	1.24	2.0				
2370		23.4	1.80	1.4				
2380		6.6	0.55	2.2				
2430		15.3	1.22	1.5	5.3	21.9	0.512676	0.7
2450(2)		9.7	0.82	1.1				
average		*11.4*		*1.7*				
1σ stdev		*4.6*		*2.2*				
eolian dust								
PHS-1		19.8	0.49	-1.2	5.6	28.2	0.512252	-7.5
PHS-1*		17.7		-1.9				
Palous-1		24.4	0.65	1.6	6.0	32.1	0.512101	-10.5
Palous-1**		22.4		1.7				

Note: (#) number of mass spectrometry analyses; values are average of individual runs; * repeat column chemistry for the same sample solution; and ** redissolved and run through column chemistry from the same sample powder.

20% ferric iron are bauxites and rocks with more than 20% total iron are laterites (< 45.5% alumina) or lateritic bauxites (> 45.5% alumina). Therefore, most of the drill core samples are lateritic bauxites. Some drill core samples have less than 45.5% alumina, and would be classified as laterites. Jackson (1974) refers to ferruginous bauxite as a laterite formed from weathering processes in which the weathered residues contain relatively high alumina and iron oxide and low silica content. Thus, we adopt this qualitative definition and refer to our drill core samples as bauxites.

The Chemical Index of Alteration, CIA, the widely used weathering intensity tracer, is defined in molar ratio as $Al_2O_3/(Al_2O_3+CaO^*+Na_2O+K_2O)$, where CaO* is the CaO that is not from carbonate or phosphate (Nesbitt and Young, 1982). However, due to the very low CaO contents in the bauxites, we do not make this correction. CIA values for fresh basalts range from 38 to 40, within the range of unweathered basalts (30 - 45) noted by Nesbitt and Young (1982). By contrast, CIA values in all bauxites are 99 or higher, which places them in the "most weathered" category. Thus, CIA values in bauxites cannot distinguish differences in weathering intensity among these bauxites (Table 2).

In order to evaluate the relative depletion or enrichment of elements during weathering of the basalts, the most immobile element is generally chosen as the normalization standard. In their study of strongly weathered Hawaiian soil profiles, Kurtz et al. (2000) demonstrated that Nb and Ta are the most immobile elements amongst the commonly considered immobile elements, such as Al, Fe ($^{3+}$), Ta, Zr and Hf. Here, we use Nb to normalize other elements in order to evaluate element depletion.

A widely adopted way to quantify weathering loss or addition is based on mass balance, originally developed by Brimhall and Dietrich (1987) and Chadwick et al. (2006b). The parameter tau ($\tau_{j,w} = \frac{C_{j,w} \times C_{i,p}}{C_{j,p} \times C_{i,w}} - 1$) is defined as the mass fraction of element *j* added or subtracted from the system during weathering relative to the mass of *j* originally present in the parent rock ($\tau_{j,w} = 100 \frac{m_{j,flux}}{C_{j,p} \rho_p V_p}$), *C* is the concentration of the immobile (*i*) or mobile (*j*) elements in weathered (*w*) or parent (*p*) materials, $m_{j,flux}$ is the mass addition of element *j* during weathering, ρ_p is density of the parent rock and V_p is volume of the parent rock (see Eq. (B.1) for details of the derivation). Negative $\tau_{j,w}$ values indicate net loss of element *j* ($\tau_{j,w} \geq -1$), and positive values indicate net gain of the element *j* relative to the stock of the rock's immobile element *i*. In the following discussion and elemental behavior plots, we use Nb as element *i*.

Figure 2 shows tau values for major and trace elements $\tau_{j,w}$) as a function of depth in the Cowlitz and Columbia profiles. In general, all major and trace elements in both bauxite profiles are depleted compared to Nb and their parent basalts, except for Al2O3 in the Cowlitz profile, and Zr in one Cowlitz sample. Plots of tau for trace elements vs. depth show that, as expected, soluble elements, such as Mg, Rb, and Sr, are strongly depleted. In addition to the depletion of transition metals, such as V, Ni,

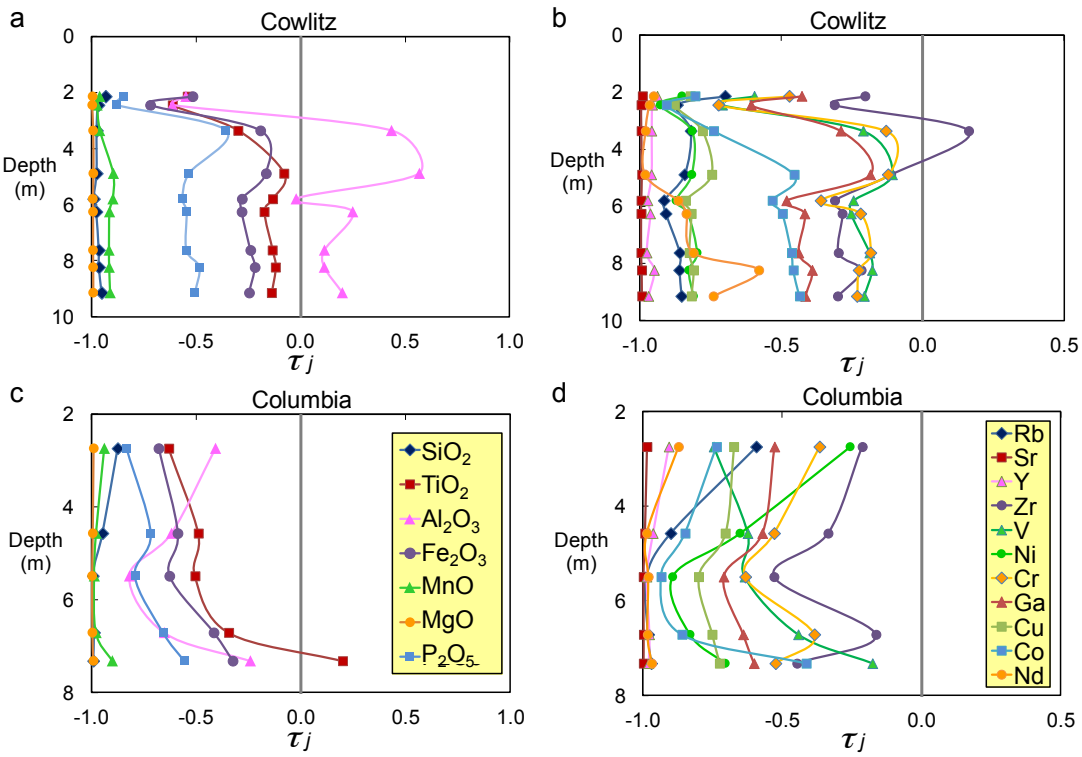

Figure 2. Major and trace element τ values vs. depth in Cowlitz and Columbia profiles.

a and b: Major element and trace element τ in Cowlitz bauxites, respectively. c and d: Major element and trace element τ in Columbia bauxites. τ is calculated using Nb as the reference immobile element. Details of τ calculations are discussed in the main text. Gray lines indicate the τ value of fresh basalts (τ = 0). Data are reported in Table 1.

Cr, Cu, and Zn, some elements that are traditionally considered "immobile", such as Al, Fe (3+), some REE, Y, and Zr, show strong depletion as well in these two extremely weathered profiles. In general, element depletion is more significant towards the tops of the profiles.

4.3 Li concentration and isotopic composition

4.3.1 Fresh basalts

Li concentrations ([Li]) and δ^7Li in fresh basaltic parents are given in Table 4 and plotted in Figure 3. The Pomona basalts show relatively small variations in [Li] and δ^7Li, though they do vary beyond analytical precision, ranging from 3 to 9 ppm and from -1 to +2, respectively. By contrast, Sentinel Bluffs basalts show a significantly larger degree of [Li] (7-23ppm) and δ^7Li (-1 to +5) variation than the Pomona samples. The average δ^7Li of Pomona basalts (0.5 ± 1.0) falls distinctly below typical mantle values (as seen in mid-ocean ridge basalts, Tomascak et al., 2008), whereas the average δ^7Li for the Sentinel Bluffs basalts (1.7 ± 2.2) falls at the lower range of mantle values. These values are similar to the isotopic composition of BCR-1 and -2 (2.1 ± 0.4 and 2.8 ± 0.7, respectively, see Table A4), which come from the Wapshilla Ridge member of the Grande Ronde basalt within the CRBs.

4.3.2 Cowlitz and Columbia profiles

[Li] and δ^7Li in the Cowlitz and Columbia profiles are reported in Table 4. Plots of normalized concentration, $\tau_{Li,w}$ versus depth in these two profiles are shown in Figure 4. $\tau_{Li,w}$ in both profiles indicates a large degree of Li depletion relative to fresh parent basalt, with the bottom four meters in the Cowlitz profile showing

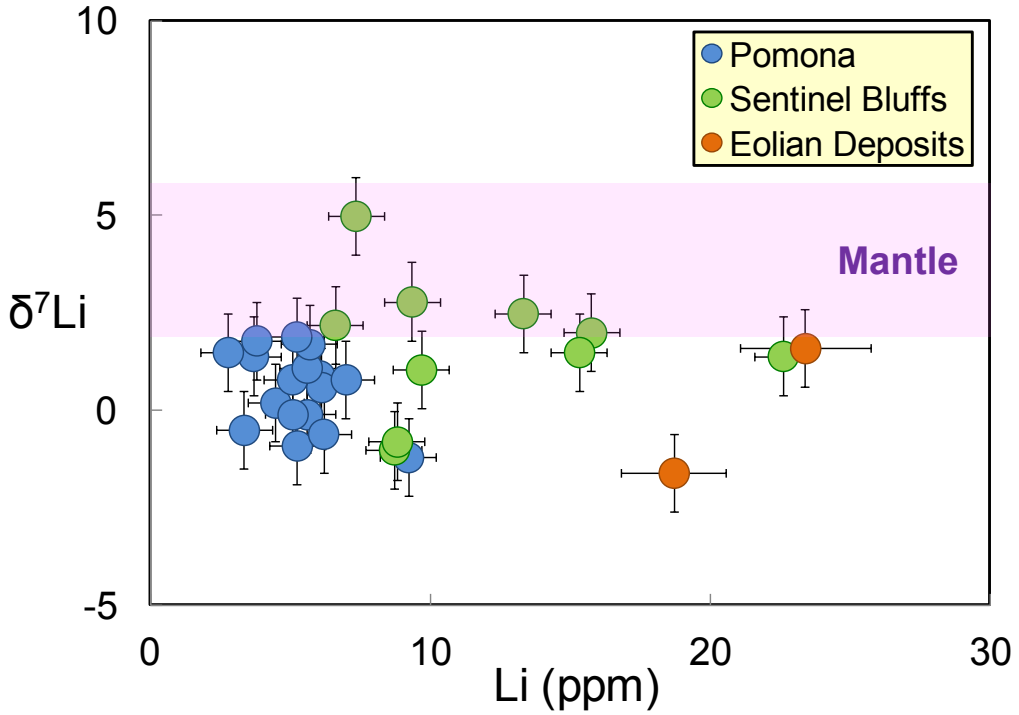

Figure 3. δ^7Li vs. [Li] (ppm) in basalt parents and eolian deposits.
Pomona basalts (CRB), parental to the Cowlitz bauxite profile, are shown as blue circles, Sentinel Bluffs basalts (CRB), parental to the Columbia bauxite profile, are shown as green circles, and eolian dust deposits are shown as orange circles. Purple field marks range of mantle δ^7Li values (+4 ± 2), according to the world-wide compilation by Tomascak et al. (2008). Error bars represent 2 standard deviations (2σ). Data are reported in Table 3.

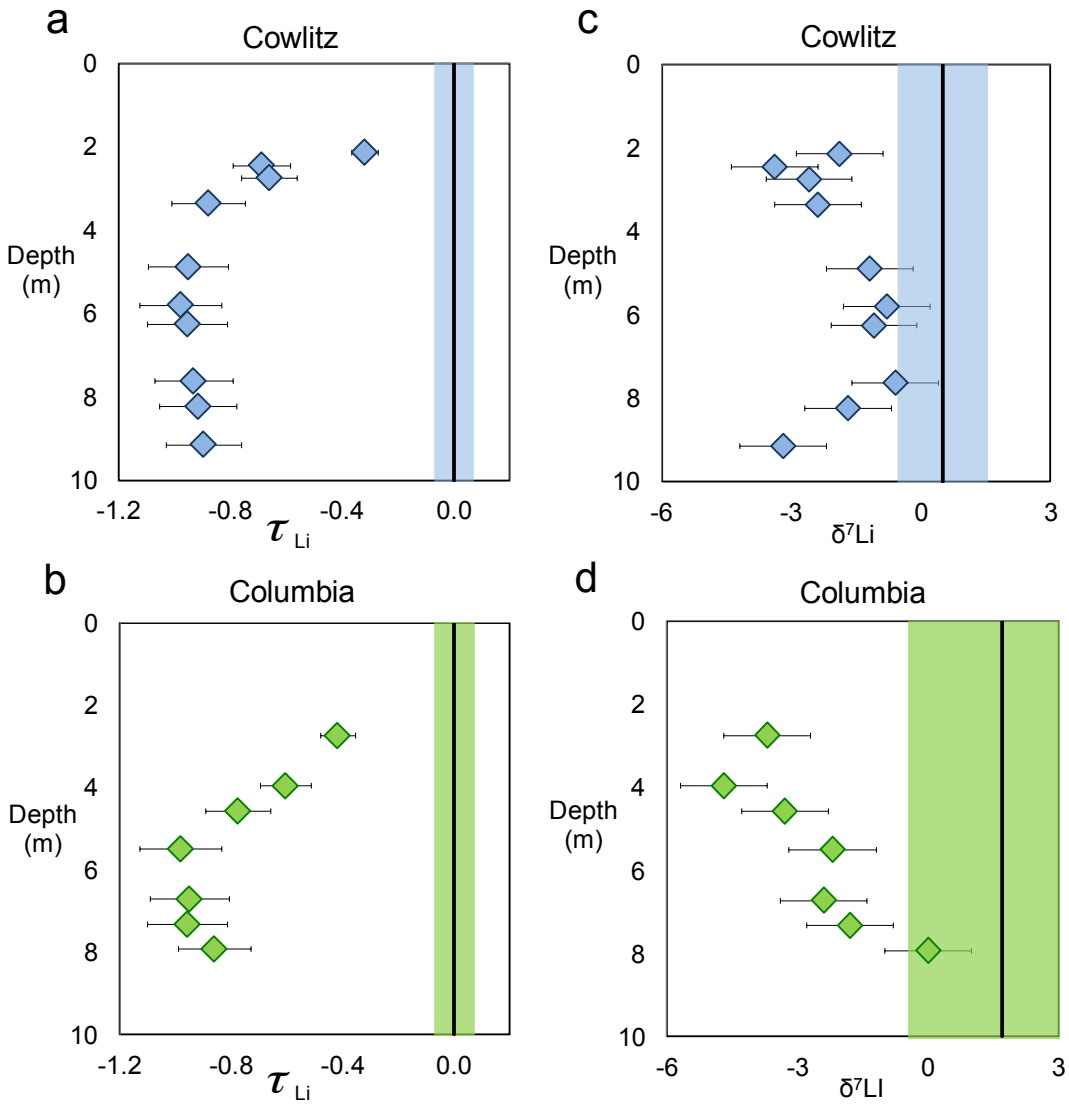

Figure 4. τ_{Li} and δ^7Li vs. depth for both Cowlitz (upper, in blue), formed on the Pomona basalt, and Columbia (lower, in green), formed on the Sentinel Bluffs basalt drill cores.
Bauxites are shown as symbols and average parent basalt compositions are shown in black lines; rectangular fields show 1σ of the average values. Error bars represent 2σ. Data are reported in Table 3.

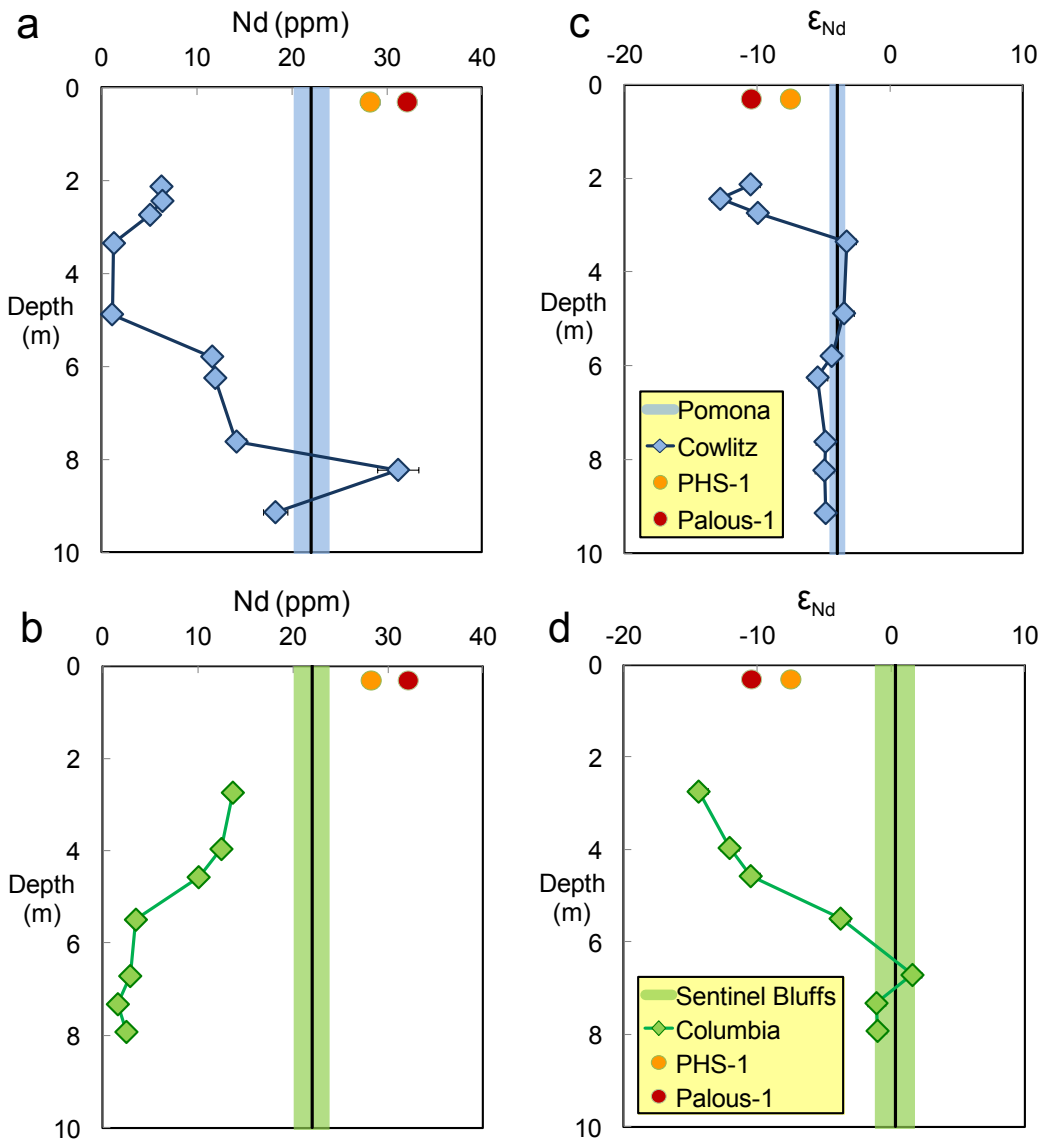

Figure 5. [Nd] and εNd vs. depth for both Cowlitz (upper, in blue) and Columbia (lower, in green) drill cores.
Eolian samples are plotted in red (east of the Cascades) and orange (west of the Cascades) circles at the top of the diagram. Analytical error bars are smaller than symbols. Average compositions of the unweathered basaltic parent are shown in black lines; with the colored field indicating the possible range in composition for the parental basalts. The widths of the colored field represent the accuracy of [Nd] analyses (< 7%, see Table A. 3) and 1σ variation of available ε_{Nd} in fresh parental basalts, for [Nd] and ε_{Nd} plots, respectively (see text for data sources).

progressive Li depletion towards the surface (Figure 4a). However, in the upper three meters of this profile, $\tau_{Li,w}$ systematically increases towards the surface. A similar trend is observed in the Columbia profile (Figure 4b).

The δ^7Li values in both bauxite profiles are lower than the average of the fresh basalt parents (vertical bars in Figure 4), though the deepest bauxite in the Columbia profile overlaps with the range of δ^7Li values seen in fresh Sentinel Bluffs basalts. The δ^7Li values of the bauxites are up to 4‰ lower than average fresh Pomona basalt (Figure 4c), and up to 7‰ lower than average fresh Sentinel Bluffs basalt (Figure 4d). In both profiles, δ^7Li values decrease systematically towards the surface.

4.3.3 Eolian deposits

Samples from both of the eolian deposits have higher [Li] (19 and 23 ppm for the Portland Hill Silt and Palouse Formation, respectively) compared to most of the fresh CRBs (Table 4 and Figure 3). The δ^7Li values of the eolian samples overlap those of the fresh CRBs (+1.6 for Palouse Formation, and -1.6 for Portland Hills Silt).

4.4 Neodymium isotopes

4.4.1 Parent basalts

Nd concentrations ([Nd]) and $^{143}Nd/^{144}Nd$ ratios (plotted as ε_{Nd}) in basaltic parents are given in Table 4 and shown as a colored vertical band depicting the average and one standard deviation in Figure 5, where we plot [Nd] instead of τ_{Nd} so that the eolian deposits can be shown on the same plot. One analysis of a Pomona basalt gives [Nd] and $^{143}Nd/^{144}Nd$ of 20 ppm and 0.512415, respectively. Combined with published data from Carlson et al. (1981), where [Nd] and $^{143}Nd/^{144}Nd$ are 24 ppm and 0.512451, respectively, we calculate an average [Nd] and $^{143}Nd/^{144}Nd$ of 22

ppm and 0.512433, respectively, for fresh Pomona basalt. By contrast, two Sentinel Bluffs basalts analyzed here have more radiogenic compositions, with average [Nd] of 22 ppm and $^{143}Nd/^{144}Nd$ of 0.512655.

4.4.2 Bauxite profiles

[Nd] and $^{143}Nd/^{144}Nd$ in the Cowlitz and Columbia profiles are reported in Table 4 and plotted as a function of depth in Figure 5. Like Li, Nd in the Cowlitz profile shows a large degree of depletion relative to fresh basalt, with an increase in concentration towards the surface and a systematic enrichment in the top three meters of the profile (Figures 5a, b). The $^{143}Nd/^{144}Nd$ values for the bauxites overlap those of the fresh basalts at depth, but trend towards less radiogenic values towards the surface, reaching ε_{Nd} values down to -12.8 for the shallowest Cowlitz samples, compared to those of -4.0 in averaged fresh Pomona basalts (Figure 5c) and ε_{Nd} values down to -14.4 for the shallowest Columbia sample, compared to those of +1.3 in averaged fresh Sentinel Bluffs basalts (Figure 5d).

4.4.3 Eolian Deposits

Both samples of eolian deposits have higher [Nd] (28 and 32 ppm for the Portland Hill Silt and Palouse Formation, respectively), compared to the fresh CRBs (Table 4 and Figure 5), and are less radiogenic (ε_{Nd} = -7.5 for Portland Hills Silt and -10.5 for the Palouse Formation). However, these isotopic compositions are more radiogenic than the least radiogenic bauxites near the tops of the profiles. This is especially apparent in the Columbia profile (Figure 5d).

5. Discussion

We first discuss the factors that may control the chemical composition of basalts that experienced extreme weathering, we then compare our results to global observations of Li isotopic behavior during basalt weathering, and, finally, we discuss the insights that Li isotopes can provide regarding chemical weathering of basalts and the implications of our study for the mass and compositional evolution of the continental crust.

5.1 Factors influencing compositional changes during basalt weathering

The significant depletion of [Li] and many other elements in the bauxites relative to fresh basalts are consistent with elemental loss via leaching during weathering. However, Li concentrations, as well as those of other potentially soluble, incompatible elements (e.g., SiO_2, Rb, Y) increase upwards in the profiles within the top five meters (Figures 2 and 4). Such increases are not an expected outcome of leaching. Other observations, described below, such as the presence of quartz in the upper five meters of the profiles, and the unradiogenic Nd isotopic compositions of the upper portions of the profiles are consistent with these profiles having experienced mass addition from the top.

5.1.1 Eolian addition

Eolian dust addition to soil profiles developed on basalts has long been recognized (e.g., Jackson et al., 1972; Kurtz et al., 2001; Rex et al., 1969). Minerals absent from the fresh basalt (e.g., quartz and mica) and variable radiogenic isotope compositions (Nd and Sr isotopes) have been used to identify and quantify the eolian inputs and their sources (Das et al., 2006; Pett-Ridge et al., 2009; Viers and

Wasserburg, 2004). Quartz was detected in the upper five meters of both the Cowlitz and Columbia bauxite profiles (Table 3), but quartz is not present in the CRBs, suggesting eolian dust addition to the tops of the profiles. Neodymium concentrations also show depletion in bauxites relative to parent basalts, with increasing concentrations towards the tops of the profiles. Most compellingly, Nd isotopes in these uppermost bauxites are less radiogenic than the fresh basalts, with ε_{Nd} decreasing towards the surface (Figure 5). Collectively, these observations suggest that wind-blown dust was added to the top five meters of the bauxite profiles, with the proportion of dust decreasing systematically with depth.

A potential source of such dust is the rather extensive eolian deposits that are associated with the last glaciation, and which blanket large areas in the region (Busacca, 1989; Sweeney et al., 2007). However, the Nd isotopic compositions of two of the two eolian deposits analyzed here (Table 4) are more radiogenic than what is observed near the tops of the profiles, suggesting one of the following possibilities: a) the dust incorporated into the weathered basalt is derived from an older continental region than the source region of these eolian deposits, b) that the eolian deposits are more heterogeneous in Nd isotopic composition than our two analyses indicate (Jagoutz and Schmidt, 2012), or c) that the dust has been added over a long time period and includes dust from a multitude of sources, such as dust from eastern Asia, which has been seen in Hawaiian soils (Kurtz et al., 2001).

Sediments deposited in the Astoria fan, delivered by the Columbia River drainage system, are believed to derive mainly from two sources, namely, Proterozoic Belt Supergroup metasediments and the CRBs. The Proterozoic Belt Supergroup

metasediments have similar or less radiogenic Nd isotopic signatures (ε_{Nd} = -12 to -30) (Prytulak et al., 2006) as the least radiogenic bauxites near the tops of the profiles (ε_{Nd} is down to -14). Therefore, if the two eolian samples analyzed here are representative of the eolian dusts from the last glacial episode, it is likely that the dust incorporated into these bauxites derived, at least in part, from more ancient continental crustal sources, such as the Proterozoic Belt Supergroup. Interestingly, the Li isotopic compositions of the tops of both profiles are lighter than typical sedimentary materials, suggesting either that the source region was strongly weathered, or that the dust component also experienced weathering after its incorporation into the soils.

5.1.2 Mechanism controlling Li isotopic fractionation

The isotopically light Li compositions of the profiles are likely caused by fractionation during weathering. As a start, we use a Rayleigh fractionation model to quantify lithium isotopic fractionation produced by Li leaching from the basalts, assuming equilibrium fractionation between fluid and bauxites. Because of the uncertainty regarding the original Li isotopic composition of the eolian component, as well as its mass fraction, we exclude samples containing the eolian component (i.e., quartz-bearing samples) from these calculations. The fractionation factor (α), is defined as $\alpha = (^7Li/^6Li)_{fluid}/(^7Li/^6Li)_{bauxite}$. Therefore, the Rayleigh fractionation equation can be written as: $\delta^7 Li_{bauxite} = (\delta^7 Li_{basalt} + 1000) f^{(\alpha-1)} - 1000$, where $\delta^7Li_{bauxite}$ and δ^7Li_{basalt} are Li isotopic composition in bauxite and basalt, respectively; f is the fraction of Li remaining in the residue, calculated from $[Li]_{bauxite}/[Li]_{basalt}$. Using average lithium concentration and δ^7Li in the parental basalts, the

models indicate α values ranging from 1.001 to 1.004 in bauxites from both the Cowlitz and Columbia profiles. We then plot δ^7Li against $1/[Li]_{norm}$ (using $1/[Li]_{norm}$ instead of $1/\tau_{Li}$ because τ_{Li} in parental basalt is zero), defined as $[Li]_{norm} = [Li]_{bauxite}/[Li]_{basalt}$ (Figure 6).

It is known that lithium is preferentially incorporated into secondary minerals, such as the clay minerals smectite and illite, where Li can substitute in octahedral sites (Calvet and Prost, 1971; Williams and Hervig, 2005). By contrast, Li^+ forms stable tetrahedral complexes with water molecules (Olsher et al., 1991). The bonds in such tetrahedra are stronger than those for Li in octahedral sites in minerals or Li adsorbed onto mineral surfaces, leading to a preference for heavy Li (^{7}Li) in water. Alternatively, Li can be adsorbed onto the surface or into the interlayers of minerals such as kaolinite (Zhang et al., 1998) and gibbsite (Pistiner and Henderson, 2003). Indeed, experimental studies have documented that light Li (^{6}Li) is preferentially incorporated into secondary minerals. For example, the experimental study of Pistiner and Henderson (2003) suggests that ^{6}Li preferentially sorbs to the surface of gibbsite, leading to large Li isotopic fractionation between gibbsite and water (~14‰). Gibbsite is likely to be the dominant Li-containing mineral in the bauxites studied here, as it is the major Al-bearing mineral (comprising between 20% to 70% of the bauxites, Table 3). In addition, kaolinite and/or halloysite are other possibly significant hosts for Li in bauxites, and they have even larger Li isotopic fractionation factors (α=1.021, Zhang et al., 1998). However, the inferred fractionation factor associated with the bauxites in the Rayleigh calculations (α up to 1.004) is significantly smaller than the fractionation found in these sorption experiments.

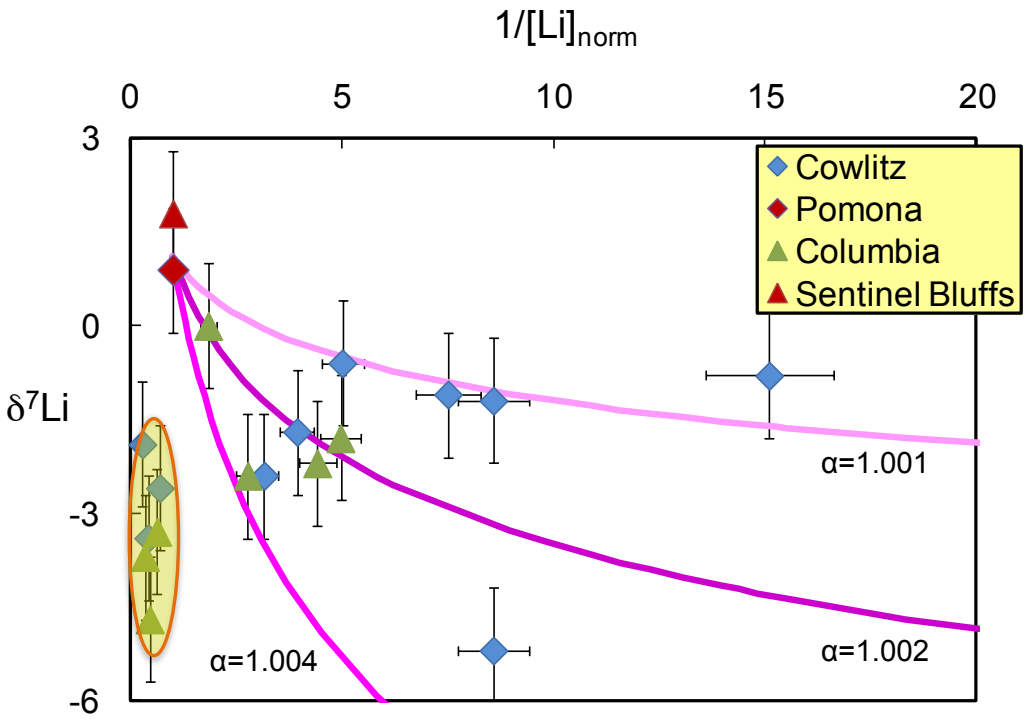

Figure 6. Rayleigh fractionation modeling of Li isotopic fractionation in bauxites. $[Li]_{norm}$ is defined as $[Li]_{norm}= [Li]_{bauxite} /[Li]_{basalt}$. The parent of Cowlitz bauxites (blue diamonds) is Pomona basalt (red diamond) and parent of Columbia bauxites (green triangles) is Sentinel Bluffs. Note that all bauxites except for the top three (circled by orange ellipse) from both Cowlitz and Columbia are plotted. We model Li depletion in non-eolian influenced bauxites via Rayleigh fractionation model, where these bauxites fit Rayleigh fractionation curves (pink) with different fractionation factors, α, defined as $\alpha = (^7Li/^6Li)_{fluid} /(^7Li/^6Li)_{bauxite}$. Error bars represent 2σ. Data are reported in Table 3.

The above discrepancy shows that a simple Rayleigh fractionation process does not account for the observed Li isotope fractionation in bauxites. The Rayleigh modeling assumes a constant fractionation factor between the fluid and rock during leaching, where primary mineral dissolution is accompanied with secondary mineral formation, with the fluid ultimately leaving the system. However, the natural processes of weathering are more complex: basalts may first experience primary dissolution (e.g., of olivine, glass), with little formation of secondary minerals. During such dissolution processes most of Li is lost to the interacting fluid, such as pore water, and is accompanied by little to no lithium isotopic fractionation (Pistiner and Henderson, 2003; Wimpenny et al., 2010a). Secondary minerals formed later may adsorb light Li from pore waters, as documented by both experimental studies and field observations (e.g, Huh et al., 2002; Huh et al., 1998; Kisakürek et al., 2004; Pistiner and Henderson, 2003; Pogge von Strandmann et al., 2006; Rudnick et al., 2004; Vigier et al., 2009). Therefore, the relatively low α inferred here from the Rayleigh modeling may reflect a combination of dissolution, leaching, and equilibrium partitioning between secondary minerals and isotopically heavy pore waters in soils.

The δ^7Li values in bauxites decrease systematically towards the surface in the upper five meters, reaching values that are 6 to 7‰ lower than those of the average fresh basalt. The light δ^7Li values (-5‰) combined with their high Li concentrations near the surface of the profiles may reflect weathering of a mixture of basalt and dust, the latter of which is enriched in lithium compared to basalts. Moreover, the Li isotopic compositions of the two eolian deposits analyzed here (average δ^7Li = 0) are

lighter than that of the basalts (average δ^7Li = 2), and is consistent with Li found in terrigneous sediments, loess and shale, which tends to have δ^7Li that is lower than that of the mantle (Chan et al., 2006a; Qiu et al., 2011a; Qiu et al., 2009; Teng et al., 2004). Although, based on their Nd isotopic compositions, these two eolian samples may not be the source of the dust added to the top of the bauxites, their δ^7Li values are similar to typical eolian sediments (Figure 7). Thus, the isotopically unusually light eolian components seen near the surface of the bauxite profiles may have also experienced weathering, lowering the δ^7Li values (down to -5‰). Therefore, chemical weathering likely post-dated or was concurrent with eolian addition.

5.2 Insights regarding chemical weathering of basalts and continental crust composition

Our results are remarkably similar to those found for a 50 m laterite profile developed on the Deccan basalts (Kisakürek et al., 2004), suggesting a global similarity in process. Although the latter results were attributed to mixing with an unusually isotopically light (- 5‰) eolian component, another possible interpretation is that the eolian component is also weathered, as discussed above. Weathering of the eolian component following its deposition was also documented for Hawaiian soils (Kurtz et al., 2001).

We document an outcrop-scale case study that supports the notion that chemical weathering removes mass from the continental crust and may modify the crust's chemical composition. Chemical weathering of basalts can significantly change the mass and chemical composition of the parental rock by preferential depletion of more soluble elements. According to this case study, more than 95% of

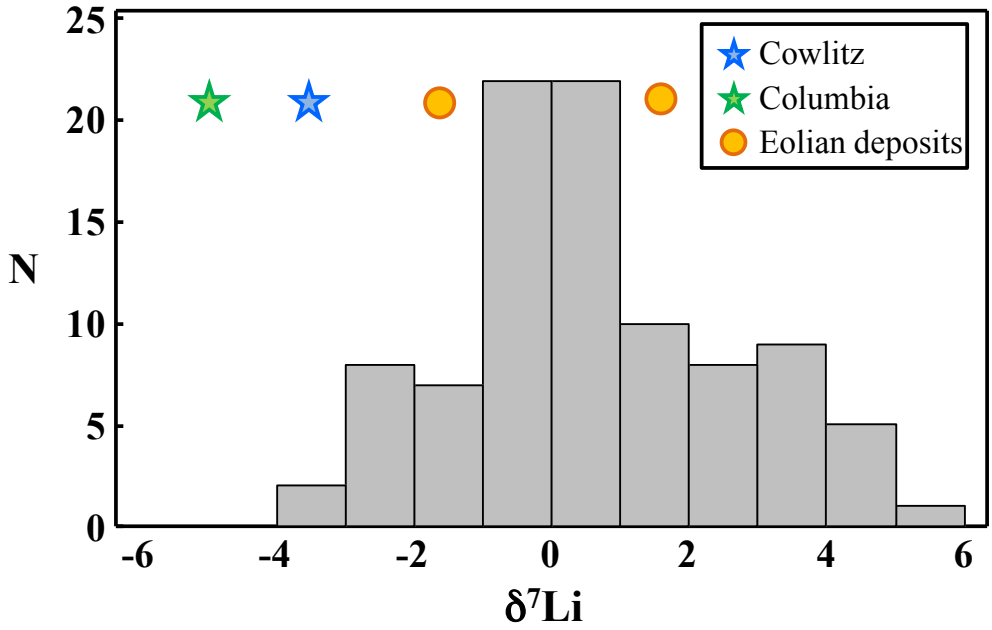

Figure 7. Comparison of δ^7Li at the top of the bauxite profiles (blue and green stars) to δ^7Li in the upper continental crust (UCC, as sampled by shales, loess and granites: histogram) and the two eolian deposits analyzed here (orange stars).
Data for shales, loess, and granites are from Teng et al. (2004), Qiu et al. (2011a; 2009).

mobile major elements, such as Na, Mg, K, and Ca were lost during this extreme weathering; significant loss (mostly > 50%) of other "immobile elements", such as Al, Fe ($^{3+}$), REE, Y, and Zr are also observed (Figure 2). The strong depletion of mobile and even "immobile elements" during extreme weathering supports previous suggestions (Albarède, 1998; Lee et al., 2008; Liu and Rudnick, 2011) that significant mass loss, perhaps more than 15%, of juvenile continental crust materials (i.e., basalts), may occur due to chemical weathering.

Weathering may also have implications for the trace element signature of the continental crust. It is well established that the continental crust is depleted in Nb and Ta relative to other highly incompatible elements such as La (Rudnick, 1995 and references therein). However, the degree of Nb depletion in the crust is smaller than that seen in arc magmas (Barth et al., 2000), which are widely considered to represent the building blocks of the continental crust (Hawkesworth and Kemp, 2006; Plank, 2005). Thus, it has been suggested that this Nb depletion may reflect a continental crust that is a mixture between intraplate (no Nb depletion) and convergent margin magmas (e.g., Barth et al., 2000). An alternative, or additional possibility, is that chemical weathering, which depletes REE relative to Nb (Figure 2), could also be important in reducing the magnitude of the Nb anomaly of the continental crust.

6. Conclusions

The main conclusions from this study are:

1. As demonstrated in previous studies, extreme depletion of elements in bauxite profiles indicate intense weathering can remove elements traditionally considered as "immobile", such as Al, Fe ($^{3+}$), REE, Zr, Y, etc.

2. This study demonstrates the open and dynamic characteristics of terrestrial weathering. Leaching, secondary mineral formation, and eolian addition are the main processes controlling lithium and its isotopic composition in these bauxite profiles.

3. Our study demonstrates that Li concentrations and its isotopic compositions are sensitive tracers of chemical weathering, especially for extreme weathering conditions, where traditional weathering intensity indicators such as CIA fail to discriminate different degrees of weathering. In addition, we demonstrate that Li isotopes can trace both origin and processes (e.g., eolian inputs and weathering), whereas Nd isotopes can only trace origin.

4. Our results support previous suggestions that significant mass loss due to chemical weathering is one of the possible mechanisms that drove the bulk continental crustal composition from basalt to andesite.

5. Chemical weathering may also decrease the magnitude of Nb anomaly of the bulk continental crust.

Appendices

Table A.1. Precision evaluation of typical bauxite.

	O	#1	#2	#3	#4	#5	mean	2σ	% error
SiO2	33.95	34.04	34.18	34.09	34.24	34.05	34.09	0.21	0.6
TiO2	4.61	4.65	4.61	4.62	4.62	4.59	4.62	0.04	0.9
Al2O3	29.18	29.03	28.93	28.77	28.98	28.85	28.96	0.29	1.0
Fe2O3T	29.84	29.86	29.76	29.67	29.79	29.83	29.79	0.14	0.5
MnO	0.950	0.981	0.976	0.945	0.986	0.944	0.96	0.04	4.0
MgO	0.143	0.157	0.155	0.152	0.152	0.155	0.15	0.01	6.5
CaO	0.098	0.090	0.088	0.089	0.087	0.088	0.09	0.01	9.0
Na2O	0.061	0.074	0.072	0.071	0.071	0.069	0.07	0.01	13.1
K2O	0.018	0.020	0.028	0.019	0.018	0.018	0.02	0.01	38.9
P2O5	0.437	0.437	0.441	0.435	0.437	0.436	0.44	0.00	0.9
Total	99.310	99.339	99.240	98.861	99.381	99.030	99.19	0.41	0.4
LOI	18.57	18.47	18.60	18.29	18.30	18.39	18.44	0.27	1.44
Rb	4.6	4.4	4.8	4.0	4.1		4.4	0.7	15.3
Sr	38	37	38	37	38	37	38	1.1	2.9
Y	4.8	4.8	4.0	4.9	4.8		4.7	0.7	15.9
Zr	289	290	287	285	288	289	288	3.6	1.2
V	645	645	640	644	652	668	649	20.2	3.1
Ni	46	45	45	45	45		45	0.9	2.0
Cr	40	41	44	37	39	40	40	4.6	11.5
Nb	24.9	23.9	25.3	23.8	24.5		24.5	1.3	5.2
Ga	29.7	29.1	29.0	29.1	29.4		29.3	0.6	2.0
Cu	102	91	91	93	91		94	9.5	10.2
Zn	159	158	158	157	158		158	1.4	0.9
Co	67	66	68	65	65		66	2.6	3.9
Ba	404	408	404	400	389		401	14.6	3.6
La	4	2	3	2	2		3	1.8	68.8
Ce	17	17	18	18	18		18	1.1	6.2
U	<0.5	<0.5	<0.5	0.8	<0.5		<0.5	-	-
Th	38.2	36.4	38.4	43.4	35.3		38.3	6.2	16.2
Sc	53	54	56	56	57		55	3.3	6.0
Pb	10	8	9	15	12		11	5.5	51.4

Notes: 1.O indicates the original measurement and # indicates the number of replicates. 2. Units of all the major elements and LOI are in wt % and all trace elements are reported in ppm.

Table A.2. Accuracy evaluation of Li concentration and isotopic compositions.

Standard Name	Date Run	[Li] (ppm)	δ^7Li	Source
Basalt, Hawaii				
BHVO-1	2010 08 18	4.3	4.6	this study
BHVO-1	2011 09 02	3.8	4.1	this study
BHVO-1	2011 08 05	3.8	5.2	this study
BHVO-1	2010 09 17	4.3	5.2	this study
BHVO-1	2010 12 11	4.5	4.1	this study
Average		4.1	4.7	
BHVO-1		4 ~ 5	4.0 ~ 5.6	GEOREM database
Andesite, Oregon				
AGV-1	2010 08 18	10.9	4.4	this study
AGV-1	2010 12 11	9.2	4.9	this study
Average		10.0	4.6	this study
AGV-1		10 ~ 12	4.6 ~ 6.7	GEOREM database
Basalt, Oregon				
BCR-2	2011 09 02	9.6	3.4	this study
BCR-2	2011 03 04	9.1	2.1	this study
Average		9.3	2.7	this study
BCR-2		8 ~ 10	2.6 ~ 4.6	GEOREM database

Table A.3. Accuracy evaluation of Nd concentration and isotopic compositions.

Standard Name	Date Run	[Nd] (ppm)	% Error	$^{143}Nd/^{144}Nd$	Source
Basalt, Hawaii					
BHVO-1	2012 02 20	27.5		0.513036	this study
BHVO-1	2012 02 21	25.3		0.513022	this study
Average		26.4		0.513029	
GeoReM prefered		24.7	6.8		
BHVO-1		22.1-28.5		0.512949 - 0.513048	GeoReM database
Basalt, Oregon					
BCR-2	2012 02 21	28.0		0.512651	this study
GeoReM prefered		28.7	2.6		
BCR-2		26.7-31.4		0.512608 - 0.512656	GeoReM database

Table A.4. Li isotopic compositions of BCR-1 and BCR-2.

BCR-1	δ^7Li	2 sigma	n
Rudnick et al. (2004)	2.7	1	1
Magna et al. (2004)	2.4	0.5	2
Teng et al. (2006)	2.0	0.7	10
Aulbach et al. (2008)	3.0	0.5	1
Qiu et al. (2009)	2.0	0.3	2
Teng et al. (2009)	2.0	0.7	10
Qiu et al. (2011)	2.2		1
weighted average	**2.1**	**N =**	**27**
1 sigma stdev	**0.4**		
BCR-2	δ^7Li	2 sigma	n
Jochum et al. (2006)	4.4	0.3	2
Rosner et al. (2007)	2.9	0.4	2
Kosler et al. (2009)	3.19	0.12	4
Janosek et al. (2010)	3.0	0.3	3
Pogge von Strandmann et al. (2011)	2.6	0.3	18
Penniston-Dorland et al. (2012)	2.6	0.3	19
weighted average	**2.8**	**N =**	**48**
1 sigma stdev	**0.7**		

Eq. (B.1). Derivation of the mass balance of chemical composition during weathering

Base on mass balance of element before and after weathering, we have

$$m_{j,p} + m_{j,flux} = m_{j,w} \quad \text{(A1)},$$

where m is the mass of element *j* in parent rocks (p), flux into the system (flux) and weathered rocks (w). Given density (ρ) and volume (V), and concentration (C), equation A1 can be written as

$$\frac{V_p \rho_p C_{j,p}}{100} + m_{j,flux} = \frac{V_w \rho_w C_{j,w}}{100} \qquad \text{(A2)}.$$

If we define the mass fraction of element *j* added to the system during weathering relative to the mass of originally present in the parent material, we have

$$\tau_{j,w} = 100 \frac{m_{j,flux}}{C_{j,p} \rho_p V_p} \quad \text{(A3)}.$$

Also, we define the volume change during weathering $\varepsilon_{i,w}$, as $\varepsilon_{i,w} = \frac{V_w - V_p}{V_p}$ (A4),

where *i* represents the chosen immobile element. Combine equations (A2)-(A4), we have

$$\tau_{j,w} = \frac{\rho_w C_{j,w}}{\rho_p C_{j,p}} (\varepsilon_{i,w} + 1) - 1 \qquad \text{(A5)}.$$

If we assume the immobile element *i* has zero influx during weathering, that is to say $\tau_{i,w}$=0, and rewrite equation A5 in terms of element *i* (replace *j* with *i*), we have

$$\varepsilon_{i,w} = \frac{\rho_p C_{i,p}}{\rho_w C_{i,w}} - 1 \qquad \text{(A6)}.$$

Then we substitute equation A6 into equation A5, we then have

$$\tau_{j,w} = \frac{C_{j,w} \cdot C_{i,p}}{C_{j,p} \cdot C_{i,w}} - 1 \quad \text{(A7)}.$$

Chapter 3: Massive magnesium isotopic fractionation produced by basalt weathering

Abstract

Chemical weathering of juvenile continental crust, specifically basalts, impacts the evolution of the continental crust and the global CO_2 cycle. Several non-traditional stable isotope tracers, such as Mg isotopes, have been developed in the last decade to study weathering. However, the mechanisms of Mg isotope fractionation during continental weathering are still unclear. Here we present Mg isotope data from two ~10 m deep drill cores, which traverse bauxites developed on Columbia River Basalts (CRBs), and use these data to unravel the main factors responsible for Mg isotope behavior during basalt weathering. Bauxites have extremely high $\delta^{26}Mg$ values (up to +1.8) and low MgO contents (0.12 wt. %) relative to the fresh basalts ($\delta^{26}Mg = -0.24 \pm 0.07$ and MgO = 5.9 wt. %). $\delta^{26}Mg$ is positively correlated with gibbsite abundance, suggesting that gibbsite controls the Mg isotopic fractionation. Additionally, dust addition at the surface lowered $\delta^{26}Mg$ towards values more typical of the original basalt. The significant Mg isotope fractionation reported here demonstrates that Mg isotopes can be useful tracers of chemical weathering, especially under intense weathering conditions, where traditional tracers such as Chemical Index of Alteration (CIA) are less sensitive to weathering processes.

1. Introduction

The development of MC-ICP-MS techniques has enabled the use of non-traditional stable isotopes for a variety of applications, one of which is their use as tracers of chemical weathering. Magnesium isotopes have several advantages as potential geochemical tracers of chemical weathering. First, magnesium is one of the most abundant elements in the continental crust (e.g., Rudnick and Gao, 2003b; Taylor and McLennan, 1995), and it is also water-soluble, preferentially dissolving in water during continental weathering. Magnesium has only one redox state (+2), and is thus insensitive to changes in oxygen fugacity (cf. Fe, Cu, Mo, etc.). In addition, no significant Mg isotopic fractionation has been observed during igneous differentiation (e.g., Liu et al., 2010a; Teng et al., 2010b; Teng et al., 2007b). Most importantly, Mg isotopes are significantly fractionated from the mantle value in both soils and river waters, indicating that they are fractionated by continental weathering (e.g., Pogge von Strandmann et al., 2008; Teng et al., 2010a; Tipper et al., 2006a; Wimpenny et al., 2010a).

Nevertheless, there is no consensus on either the direction or mechanisms of Mg isotope fractionation during chemical weathering. In a study of a weathering profile developed on a meta-diabase, Teng et al. (2010a) suggested that Mg isotope fractionation follows simple Rayleigh fractionation and is controlled by the formation of secondary minerals, producing regoliths enriched in heavy Mg isotopes by up to 0.65‰. The experimental study of Ryu et al. (2011) suggested that preferential dissolution of isotopically light minerals, such as chlorite (δ^{26}Mg is as low as -1.82), may lead to isotopcally light Mg in solution (δ^{26}Mg down to -1.59). By contrast,

Pogge von Strandmann et al. (2008) analyzed Icelandic rivers and found a very large range in $\delta^{26}Mg$ (-0.96 to 0.64), suggesting that some secondary minerals preferentially incorporate light Mg isotopes, leaving residual water to be isotopically heavy. In another experimental study, Wimpenny et al. (2010a) suggested that light Mg isotopes are preferentially incorporated into water during dissolution of certain minerals, such as forsterite, and then precipitation of certain secondary minerals (chrysotile) preferentially removes light Mg isotopes from solution, leaving the residual water with a heavy Mg isotopic composition. Note that the Mg isotope behavior in the experimental results of Wimpenny et al. (2010a) is opposite to most natural observations, where waters tend to be isotopically light and regoiliths heavy, except for those of Pogge von Strandmann et al. (2008).

This study aims to determine the factors controlling Mg isotope fractionation during basalt weathering, especially under intense weathering conditions. The findings help to illuminate the role of chemical weathering in changing the juvenile continental composition from basaltic to andesitic.

2. Method of Mg isotope analyses

MgO content, along with other major and trace elements, were analyzed by X-Ray Fluorescence analysis (XRF) at Franklin and Marshall College. The uncertainty of MgO content in fresh basalts and eolian samples is better than 1% (2 σ), based on repeat analyses of BHVO-2 (http://www.fandm.edu/earth-and-environment/precision-and-accuracy). However, due to the low MgO concentrations in bauxites, the above precision is not representative of the bauxites. To determine precision, one bauxite

sample with typical MgO concentration was repeatedly analyzed. We find a precision better than 6.5% (2 σ, n=6) (Table A.2).

Magnesium isotope analyses were carried out using a Nu Plasma Multi Collector-Inductively Coupled Plasma-Mass Spectrometer (MC-ICP-MS) at the Isotope Laboratory of the University of Arkansas, Fayetteville, using the method described in Teng et al. (2011). A brief description of sample dissolution, column chemistry and instrumental analysis is provided below.

The same rock powers that were analyzed for Li isotopes were used here: 2-30 mg of sample powders were dissolved, depending on their Mg concentrations, to obtain ~10 mg Mg for isotopic analysis. First, rock powers are dissolved in a 3:1 (v/v) mixture of Optima-grade HF and HNO_3 acids in separate screw-top teflon beakers. Then the capped beakers are heated at 160 ^oC on a hotplate in a laminar flow exhaust hood (for 1-3 days). After total dissolution, they are evaporated to dryness. Second, samples are dissolved in HCl - HNO_3 (~3:1, v/v) at the same temperature and evaporated to dryness. Third, samples are dissolved in HNO_3 and evaporated to dryness. Finally, sample solutions are dissolved in 1 N HNO_3 in preparation for column chemistry. Chemical separation of Mg is achieved using Bio-Rad AG50W-X8 resin (200-400 mesh). The resins were pre-cleaned with 6M HCl and 18.2 MΩ Milli-Q® water. Sample solutions in 1 N HNO_3 are loaded to the columns and eluted with 1 N HNO_3. The same column chemistry is then repeated to get purified solutions. A "Wet" introduction system equipped with a quartz cyclonic spray chamber and a MicroMist micro-uptake glass concentric nebulizer, was used for the analysis of purified Mg solution (~300 ppb Mg in ~0.45 N HNO_3). Purified Mg

solutions were analyzed by the standard bracketing method. Analyses were performed in low resolution mode, with simultaneous measurements of ^{26}Mg, ^{25}Mg and ^{24}Mg in separate Faraday cups (H5, Ax and L4). The background Mg signals for ^{24}Mg ($<10^{-4}$ V) are negligible compared to the typical sample signals (2-4 V). Standard bracketing, using DSM3 (solution of pure Mg metal, Galy et al. (2003)), is performed for all analyses. The Mg isotopic composition is reported as $\delta^{26}Mg$, where $\delta^{26}Mg_{sample} = [(^{26}Mg/^{24}Mg)_{sample}/(^{26}Mg/^{24}Mg)_{DSM3}-1]\times1000$. The external precision, based on 2σ of duplicate runs of pure Mg standard solutions, is $\leq \pm 0.07‰$ (Teng et al., 2010b). For example, KH olivine, which was run during the course of these analyses (May, 2011 – June, 2011) gives $\delta^{26}Mg = -0.27 \pm 0.04‰$ (2 σ, n = 8) comparable to values reported in the literature (e.g., Teng et al., 2010b); and seawater gives $\delta^{26}Mg = -0.86 \pm 0.07‰$ (2 σ, n = 8), which agrees with seawater value of $\delta^{26}Mg = -0.83 \pm 0.09‰$ (2 σ, n = 40) (e.g., Ling et al., 2011). In addition, two USGS standards were analyzed (see Table A.3), with BHVO-1 yielding $\delta^{26}Mg$ of $-0.24 \pm 0.04‰$ (2 σ, n=2), and G-2 yielding $\delta^{26}Mg = -0.12 \pm 0.03‰$ (2 σ, n=3). These values are comparable to those reported in Huang et al. (2009).

There is a linear correlation between $\delta^{26}Mg$ and $\delta^{25}Mg$ for all analyses. The slope of the liner correlation is 0.509 (Figure A.1), therefore no mass independent Mg isotope fractionation is observed and we discuss Mg isotopic composition in terms of $\delta^{26}Mg$ values.

3. Sample selection and results

The samples studied here are the same as those in a companion Li isotope study (Li et al., 2010). The samples include: 1) fresh parental basalts from two

different flows of the Columbia River Basalts: the Pomona Member of the Saddle Mountains Basalt and the Sentinel Bluffs Member of the Grande Ronde Basalt; 2) two ~10 m drill cores through bauxites developed on the two different flows; 3) two samples of recent eolian deposits (Portland Hills Silt and Palouse Formation), which have compositions similar to the dust that may have been added to the weathering profiles.

The MgO concentration ([MgO]) and δ^{26}Mg in fresh basalts, drill core bauxites and eolian deposits are reported in Table 5. The δ^{26}Mg values in both parental basalts are relatively homogeneous (-0.24 ± 0.08, n = 17, 2 σ, and -0.22 ± 0.10, n = 10, 2 σ, for Pomona and Sentinel Bluffs basalts, respectively), and fall within the δ^{26}Mg range of the mantle (-0.25 ± 0.07, 2 σ, n=139) (Teng et al., 2010b).

To quantify relative mass loss or addition during chemical weathering, Mg concentration is normalized to Nb, a presumed immobile element (Kurtz et al., 2000). Mg/Nb versus depth in these two profiles reflects extreme depletion of Mg relative to fresh basalts (> 99% Mg loss, Figures 8a and 8b). δ^{26}Mg values in bauxites are systematically heavier than their corresponding parental basalts, reaching values that are up to 2.0‰ heavier than those of fresh Pomona basalt (Figure 8c), and 0.7‰ heavier than those of fresh Sentinel Bluffs basalt (Figure 8d), as sampled in the Cowlitz and Columbia profiles, respectively. Both eolian samples have lower [MgO] compared to the fresh CRBs: [MgO] = 1.4 and 1.8 wt. % for Portland Hills Silt and

Table 5. Mg, Li and Nd concentrations and isotopic compositions in bauxites, parents, and eolian deposits.

Sample #	Depth (m)	MgO (wt. %)	[Mg] (ppm)	Mg/Nb	δ^{26}Mg	δ^{25}Mg	[Li] (ppm)	Li/Nb	δ^{7}Li	Sm (ppm)	Nd (ppm)	^{143}Nd/^{144}Nd	ε_{Nd}
Cowlitz													
9/3-1	2.13	0.19	1140	18	0.16	0.08	21.7	0.35	-1.9	7.3	6.3	0.512121	-10.1
9/3-2	2.44	0.18	1080	12	0.22	0.08	14.5	0.16	-3.4	-	6.4	0.512004	-12.4
9/3-3	2.74	0.15	900	18	0.20	0.07	8.7	0.18	-2.6	-	5.1	0.512149	-9.5
9/3-3*					0.15	0.09							
9/3-5	3.35	0.14	840	27	1.15	0.56	1.9	0.06	-2.4	0.4	1.3	0.512492	-2.8
9/3-5*					0.90	0.45							
9/3-9	4.88	0.15	900	31	1.52	0.72	0.7	0.02	-1.2	0.3	1.1	0.512482	-3.0
9/3-9**					1.48	0.74							
9/3-10(2)	5.79	0.15	900	22	0.60	0.28	0.4	0.01	-0.8	4.0	11.6	0.512420	-4.3
9/3-19	6.25	0.15	900	26	1.26	0.65	0.8	0.02	-1.1	2.1	12.0	0.512366	-5.3
9/3-21	7.62	0.15	900	25	1.72	0.85	1.2	0.03	-0.6	-	14.2	0.512396	-4.7
9/3-21**					1.81	0.92							
9/3-22	8.23	0.16	960	27	1.28	0.68	1.5	0.04	-1.7	9.1	31.2	0.512392	-4.8
9/3-22*					1.37	0.73							
9/3-23	9.14	0.16	960	29	1.55	0.81	1.8	0.05	-3.2	-	18.29	0.512397	-4.7
9/3-23*					1.60	0.83							
Pomona basalts													
WC-6(2)		6.10	36600	3450	-0.33	-0.16	4.5	0.42	0.2				
WC-7		6.37	38220	3710	-0.27	-0.12	3.3	0.32	-0.5				
WC-8		6.76	40560	3980	-0.25	-0.14	5.2	0.51	-0.9				
WC-9		6.02	36120	3110	-0.24	-0.12	9.2	0.79	-1.2				
WC-10		6.35	38100	3590	-0.29	-0.13	3.7	0.35	1.4				
WC-12		6.36	38160	3630	-0.27	-0.14	5.6	0.53	-0.1				
WC-13		6.50	39000	4060	-0.28	-0.13	6.1	0.64	0.6				
WC-14		5.62	33720	3270	-0.25	-0.14	5.1	0.49	0.8				
WC-15		6.53	39180	3840	-0.26	-0.14	5.1	0.50	-0.1				
WC-16		6.89	41340	3720	-0.25	-0.12	5.6	0.50	1.1				
WC-17		6.57	39420	3900	-0.21	-0.08	5.7	0.56	1.7				
WC-18		6.63	39780	4020	-0.20	-0.09	5.2	0.53	1.9				
WC-19		6.47	38820	3840	-0.24	-0.12	2.8	0.27	1.5				
WC-20		6.50	39000	4020	-0.22	-0.12	3.8	0.39	1.8				
WC-21		6.54	39240	3600	-0.21	-0.09	7.0	0.64	0.8				
WC-22		6.59	39540	3560	-0.16	-0.09	6.2	0.56	-0.6				
Pomona-1(2)		6.74	40440	4490	-0.19	-0.11	6.0	0.67	0.9	4.8	20.1	0.512426	-4.1
average		*6.44*			*-0.24*								
1σ stdev		*0.30*			*0.04*								

Note: (#) number of mass spectrometry analyses; values are average of individual runs; * repeat column chemistry for the same sample solution; and ** redissolved and run through column chemistry from the same sample powder. The external precision, based on 2σ of duplicate runs of pure Mg standard solutions, is ≤ ± 0.07‰ (Teng et al., 2010b). Li and Nd date are previously reported in Liu et al. (2010).

Table 5, continued. Mg, Li and Nd concentrations and isotopic compositions in bauxites, parents, and eolian deposits.

Sample #	Depth (m)	MgO (wt. %)	[Mg] (ppm)	Mg/Nb	δ^{26}Mg	δ^{25}Mg	[Li] (ppm)	Li/Nb	δ^{7}Li	Sm (ppm)	Nd (ppm)	^{143}Nd/^{144}Nd	ε_{Nd}
Columbia													
5/1-4	2.74	0.25	1500	26	-0.12	-0.07	35.4	0.61	-3.7	2.4	13.7	0.511884	-14.7
5/1-6	3.96	0.21	1260	23	0.08	0.04	23.0	0.41	-4.7	2.3	12.5	0.512040	-11.7
5/1-8	4.57	0.19	1140	14	0.30	0.17	19.0	0.23	-3.3	1.7	10.1	0.512121	-10.1
5/1-10	5.49	0.12	720	5	0.51	0.25	2.7	0.02	-2.2	0.9	3.5	0.512466	-3.4
5/1-12	6.71	0.12	720	9	0.31	0.14	4.3	0.05	-2.4	7.4	2.9	0.512742	2.0
5/1-14[(2)]	7.32	0.20	1200	22	0.21	0.09	2.4	0.04	-1.8	5.4	1.6	0.512599	-0.8
5/1-15	7.92	0.20	1200	27	0.41	0.21	6.5	0.15	0.0	0.7	2.5	0.512603	-0.7
Sentinel Bluffs basalts													
SB-1		4.91	29460	3510	-0.21	-0.12	8.0	0.95	-0.8	5.3	21.8	0.512618	-0.4
SB-2		4.66	27960	2540	-0.21	-0.10	9.3	0.85	2.8				
2170		4.90	29400	2850	-0.30	-0.15	13.3	1.29	2.5				
2242		5.17	31020	2520	-0.16	-0.09	8.7	0.70	5.5				
2256.5		4.97	29850	2740	-0.26	-0.12	10.1	0.93	-0.9				
2340		4.38	26290	2070	-0.30	-0.13	15.7	1.24	2.0				
2370		4.90	29410	2260	-0.19	-0.10	22.6	1.74	1.4				
2380		4.85	29100	2450	-0.19	-0.06	6.6	0.55	2.2				
2430		5.21	31280	2480	-0.15	-0.06	15.3	1.22	1.5	5.3	21.9	0.512660	0.4
2450		4.99	29960	2540	-0.19	-0.09	9.7	0.82	1.1				
average		*4.90*			*-0.22*								
1σ stdev		*0.24*			*0.05*								
Eolian dust													
PHS-1		1.39	8340	540	-0.24	-0.13	18.7	0.49	-1.6	5.6	28.2	0.512237	-7.8
Palous-1		1.77	10620	640	-0.09	-0.03	23.4	0.65	1.6	6.0	32.1	0.512118	-10.1

Note: (#) number of mass spectrometry analyses; values are average of individual runs; * repeat column chemistry for the same sample solution; and ** redissolved and run through column chemistry from the same sample powder. The external precision, based on 2σ of duplicate runs of pure Mg standard solutions, is ≤ ± 0.07‰ (Teng et al., 2010b). Li and Nd date are previously reported in Liu et al. (2010).

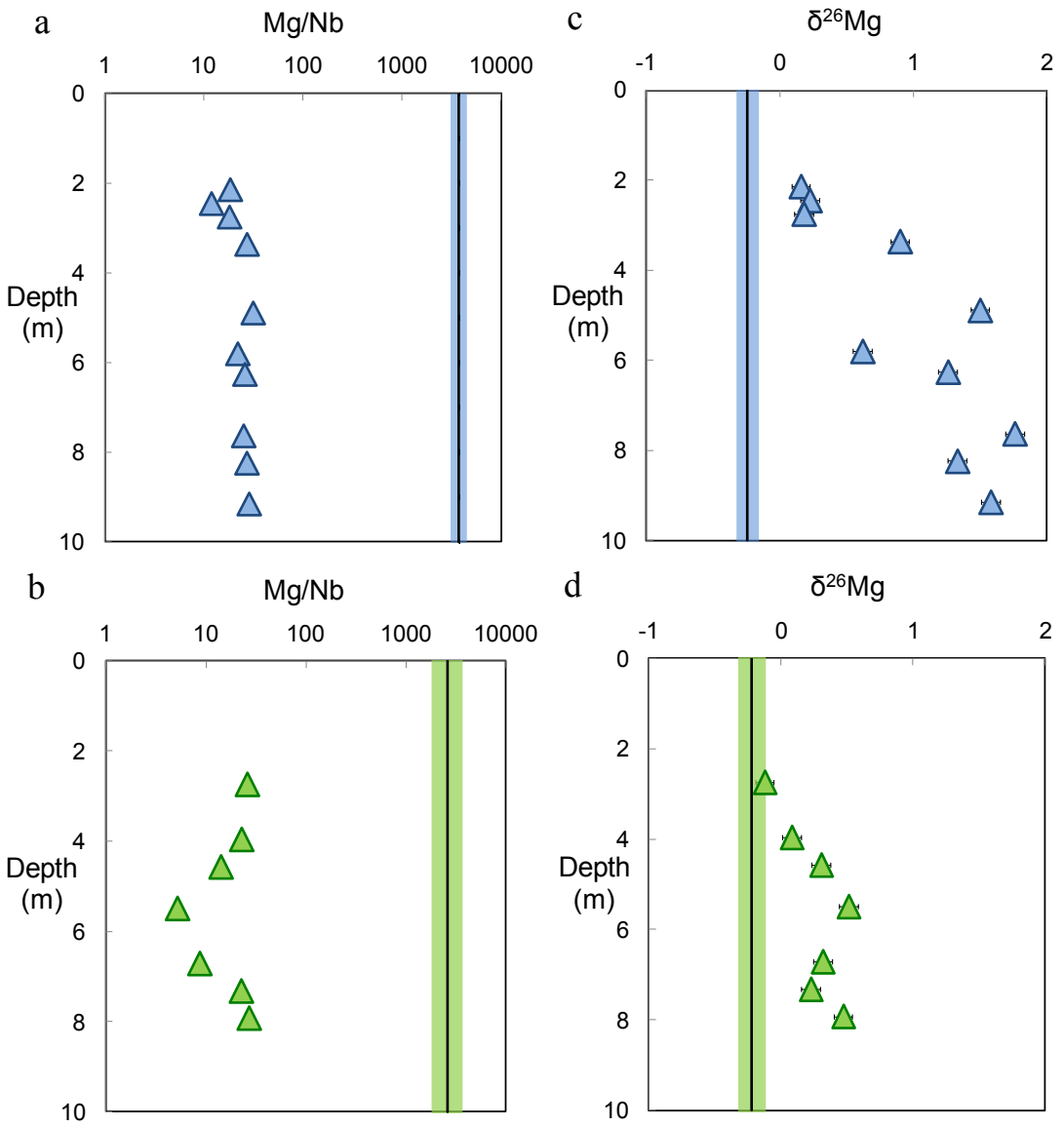

Figure 8. Mg isotopes vs. depth plots.
a. Mg/Nb (log scale) vs. depth for Cowlitz drill cores through bauxites developed on the Pomona basalt flow. b. Mg/Nb (log scale) vs. depth for both Columbia drill cores. c. δ^{26}Mg vs. depth for Cowlitz drill cores. d. δ^{26}Mg vs. depth for Columbia drill cores through bauxites developed on the Sentinel Bluffs basalt flow. Bauxites are shown as symbols and average fresh basalt compositions are shown in black lines; rectangular fields indicate 2σ of the average values. Error bars represent 2σ and errors for Mg/Nb are smaller than symbols. Data are reported in Table 5.

Palouse Formation, respectively (Table 5). The δ^{26}Mg of the Portland Hills Silt (-0.24) overlaps those of the fresh CRBs, while the δ^{26}Mg of the Palouse Formation dust (-0.09) is isotopically heavier than the basalts.

4. Discussion

Beyond the extreme depletion of [Mg] and significant fractionation of Mg isotopes in the bauxites, their most striking feature lies in the δ^{26}Mg vs. depth plots in both drill cores, where δ^{26}Mg values systematically decrease towards the tops of the profiles. These trends are opposite to the Mg isotope fractionation expected due to greater leaching at the surface. Here, we evaluate the possible mechanisms that may be responsible for the Mg isotopic fractionation.

The δ^{26}Mg values in the bauxites display the opposite trend to what is expected via Rayleigh fractionation during leaching and what was observed by Teng et al. (2010a) (see Figures 8c and 8d). This is likely due to the deposition of eolian dust at the tops of both drill cores. The abundance of the dust can be determined based on the percentage of quartz (which is not found in fresh basalt) and the nature of the Nd isotopic profiles (less radiogenic near the tops of profiles compared to lower parts) (Liu et al. 2012, Chapter 2). The slight increase in [Mg] in the Columbia profile and the decrease in δ^{26}Mg with increasing quartz contents in both profiles suggest that eolian components introduced isotopically light Mg, having a Mg isotopic composition that is close to that observed in fresh basalts to the tops of the profiles. However, the fact that [Mg] at the tops of the profiles is still strongly depleted compared to [Mg] in the analyzed possible eolian deposits indicates that

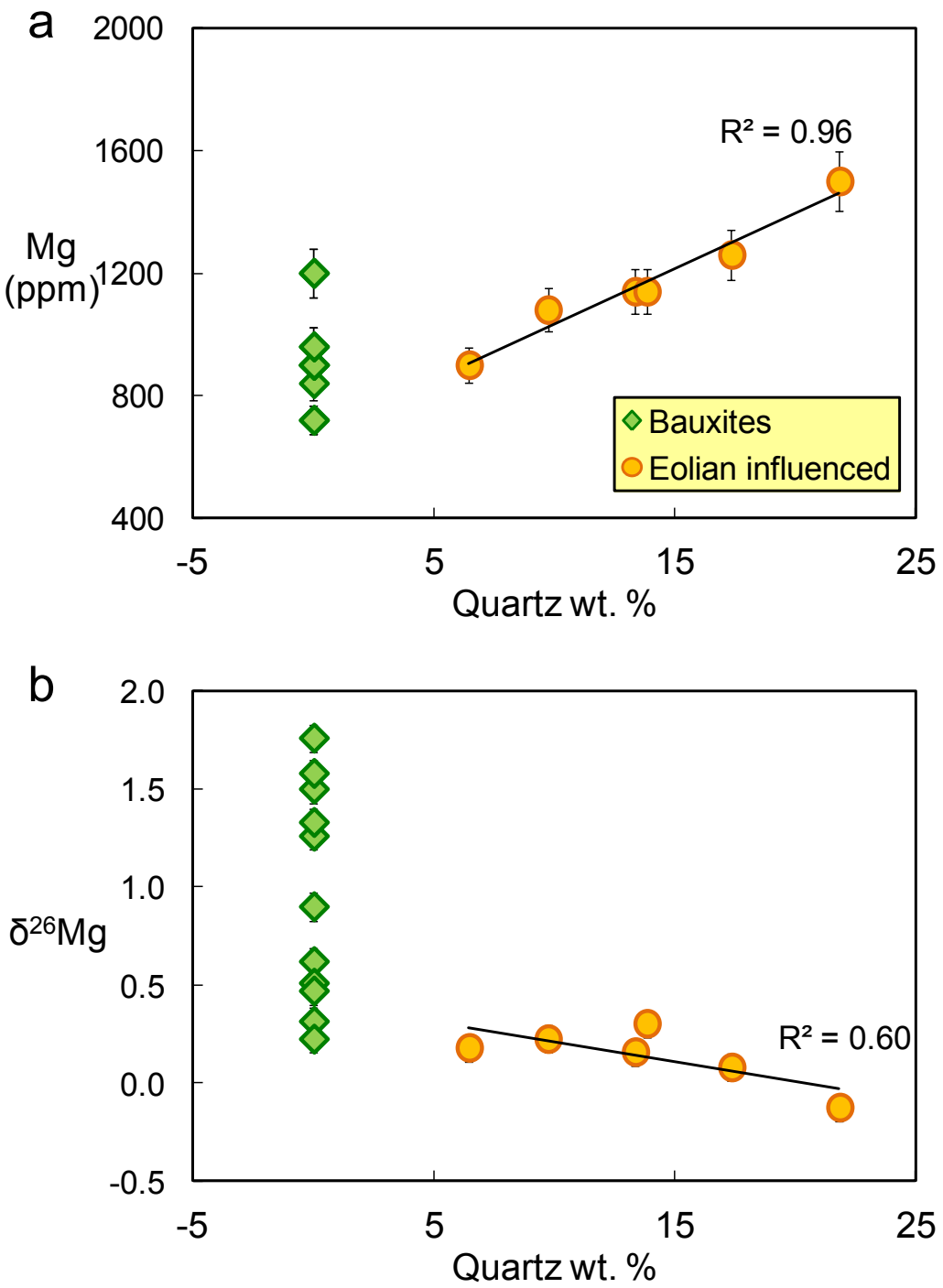

Figure 9. Variation of Mg and δ^{26}Mg in bauxites as a function of eolian component. Data shown in yellow contain quartz and are influenced by dust addition. a. [Mg] vs. wt.% quartz. b. δ^{26}Mg vs. wt. % quartz. 2σ errors are shown on [Mg] and δ^{26}Mg, which are better than 6.5% and ±0.07, respectively. 2σ errors of δ^{26}Mg data are about the size the symbols. Quartz wt. % data are from Liu et al. (2012), and is also provided in the appendix (Table A.1).

significant chemical weathering likely occurred during or after eolian deposition (Figures 9a and 9b). If eolian influenced samples for each profile are excluded (the top three samples in each profile that contain quartz), there is no systematic trend in δ^{26}Mg vs. depth plots (Figures 8c and 8d).

Two different processes associated with primary mineral dissolution have been recognized to cause fractionation of Mg isotopes: fractionation during dissolution and preferential dissolution of isotopically distinct phases. In an experimental study of olivine dissolution, Wimpenny et al. (2010) showed that light Mg isotopes are preferentially released to the solution, and later-formed secondary minerals, such as chrysotile, preferentially incorporate the light Mg isotopes, resulting in an isotopically heavy solution. Another experimental study suggests that preferential dissolution of low δ^{26}Mg minerals, such as chlorite, can lead to isotopically light Mg in solution (Ryu et al., 2011). Nonetheless, Mg isotope fractionation associated with primary mineral dissolution is not likely to be responsible for the Mg isotopic behavior observed in this study, because the bauxites are composed entirely of secondary minerals.

Major and trace cations (Li, Na, K, Mg, Ca, Fe, Cu, *etc.*) may sorb to the surfaces (adsorption) or enter into the structures (absorption) of secondary minerals, such as clays and Al- or Fe- hydroxides/oxides (e.g., Gomes et al., 2001; Kinniburgh et al., 1976; Ma and Eggleton, 1999; Sawhney, 1972; Srivastava et al., 2005; Velde, 1995; Zhong et al., 2010). Hereafter, we use the general word "sorption" to encompass both mechanisms. Investigations of many divalent metal isotopes have documented isotopic fractionation via sorption on clays or Al- or Fe-

hydroxides/oxides in both experimental and natural environments. Balistrieri et al. (2008) experimentally documented Cu and Zn isotope fractionation ($\Delta^{65}Cu_{sorbed\text{-}aqueous}$ = 0.52 and $\Delta^{66}Zn_{sorbed\text{-}aqueous}$ = 0.73) due to adsorption onto amorphous Fe oxyhydroxide. Pokrovsky et al. (2008) also observed enrichment of heavy isotopes of Cu, with $\Delta^{65}Cu_{sorbed\text{-}aqueous}$ around 1.0 and 0.78 on gibbsite and goethite surfaces, respectively. Like Cu and Zn isotopes, Mikutta et al. (2009) demonstrate that sorption of Fe^{2+} to mineral surfaces, such as goethite and quartz, causes significant Fe isotope fractionation ($\Delta^{56}Fe_{sorbed\text{-}aqueous}$ ranging from 0.73 to 0.85). The magnitudes of isotopic fractionation are dependent on the mineral species involved, as well as the experimental conditions, such as pH and metal concentrations in solution. For example, Balistrieri et al. (2008) reported a $\Delta^{66}Zn_{sorbed\text{-}aqueous}$ value of +0.52 for Zn sorbed on amorphous ferrihydrite in a laboratory study, whereas Juillot et al. (2008) found $\Delta^{66}Zn_{sorbed\text{-}aqueous}$ around +0.29 and +0.53 for goethite and ferrihydrite, respectively. Moreover, Pokrovsky et al. (2005) found $\Delta^{66}Zn_{sorbed\text{-}aqueous}$ ranging from +0.02 (5.8<pH<6.7) to +0.61 (pH = 5.5) for Zn sorption on hematite. Unfortunately, no experimental studies on Mg isotope fractionation related to sorption on clays or Al- or Fe- hydroxides/oxides yet exist.

We investigate the possible mineralogical control on $\delta^{26}Mg$ in these bauxites by plotting $\delta^{26}Mg$ against mineral modes, derived from XRD. A recent study by Huang et al. (2012) showed that $\delta^{26}Mg$ is controlled by the abundance of kaolin minerals in a saprolite profile on weathered basalts. They found a positive correlation between $\delta^{26}Mg$ and the abundance of kaolin minerals in the bottom section of their profile, which they attributed to adsorption of heavy Mg. By contrast, $\delta^{26}Mg$ values in

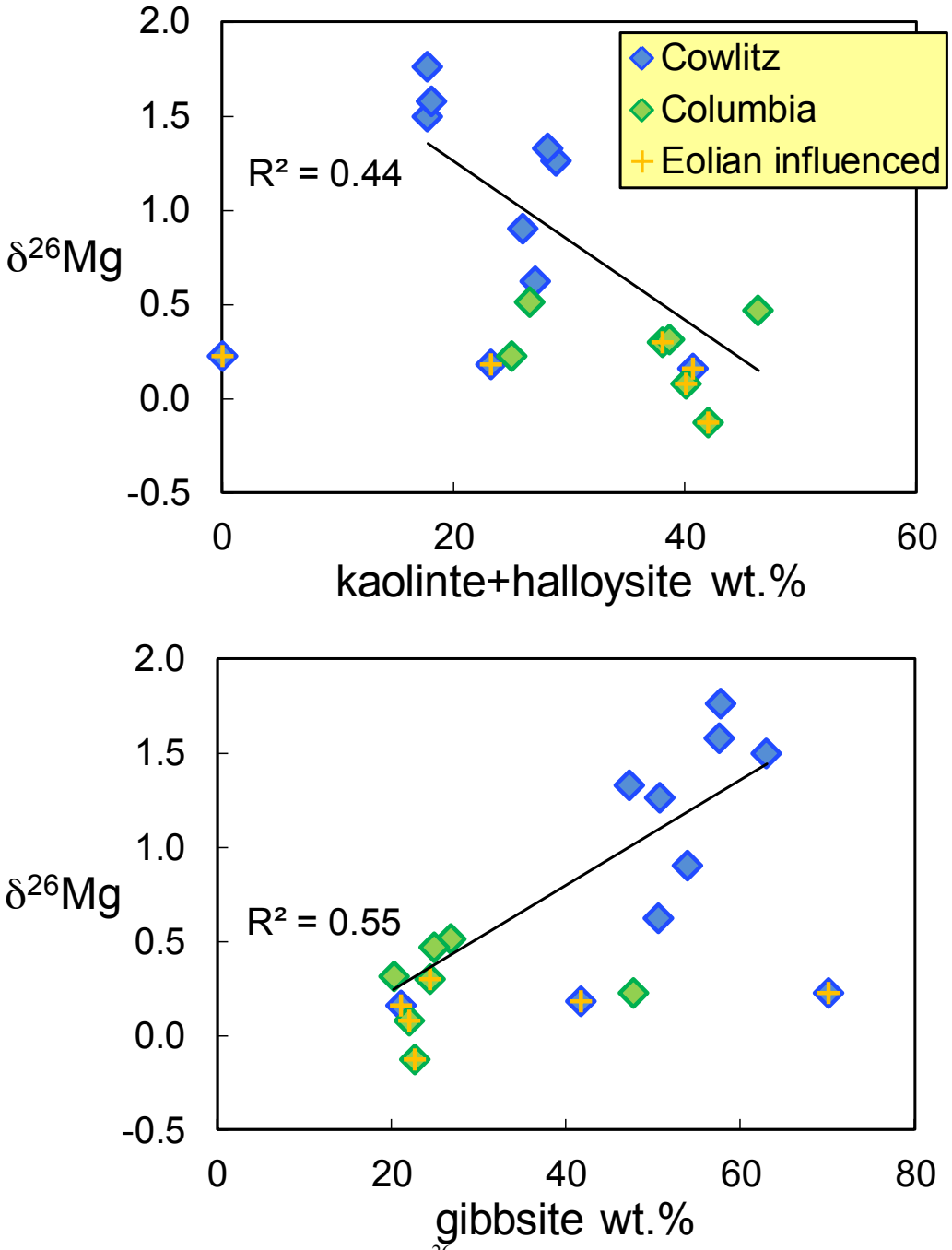

Figure 10. Mineralogical control of $\delta^{26}Mg$ in bauxites.
a. $\delta^{26}Mg$ vs. wt.% kaolinite & halloysite in bauxites. b. $\delta^{26}Mg$ vs. wt. % gibbsite in bauxites. Bauxites influenced by eolian addition are shown in yellow cross. R^2 is calculated based on bauxites with no eolian component. 2σ errors of $\delta^{26}Mg$ data are about the size the symbols. Mineral percentage data were determined by XRD (Liu et al., 2012), and are provided in the appendix (Table A.1).

the bauxites investigated here do not correlate with clay minerals such as kaolinite and halloysite (Figure 10a), but positively correlate with gibbsite content (Figure 10b), indicating that gibbsite may preferentially sorb the heavy Mg isotopes and cause extreme magnesium isotope fractionation (δ^{26}Mg up to +1.8, the highest δ^{26}Mg yet reported). The negative correlation between δ^{26}Mg and clays (kaolinite plus halloysite) is expected as a consequence of dilution of gibbsite. Therefore, preferential sorption of the heavy Mg isotopes onto gibbsite is probably responsible for the massive Mg isotopic fractionation observed during intense chemical weathering of the CRBs.

5. Implications for continental weathering

All bauxite samples studied here have heavier Mg isotopic composition compared to their parental material (CRBs). This result is consistent with the majority of previous investigations of continental materials, as well as rivers, where chemical weathering of silicate rocks produces a high δ^{26}Mg regolith in the upper continental crust and low δ^{26}Mg in rivers (e.g., Brenot et al., 2008; Gomes et al., 2001; Huang et al., 2012; Opfergelt et al., 2012; Shen et al., 2009; Teng et al., 2010a; Tipper et al., 2006a; 2006b; Wimpenny et al., 2011). Moreover, because the degree of weathering in this study is more intense compared to most previous studies, the Mg isotope fractionation is the largest observed (δ^{26}Mg is up to +1.8). Regolith generated by high degrees of chemical weathering could serve as an end member with extreme δ^{26}Mg that helps to produce the large variations of Mg isotopic compositions observed in the upper continental crust (Gomes et al., 2001).

This study has implications for understanding Mg isotopic behavior in weathering and the use of Mg isotopes as tracers of chemical weathering: the formation of different secondary minerals greatly influences the behavior of Mg isotopes, especially under intense weathering conditions, where Al- or Fe-hydroxides/oxides dominate over clay minerals in soils. Formation of gibbsite, in particular, seems to the produce significant Mg isotope fractionation, as bauxites with more than 50% of gibbsite show the heaviest Mg isotopes. Better quantification of Mg isotopic fractionation factors in single mineral species, such as gibbsite, could make Mg isotopes useful tracers of chemical weathering intensity.

6. Conclusions

The main conclusions from this study are:

1. Extreme Mg depletion (> 99%) and Mg isotopic fractionation (δ^{26}Mg up to 1.8‰) are observed in bauxites developed on CRBs due to intense chemical weathering of basalts. Both Mg concentrations and δ^{26}Mg values are distinct from those in fresh basalts (CRBs), whose isotopic signatures are similar to that of the mantle.

2. δ^{26}Mg correlates with the abundance of gibbsite, with the isotopically heaviest samples having the greatest gibbsite abundance, demonstrating that Mg partitioning between water and gibbsite leads to large isotopic fractionation.

3. Addition of eolian dust is marked by the presence of quartz, less radiogenic Nd, a very slight increase in MgO and lighter Mg isotopic compositions in the upper three to five meters compared to deeper bauxites of the profiles.

4. Mg isotopes have the potential to be useful in tracing continental chemical weathering, especially for extreme weathering conditions, where strong depletion of elements occurs.

Appendices

Table A.1. Mineral phases in bauxites.

Sample #	Gibbsite	Halloysite	Kaolinite	Hematite	Goethite	Maghemite	Quartz
Cowlitz County							
9/3-1	21	25	15	6	11	8	13
9/3-2	70	-	-	13	-	7	10
9/3-3	42	23	-	14	15	-	6
9/3-5	54	26	-	7	7	4	-
9/3-9	63	-	18	6	5	7	-
9/3-10	51	27	-	11	-	10	-
9/3-19	51	29	-	6	7	5	-
9/3-21	58	18	-	7	6	8	-
9/3-22	47	28	-	5	7	8	-
9/3-23	58	18	-	11	9	-	-
Columbia County							
5/1-4	23	16	26	6	7	-	22
5/1-6	22	15	25	10	10	-	17
5/1-8	24	15	23	24	0	-	14
5/1-10	27	27	-	19	24	-	-
5/1-12	20	17	21	17	20	-	-
5/1-14	48	25	-	8	9	8	-
5/1-15	25	16	30	7	6	8	-

Notes: Mineral abundances are shown in percentage (%), which is calculated from combined XRD spectrum and major element analyses. - indicate the mineral phase is not detected.

Table A.2. Evaluation of analytical precision in typical bauxite via multiple XRF analyses.

	O	#1	#2	#3	#4	#5	mean	2σ	% error
SiO2	33.95	34.04	34.18	34.09	34.24	34.05	34.09	0.21	0.6
TiO2	4.61	4.65	4.61	4.62	4.62	4.59	4.62	0.04	0.9
Al2O3	29.18	29.03	28.93	28.77	28.98	28.85	28.96	0.29	1.0
Fe2O3T	29.84	29.86	29.76	29.67	29.79	29.83	29.79	0.14	0.5
MnO	0.950	0.981	0.976	0.945	0.986	0.944	0.96	0.04	4.0
MgO	0.143	0.157	0.155	0.152	0.152	0.155	0.15	0.01	6.5
CaO	0.098	0.090	0.088	0.089	0.087	0.088	0.09	0.01	9.0
Na2O	0.061	0.074	0.072	0.071	0.071	0.069	0.07	0.01	13.1
K2O	0.018	0.020	0.028	0.019	0.018	0.018	0.02	0.01	38.9
P2O5	0.437	0.437	0.441	0.435	0.437	0.436	0.44	0.00	0.9
Total	99.310	99.339	99.240	98.861	99.381	99.030	99.19	0.41	0.4
LOI	18.57	18.47	18.60	18.29	18.30	18.39	18.44	0.27	1.44
Rb	4.6	4.4	4.8	4.0	4.1		4.4	0.7	15.3
Sr	38	37	38	37	38	37	38	1.1	2.9
Y	4.8	4.8	4.0	4.9	4.8		4.7	0.7	15.9
Zr	289	290	287	285	288	289	288	3.6	1.2
V	645	645	640	644	652	668	649	20.2	3.1
Ni	46	45	45	45	45		45	0.9	2.0
Cr	40	41	44	37	39	40	40	4.6	11.5
Nb	24.9	23.9	25.3	23.8	24.5		24.5	1.3	5.2
Ga	29.7	29.1	29.0	29.1	29.4		29.3	0.6	2.0
Cu	102	91	91	93	91		94	9.5	10.2
Zn	159	158	158	157	158		158	1.4	0.9
Co	67	66	68	65	65		66	2.6	3.9
Ba	404	408	404	400	389		401	14.6	3.6
La	4	2	3	2	2		3	1.8	68.8
Ce	17	17	18	18	18		18	1.1	6.2
U	<0.5	<0.5	<0.5	0.8	<0.5		<0.5	-	-
Th	38.2	36.4	38.4	43.4	35.3		38.3	6.2	16.2
Sc	53	54	56	56	57		55	3.3	6.0
Pb	10	8	9	15	12		11	5.5	51.4

Notes: 1.O indicates the original measurement and # indicates the number of replicates. 2. Units of all the major elements and LOI are in wt % and all trace elements are reported in ppm.

Table A.3. Magnesium isotopic measurements of standard reference materials analyzed during the course of this study, compared to literature data.

Standard Name	n	δ^{26}Mg	2σ	δ^{25}Mg	2σ	Reference
Seawater		-0.87	0.09	-0.45	0.06	
		-0.83	0.07	-0.42	0.04	
		-0.92	0.06	-0.47	0.03	
		-0.87	0.07	-0.46	0.06	
		-0.84	0.07	-0.45	0.05	
		-0.88	0.09	-0.42	0.07	
		-0.83	0.07	-0.43	0.06	
		-0.88	0.07	-0.44	0.06	
Average	**8**	**-0.86**	**0.07**	**-0.44**	**0.04**	**this study**
	90	-0.83	0.09	-0.43	0.06	Ling et al. (2011)
	20	-0.79	0.18	-	-	Higgins and Schrag (2010)
	5	-0.86	0.02	-0.45	0.02	Li et al. (2010)
	4	-0.83	0.06	-0.43	0.03	Teng et al. (2010)
	10	-0.80	0.05	-0.42	0.02	Hippler et al. (2009)
	14	-0.89	0.10	-0.47	0.08	Bolou-Bi et al. (2009)
	4	-0.83	0.07	-0.42	0.05	Yang et al. (2009)
	1	-0.84	0.13	-0.43	0.15	Tipper et al. (2006)
	4	-0.84	0.06	-0.42	0.02	Young and Galy (2004)
	4	-0.82	0.08	-0.42	0.09	Chang et al. (2003)
KH olivine		-0.26	0.07	-0.14	0.06	
		-0.28	0.07	-0.16	0.05	
		-0.28	0.08	-0.16	0.06	
		-0.29	0.06	-0.19	0.05	
		-0.28	0.08	-0.16	0.05	
		-0.27	0.07	-0.11	0.05	
		-0.27	0.07	-0.14	0.05	
		-0.22	0.07	-0.14	0.07	
Average	**8**	**-0.27**	**0.04**	**-0.15**	**0.05**	**this study**
	7	-0.31	0.06	-0.16	0.05	Li et al. (2010)
	1	-0.27	0.04	-0.12	0.05	Liu et al. (2010)
	16	-0.27	0.07	-0.14	0.04	Teng et al. (2010)
	24	-0.31	0.09	-0.14	0.08	Teng et al. (2007)
BHVO-1		-0.22	0.14	-0.11	0.08	this study
BHVO-1		-0.25	0.06	-0.13	0.04	this study
Average	**2**	**-0.24**	**0.04**	**-0.12**	**0.04**	**this study**
BHVO-1	8	-0.30	0.08	-0.14	0.04	Huang et al. 2009
G-2		-0.13	0.08	-0.05	0.06	this study
G-2		-0.10	0.07	-0.05	0.06	this study
G-2		-0.13	0.06	-0.10	0.04	this study
Average	**3**	**-0.12**	**0.03**	**-0.07**	**0.05**	**this study**
G-2	16	-0.22	0.25	-0.07	0.14	Huang et al. 2009

Notes: n indicates number of analyses; 2σ represents two standard deviation of population analyzed.

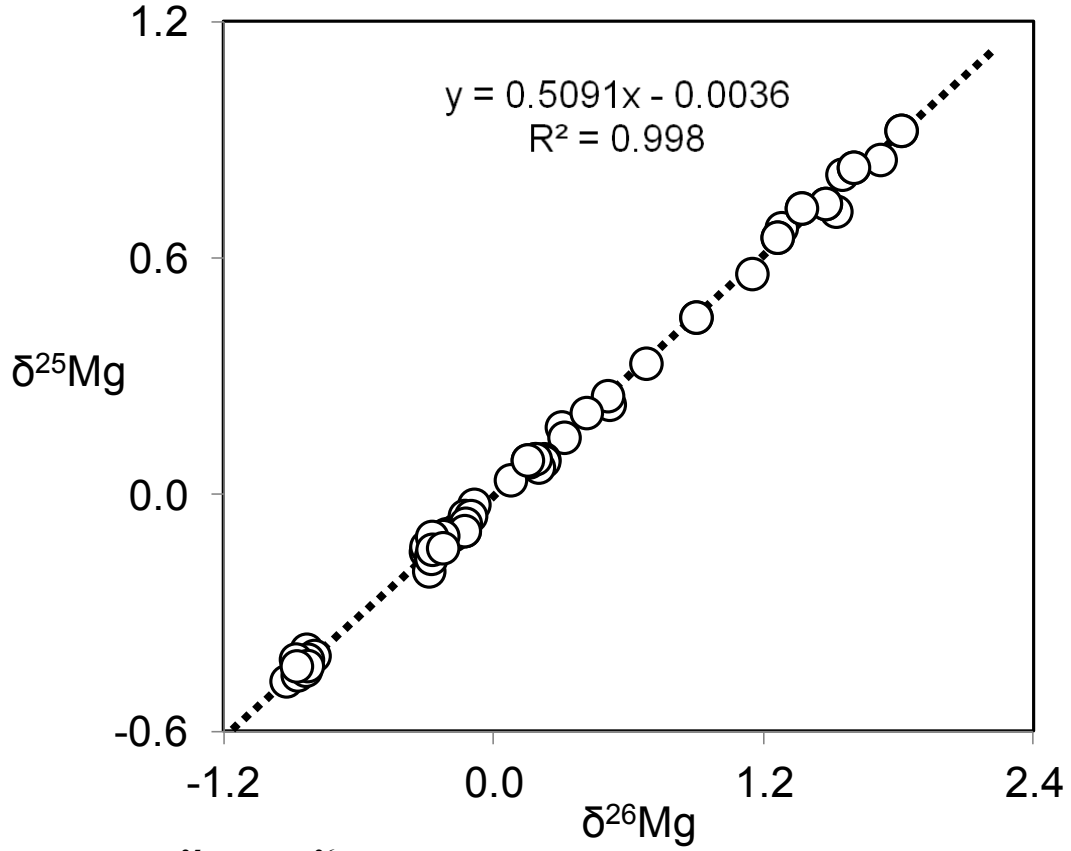

Figure A. 1. $\delta^{25}Mg$ vs. $\delta^{26}Mg$ plot of all samples and standards analyzed in the course of this study are displayed here. Dotted line indicates the liner correlation between $\delta^{25}Mg$ and $\delta^{26}Mg$.

Chapter 4: Li isotopes as chemical weathering intensity tracers in streams and ground waters draining basalts

Abstract

We analyzed Li and its isotopes in streams draining only a single lithology, the Columbia River Basalts (CRBs), and groundwaters within CRB reservoirs in varied climate zones in order to determine the degree to which climate influences weathering and to understand how Li isotopes behave during basalt weathering. In addition, we sampled streams during two different seasons (summer and late winter) to evaluate how Li isotopic composition may change through the seasons. The dissolved δ^7Li in the streams is uniformly higher than that of the basalts, but varies greatly between streams (by up to 20‰). The δ^7Li of suspended loads varies from (-6 to +4) and are lighter compared to that of the dissolved load. We find that δ^7Li and Li/Na are potentially sensitive tracers of chemical weathering intensity, which may have global significance. Moreover, chemical weathering intensity, marked by dissolved δ^7Li and Li/Na, correlates neither with climate nor distance to the coast. We confirmed that secondary minerals control Li isotopic fractionation in streams. In addition, the low δ^7Li in streams corresponds to high chemical weathering intensity of the stream catchments.

1. Introduction

Chemical weathering of silicate rocks on Earth's surface plays a critical role in regulating global carbon cycle over geological time-scales (e.g., Berner et al., 1983). Attempts to illuminate chemical weathering processes using natural samples

generally take two approaches: studies of river waters (e.g., Dessert et al., 2001; Gaillardet et al., 1999) and studies of weathering profiles or weathered regoliths (e.g., Liu et al., 2012; Nesbitt and Wilson, 1992). River chemistry is able to provide rate-related constraints, such as chemical weathering fluxes and CO_2 consumption rates (Gaillardet et al., 1999), although only for the present. As Li is contained mainly in silicates and is released, with attendant isotopic fractionation, during weathering, it has the potential to serve as an excellent proxy for silicate weathering of the continents over time (e.g., Misra and Froelich, 2012). But what causes isotopic fractionation and how variable will it be in waters draining a single lithology as a function of climate, season, topography and chemical weathering intensity? These are some of the questions we seek to address here.

2. Lithium isotopes and weathering

Lithium has two stable isotopes, ^{7}Li and ^{6}Li, with abundances of approximately 92.41% and 7.59%, respectively (Coplen et al., 2002). Thus, lithium isotopes have great mass-dependent fractionation potential due to 17% mass difference between two isotopes. The Li isotopic composition in samples is expressed as $\delta^{7}Li\ (‰) = ([^{7}Li/^{6}Li]_{sample}/ [^{7}Li/^{6}Li]_{standard}-1)\times 1000$, where the standard used is a lithium carbonate, L-SVEC (Flesch et al., 1973).

Lithium is a water-soluble trace element, but neither primary basalt dissolution nor metamorphic dehydration appear to cause Li isotopic fractionation (Marschall et al., 2007; Pistiner and Henderson, 2003; Qiu et al., 2011a; 2011b; 2009; Teng et al., 2007a; Wimpenny et al., 2010a). However, Li isotopes have been shown to fractionate significantly during incongruent continental weathering, associated with

the formation of secondary minerals, such as clays (e.g., Huh et al., 1998; Kisakürek et al., 2004; Pistiner and Henderson, 2003; Pogge von Strandmann et al., 2006; Rudnick et al., 2004; Teng et al., 2004). Lithium has a few more advantages as a potential geochemical tracer of weathering: Li has only one redox state (+1 charge), and is thus insensitive to changes in oxygen fugacity compared to Fe, Cu, Mo, etc. Also, Li is not a nutrient, so its elemental and isotopic behavior is not directly influenced by biological processes. Finally, Li is enriched in silicates and depleted in carbonates, so its abundance in rivers can reflect continental silicate weathering. Therefore, the Li isotope system could be a useful proxy to assess continental silicate weathering.

A recent study by Misra and Froelich (2012) shows a significant (~ 8 ‰) rise in δ^7Li in seawater from 60 Ma (22 ‰) to the present (30 ‰), as recorded in the Li isotope study of planktonic foraminifera. The Li isotopic composition in seawater is a function of the input of hydrothermal fluid and river water, and the output in secondary minerals formed via low temperature basalt alteration and sediment clay authigenesis. Thus, assuming a constant hydrothermal input, the significant increase in δ^7Li through the Cenozoic may indicate increases of δ^7Li in either riverine input flux (high amount of Li or high δ^7Li in weathering fluxes), the output flux, or both. Therefore, understanding the controls on riverine Li isotopes is a first-order requirement for understanding the secular evolution of continental weathering.

In a pioneering study of Li in the world's major rivers, Huh et al. (1998) suggested that the lithium isotopic composition of dissolved river loads are a function of the isotopic fractionation between water and secondary minerals, weathering

intensity in the watersheds of the rivers, as well as the composition of the bedrocks. In a study of Li isotopes in the Orinoco River, Huh et al. (2001) confirm that the δ^7Li of dissolved loads are not simply inherited from bedrock lithology or rainwater. They suggest that the largest isotopic fractionation between river water and rock occurs in relatively less weathered regions, such as the Andes. Rivers draining the Andes have a high δ^7Li of 26. By contrast, rivers draining more intensely weathered regions, such as the Guayana Shield, have a lighter isotopic composition (δ^7Li = 6.6). A later study by Kisakurek et al. (2005) on Himalayan rivers confirms the findings of Huh et al. (2001; 1998) and proposes that Li concentrations in dissolved loads reflect the silicate weathering flux, while δ^7Li is correlated with weathering intensity.

To simplify the problem of multi-lithological influence on the Li isotopic compositions of rivers, several studies have investigated rivers that only drain a single lithology, such as basalt. A study from rivers that drain mostly Icelandic basalts suggests that the δ^7Li difference between the dissolved and suspended loads is correlated with weathering intensity, with greater weathering intensity corresponding to smaller Li isotopic fractionation between the suspended and dissolved load (Pogge von Strandmann et al., 2006). By contrast, Vigier et al. (2009) performed a systematic study of Li isotopes from major rivers in Iceland and inferred an empirical law that they suggest may apply to rivers draining large areas of continental crust based on a negative correlation between δ^7Li and chemical erosion rates (instead of intensity).

More recently, Millot et al. (2010) reported Li isotopic compositions for river waters and suspended sediments from the Mackenzie River Basin in Canada that drains a wide variety of lithologies and topography. They suggest that the weathering

regime (incipient vs. intense weathering) controls the Li isotopic signature of silicate weathering, rather than weathering fluxes. In addition, Millot et al. (2010) suggest two end member processes that are responsible for the Li isotopic compositions of river waters: one is the formation of secondary minerals in the regolith due to more intense water-rock interactions, which preferentially incorporates ^{6}Li in the regolith, leaving the heavy ^{7}Li in river waters (e.g., Chan et al., 1992; Pistiner and Henderson, 2003; Rudnick et al., 2004; Vigier et al., 2008; Zhang et al., 1998); the second is preferential sorption of ^{6}Li onto Fe and Mn oxyhydroxides and/or weak (incipient) weathering, causing ^{7}Li-enriched waters, similar to that observed in rivers from Greenland (Wimpenny et al., 2010b).

From the above studies, one can conclude that, within a given river, the $\delta^{7}Li$ in suspended loads are homogeneous and isotopically lighter compared to that of dissolved loads. The $\delta^{7}Li$ in dissolved loads appears to correlate more with weathering intensity than with chemical weathering rates in most studies. However, it is still unknown what controls Li isotopic differences between dissolved river waters and suspended loads.

This study aims to understand Li isotopic behavior and possible fractionation mechanisms during chemical weathering of basalts, and to evaluate the Li isotope

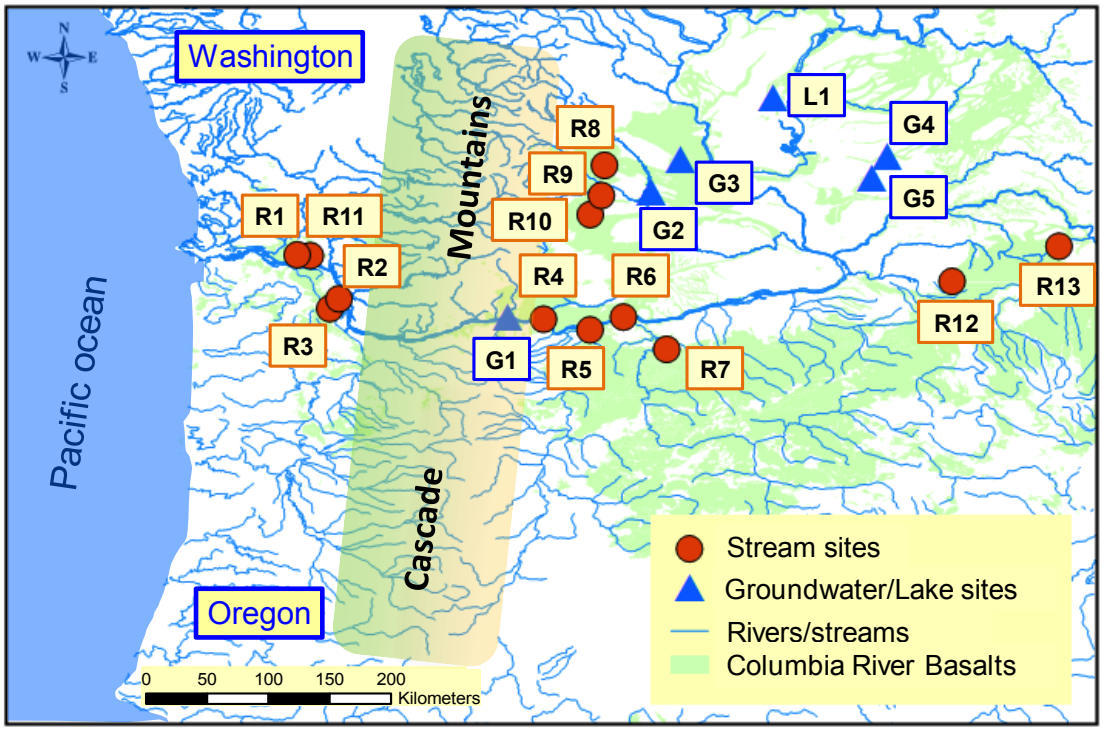

Figure 11. Map of sample locations.

system as a proxy of chemical weathering by investigating Li in streams draining a single lithology: the Columbia River Basalts, as well as groundwaters contained within these basalts.

3. Geological setting, climate and samples

The geological setting of the sampling area is described in Liu et al. (2010) and a brief description is provided here. The Columbia River Basalts (CRBs) are continental flood basalts that erupted during the Miocene (between 17 Ma to 6 Ma) in the US Pacific Northwest, covering large parts of southern Washington, northeastern Oregon and parts of western Idaho. The Cascade Mountains cut through the CRBs, dividing the CRBs into two climate zones, the wet (western) and dry (eastern) zones.

The modern mean annual temperature (MAT) and mean annual precipitation (MAP) in the study area are ~11^{o}C and ~1100 mm, respectively, according to the Western Regional Climate Center (http://www.wrcc.dri.edu). Various geological and paleofloral evidence suggest that the middle to late Miocene climate of the inland Pacific Northwest was warmer and wetter than it is today (Takeuchi et al., 2010).

The streams studied here are small and only or mainly drain the CRBs, except for the Deschutes and John Day Rivers, whose watersheds also include volcanic materials derived from the Cascades. Several groundwaters were also sampled. Sampling locations are displayed in Figure 11 and latitude and longitude of the sampling sites are reported in Table 6.

4. Field and analytical methods

4.1 Sampling

The dissolved and suspended load samples from streams were collected in July 2010, and again in March 2012; groundwaters were only collected in March 2012. At each site, pH, temperature, electrical conductivity, and total dissolved solids (TDS) were measured using a multi-meter (Hanna® Instruments) with analytical accuracy of ± 0.05, ± 0.5^{o}C, ± 2% µS/cm, and ± 2% ppm, respectively. All water samples were pumped using a peristaltic pump and filtered using a 142 mm filter holder system using 0.2 µm cellulose acetate filters. Filtered waters were collected in pre-cleaned Nalgene® bottles. The suspended loads of the stream waters were later recovered from the filters in the clean lab. The sample tubing was pumped dry after each sample collection and one liter of deionized water was pumped through the system to clean it between each sampling event. At the start of sampling at a new site, a liter of sample water was first collected into the pre-cleaned bottles and then discarded. Finally, about two liters of waters were collected, acidified using five drops (~ 0.25 ml) of concentrated HCl and stored in the Nalgene® bottles at each sampling site for Li isotopic analyses. Following this, two 125 ml pre-cleaned Nalgene® bottles were filled with water for anion (without acidification) and major and trace cation analyses (acidified using two drops of ~ 0.1 ml concentrated HCl).

4.2 Major and trace elements in dissolved loads

Major and trace cations in dissolved loads were analyzed using an Element 2 single collector Inductively Coupled Plasma-Mass Spectrometer (ICP-MS) at the

Plasma Laboratory in the Department of Geology at the University of Maryland. Calibration curves were created using pure element solutions of variable concentrations (made from purchased single elemental standards from Alfa Aesar®). Each water sample was doped with the same amount of indium to correct for instrumental drift ([In] = 2 ppb). The accuracy and precision of the analyses were determined by repeat analyses of the international river standard, SLRS-5. The accuracy of the cation analyses is better than 4% (n = 11), except for K (<10%), determined by comparing averages of repeat analyses of a certified river water standard (SLRS-5) with its certified value. The details are shown in Table A.1.

Major anion concentrations were measured by ion chromatography in the Biogeochemical Lab of the Department of Geology at the University of Maryland. Anion concentrations were measured using a Dionex ICS-1500 ion chromatograph, equipped with an AS14 4-mm analytical column and a guard column. An eluent of 3.5 mM of Na_2CO_3 with 1.0 mM $NaHCO_3$ was used at a flow rate of 0.3 mL/min. The detection limits of the ion chromatograph were 0.01 mg/L, 0.01 mg NO_3/L and 0.02 mg SO_4/L for Cl^-, NO_3^- and SO_4^{2-}, respectively. The accuracy of the analyses was evaluated to be better than 5% based on repeat analyses of standards (see Table A.2).

4.3 Lithium isotope analyses

The method for lithium isotopic analysis used here was previously described in Liu et al. (2010; 2010b), which were modified from that originally developed by Moriguti and Nakamura (1998b). All sample preparation and analyses were performed in the Geochemical Laboratory in the Department of Geology at the

University of Maryland. A brief description of sample dissolution, column chemistry and instrumental analysis is provided below.

4.3.1 Handling of dissolved loads

Approximately 30 ml to 2 L of filtered stream and ground waters (depending on the volume collected) were first weighed and then evaporated in large Savillex® Teflon beakers (160 ml) or Teflon evaporation dishes (400 ml) on a hot plate ($T < 100\ ^{o}C$). Samples were then picked up in a roughly 3:1 mixture of HF-HNO_3 in screw-top Savillex® telfon beakers (15ml) on a hot plate ($T < 120\ ^{o}C$). This was followed by treatment with concentrated HNO_3 and HCl until all solids were dissolved and the final solutions were clear. The final dried sample was picked up in 4 N HCl for column separation.

4.3.2 Dissolution of suspended loads

Suspended load samples were washed off the filters into large Savillex® Teflon beakers (160 ml) using Milli-Q water and then transferred into screw-top Teflon beakers and dried down on a hot plate ($T < 70\ ^{o}C$). The dried samples were then scraped off the beaker and weighed into clean Teflon beakers; sample sizes ranged from several milligrams to tens of milligrams. The samples were then dissolved using a roughly 3:1 mixture of HF and HNO_3 in a screw-top Teflon beaker on a hot plate ($T \approx 90^{o}C$), dried down, then pickup up by HNO_3 and HCl addition until all solids were dissolved and the final solutions were clear. The final dried sample was dissolved in 4 N HCl for column separation.

4.3.3 Column chemistry and instrumental analysis

Solutions were purified using cation exchange columns (BioRad AG50W-x12, 200-400 mesh). Four chromatographic columns were used, modified from the procedure described in Moriguti and Nakamura (1998b). The first two columns eliminate major element cations in sample solutions with 2.5M HCl and 0.15M HCl, respectively. The third column separates Na from Li with 30% ethanol in 0.5M HCl and the fourth column repeats the procedure of the third to further remove Na. Yields are determined to be greater than 95% (Marks et al., 2007).

Li solutions (~ 50 ppb Li in ~2% HNO_3) were analyzed using a Nu Plasma Multi Collector-Inductively Coupled Plasma-Mass Spectrometer (MC-ICP-MS) employing a "dry" sample introduction system, using either a CETAC Aridus or ESI Apex nebulizer. Background signals for ^7Li ($<10^{-4}$ V) were negligible compared to the typical sample signals (1-3 V). Standard bracketing, using L-SVEC (Flesch et al., 1973), was performed for each sample in all analyses and δ^7Li values were determined by comparison to the bracketing L-SVEC. The Li concentration is determined to within 10% (1σ). The external precision of δ^7Li, based on 2σ of duplicate runs of pure Li standard solutions, namely IRMM-016 and UMD-1, is ≤±1.0‰. For example, repeat analyses of these two Li solutions, analyzed during the course of this study (from 10/2010 to 07/2012) yield the following results: IRMM-016 (Qi et al., 1997) $\delta^7Li = -0.2 \pm 0.9$‰ (2 σ, n = 20); and the in-house standard, UMD-1, a purified Li solution from Alfa Aesar®, gives $\delta^7Li = +54.9 \pm 1.0$‰ (2 σ, n = 20). To evaluate the accuracy of Li isotope analyses, several USGS rock standards were run repeatedly during the course of this study (Table A.3). BHVO-1 yielded δ^7Li of 4.6 ± 1.0 (n= 5) cf. 4.0 to 5.6 in the literature (GeoReM database:

http://georem.mpch-mainz.gwdg.de/); BCR-2 yielded δ^7Li of 2.9 ± 1.5 (n = 3) cf. 2.6 to 4.6 in the literature (GeoReM database); and AGV-1 yielded δ^7Li of 5.2 ± 0.6 (n = 3) cf. 4.6 and 6.7 for AGV-1 in Liu et al. (2010b) and Magna et al. (2004), respectively.

5. Results

Data for field measurements (pH, temperature, electrical conductivity, and TDS), major and trace elements, in addition to Li isotopic data are given in Tables 6 and 7, for streams and groundwaters, respectively. Comparison of summer and late winter in streams for field and some lab data are shown in Figures A1 and A2, respectively.

5.1 Field measurements

Streams sampled in July 2010 display a temperature range from 13 to 22 ^{o}C with pH ranging from 7.2 to 8.7, while the streams sampled in March 2012 are cooler (1 to 9 ^{o}C), but have a similar range in pH (6.7 to 8.3). Groundwaters are warmer (10 to 29 ^{o}C), and have higher pH (7.7 to 9.6), compared to the streams sampled at the same time of year (March). TDS in streams are similar no matter what time of year they were sampled (10 to 154 mg/l in July, and 7 to 158 mg/l in March, Table 6). Groundwaters range to higher TDS values (90 to 253 mg/l, Table 7). The maximum TDS value was measured in a meromictic lake (i.e., a stratified lake that does not mix between layers), the TDS of which exceeded the range of the multi-meter.

Table 6. Sample locations, field measurements, major and trace element concentrations and Li isotopic compositions in dissolved and suspended loads of rivers.

2010 summer	units	Cameron	Milton	N. Scapoose	Silva	Deschutes	John Day	Hay	Wenas	Cowiche	Ahtanum	Mill	Asotin
Sample #		R1	R2	R3	R4	R5	R6	R7	R8	R9	R10	R11	R12
Logitude	^{o}	-123.16707	-122.84415	-122.91550	-121.26745	-120.90903	-120.65085	-120.31797	-120.79715	-120.82127	-120.90663	-118.11638	-117.29242
Latitude	^{o}	46.20735	45.86973	45.79293	45.71217	45.63033	45.72850	45.47992	46.89620	46.66437	46.51642	46.00358	46.27363
Location		west	west	west	east	east	east	east	east	east	east	east	east
T	^{o}C	15.6	18.6	15.2	18.1	19.2	21.9	19.6	12.6	18.8	14.6	14.1	18.1
pH		7.2	7.7	7.9	8.0	8.7	8.5	7.8	7.9	8.0	7.8	7.8	8.1
Conductivity	µS/cm	21	64	65	128	118	165	307	95	88	65	74	82
TDS	mg/l	10	32	32	64	58	82	154	47	44	32	35	41
Na	mg/l	2.7	4.9	5.3	6.5	9.6	7.0	17.1	3.9	4.0	3.2	3.8	3.5
Mg	mg/l	0.8	2.1	1.9	5.4	4.7	5.9	10.7	4.5	3.8	2.7	2.5	3.1
Al	µg/l	29.5	11.8	21.5	6.5	6.1	4.7	1.8	9.1	15.1	10.0	6.5	20.3
Si	mg/l	6.5	17.0	22.0	31.2	20.1	14.1	40.5	28.9	31.8	27.4	28.8	29.5
K	mg/l	0.4	1.1	1.3	1.5	1.7	1.4	3.7	1.6	2.1	1.8	2.3	2.3
Ca	mg/l	1.7	4.9	5.2	11.2	6.8	15.7	27.5	8.9	7.9	6.3	6.6	8.0
Fe	µg/l	129.1	315.8	173.0	27.7	20.5	31.8	54.1	127.5	184.3	78.8	50.1	34.7
F^-	mg/l	0.06	0.08	0.04	0.56	-	0.13	0.13	0.04	0.06	0.03	0.07	0.08
Cl^-	mg/l	2.65	3.95	17.72	53.51	12.88	8.53	8.60	15.65	12.89	16.02	3.18	2.82
NO_3^-	mg/l	-	-	-	-	0.00	-	0.01	-	-	0.01	-	-
SO_4^{2-}	mg/l	2.13	4.66	5.51	38.87	1.29	4.30	17.90	2.73	1.41	5.10	3.38	1.93
Li_{dis}	µg/l	0.1	0.7	1.6	0.4	4.7	1.6	3.2	0.7	1.1	0.7	0.9	1.0
δ^7Li_{dis}		21.1	22.1	14.9	30.4	12.2	16.6	20.0	20.2	17.0	13.0	10.6	9.3
Li_{sus}	µg/g	-	-	13.8	-	7.5	14.7	-	23.8	-	-	-	7.2
δ^7Li_{sus}		-	-	-5.6	-	4.2	-1.6	-	-3.1	-	-	-	-4.2

Note: "*" location relative to the Cascades (west or east). "-" under detection limit.

Table 7. Sample locations, field measurements, major and trace element concentrations and Li isotopic compositions in dissolved and suspended loads of rivers continued.

2012 winter	units	Cameron	Milton	N. Scapoose	Silva	Deschutes	John Day	Hay	Wenas	Cowiche	Ahtanum	Mill	Asotin	Mosquito
Sample #		R1	R2	R3	R4	R5	R6	R7	R8	R9	R10	R11	R12	R13
Logitude	^{o}	-123.16707	-122.84415	-122.91550	-121.26745	-120.90903	-120.65085	-120.31797	-120.79715	-120.82127	-120.90663	-118.11638	-117.29242	-123.06510
Latitude	^{o}	46.20735	45.86973	45.79293	45.71217	45.63033	45.72850	45.47992	46.89620	46.66437	46.51642	46.00358	46.27363	46.20202
Location		west	west	west	east	east	east	east	east	east	east	east	east	west
T	^{o}C	5.8	6.0	5.2	5.6	8	6.9	9	1.4	2.2	2.9	4.3	5.2	5.6
pH		6.7	6.9	8.3	7.6	8.0	7.7	7.8	7.6	7.6	7.6	7.4	7.6	6.7
Conductivity	µS/cm	14	31	37	65	105	125	316	97	102	91	51	74	20
TDS	mg/l	7	16	18	33	52	62	158	48	51	44	25	37	10
Na	mg/l	2.2	3.1	3.2	4.2	8.2	5.6	16.1	4.0	4.6	3.9	3.1	2.9	2.4
Mg	mg/l	0.6	1.0	1.0	2.7	4.0	4.4	10.2	4.3	4.4	3.6	1.7	2.7	0.8
Al	µg/l	16.4	4.9	8.9	85.9	42.5	40.0	2.1	57.4	22.5	21.7	179.5	241.3	11.9
Si	mg/l	4.1	9.2	12.2	21.3	21.7	19.3	33.6	27.3	29.7	30.0	23.7	27.1	4.8
K	mg/l	0.3	0.6	0.8	0.9	1.5	1.3	3.8	1.5	1.9	2.0	1.5	1.7	0.3
Ca	mg/l	1.6	2.8	3.1	6.3	6.4	11.6	27.2	8.6	8.8	7.9	4.8	6.9	1.9
Fe	µg/l	19.7	14.2	15.6	54.7	33.9	50.9	57.3	93.0	76.2	55.3	218.8	251.3	37.4
F^-	mg/l	0.01	0.02	0.03	0.04	0.10	0.08	0.42	0.09	0.10	0.07	0.15	0.08	0.01
Cl^-	mg/l	3.31	2.58	2.90	1.62	1.76	1.24	10.83	0.42	0.93	0.45	0.49	0.66	2.68
NO_3^-	mg/l	2.05	3.30	2.79	0.04	0.40	0.32	1.55	0.01	0.01	0.02	0.22	0.33	4.76
SO_4^{2-}	mg/l	0.51	1.16	1.62	0.68	1.78	3.92	14.75	2.03	3.19	1.57	0.61	1.29	0.53
Li_{dis}	µg/l	0.1	0.4	0.9	0.3	3.5	1.1	2.9	0.5	1.1	0.8	0.7	0.7	0.2
δ^7Li_{dis}		17.4	13.0	8.8	14.0	12.5	13.5	18.8	21.6	16.1	13.1	10.9	8.9	15.9
Li_{sus}	µg/g	15.8	20.2	66.5	17.8	12.9	20.1	21.3	24.3	15.6	16.1	19.3	36.3	16.9
δ^7Li_{sus}		-1.4	-2.5	-4.5	-0.9	-0.3	-1.5	-0.2	-3.1	-5.7	-5.9	-2.8	-5.2	-1.0

Note: "*" location relative to the Cascades (west or east). "-" under detection limit.

Table 8. Sample locations, field measurements, major and trace element concentrations and Li isotopic compositions of groundwaters.

Groundwater	units	Spring Creek	Selah	Ryegrass	Lind	Hatton	Soap Lake
Sample #		G1	G2	G3	G4	G5	L1
Logitude	^{o}	-121.54613	-120.44327	-120.20900	-118.62250	-118.74282	-119.49877
Latitude	^{o}	45.72737	46.69758	46.94738	46.96828	46.79410	47.42263
Sampling*		well	faucet	faucet	well	faucet	
T	^{o}C	17.6	18.1	14.7	28.6	10.9	10.2
pH		8.8	8.0	7.7	9.1	7.9	9.6
Conductivity	µS/cm	180	315	341	350	505	> 3999
TDS	mg/l	90	157	173	175	253	>2000
Na	mg/l	33.3	20.9	12.9	78.3	18.9	284.0
Mg	mg/l	0.4	12.0	15.4	0.3	18.8	4.4
Al	µg/l	6.9	27.4	0.5	4.9	0.1	-
Si	mg/l	44.8	33.3	40.1	64.1	34.8	4.9
K	mg/l	4.5	3.9	2.9	3.9	4.0	588.6
Ca	mg/l	1.9	16.6	19.0	3.1	40.4	6.9
Fe	µg/l	46.6	6.9	5.7	16.6	53.7	1.3
F^{-}	mg/l	0.76	0.48	0.39	3.30	0.28	0.31
Cl^{-}	mg/l	3.63	8.60	6.96	7.89	46.13	131.7
NO_3^{-}	mg/l	0.01	-	10.56	0.13	18.30	-
SO_4^{2-}	mg/l	1.48	3.73	12.30	4.66	49.79	206.2
Li_{dis}	µg/l	21.1	9.8	6.5	8.9	3.3	1.5
δ^7Li_{dis}		6.8	8.1	9.4	21.4	6.7	20.5

Note: "*" sampling methods (well or faucet). "-" under detection limit.

5.2 Major elements

Major elements in stream dissolved loads, such as Na, Si and Ca, correlate with Mg (Figure 12). Similarly, the total cation charge, TZ^+ ($TZ^+ = Na^+ + 2Mg^{2+} + K^+ + 2Ca^{2+}$ in 10^{-3} equivalents per liter, mEq/L), also correlates (R^2 = 0.98) with Mg concentrations ([Mg]) in summer and late winter stream waters. Some groundwaters follow the major element correlation trend, but with higher elemental concentrations. However, the two deep groundwaters have low [Ca] (< 3 mg/l) and [Mg] (< 0.5 mg/l), such as Spring Creek (fish hatchery) and Lind Well (municipal city well). The sample from Silva Creek in July 2010 has much higher [Cl^-] (54 mg/l) and [SO_4^{2-}] (39 mg/l), compared to the other streams studied here and natural streams elsewhere (where [Cl^-] is typically less than 10 mg/l), indicating that this creek may have been subjected to anthropogenic contamination from fertilizer in the summer months.

5.3 Li elemental and isotopic data

The Li concentrations ([Li]) vary from 0.2 to 4.7 µg/l in dissolved loads of streams for both sampling seasons. In both summer and late winter dissolved load [Li] positively correlates with [Mg] (R^2 = 0.7), but not so much with [Si] (R^2 = 0.4), indicating [Li] contains additional information that major elements, such as Mg, cannot provide (Figures 13a and 13b). In groundwaters, [Li] varies from 2 to 21 µg/l and δ^7Li ranges from 7 to 21. [Li] in groundwaters does not show the correlation with major elements as seen in stream waters (Figure 13). In addition, there is little

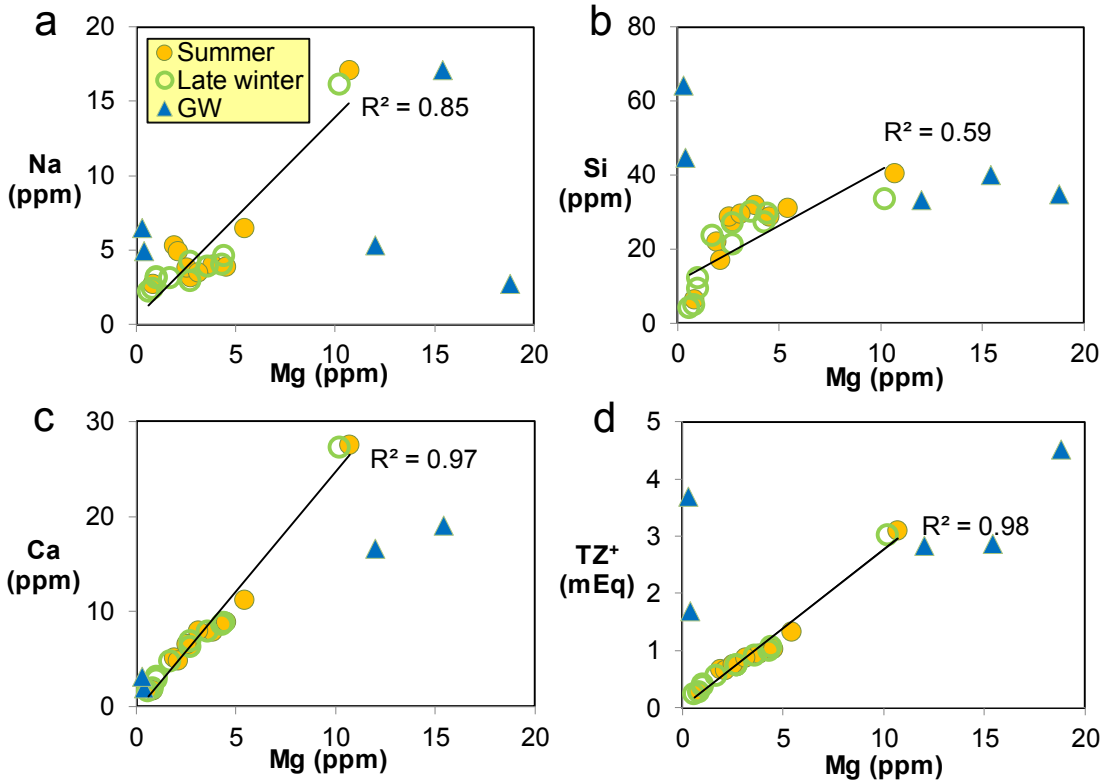

Figure 12. Major elements in streams and groundwaters.
Summer (July) and late winter (March) stream waters are shown in yellow and green circles, respectively. Groundwaters are plotted as blue triangles. R^2 values are calculated based on stream data only.

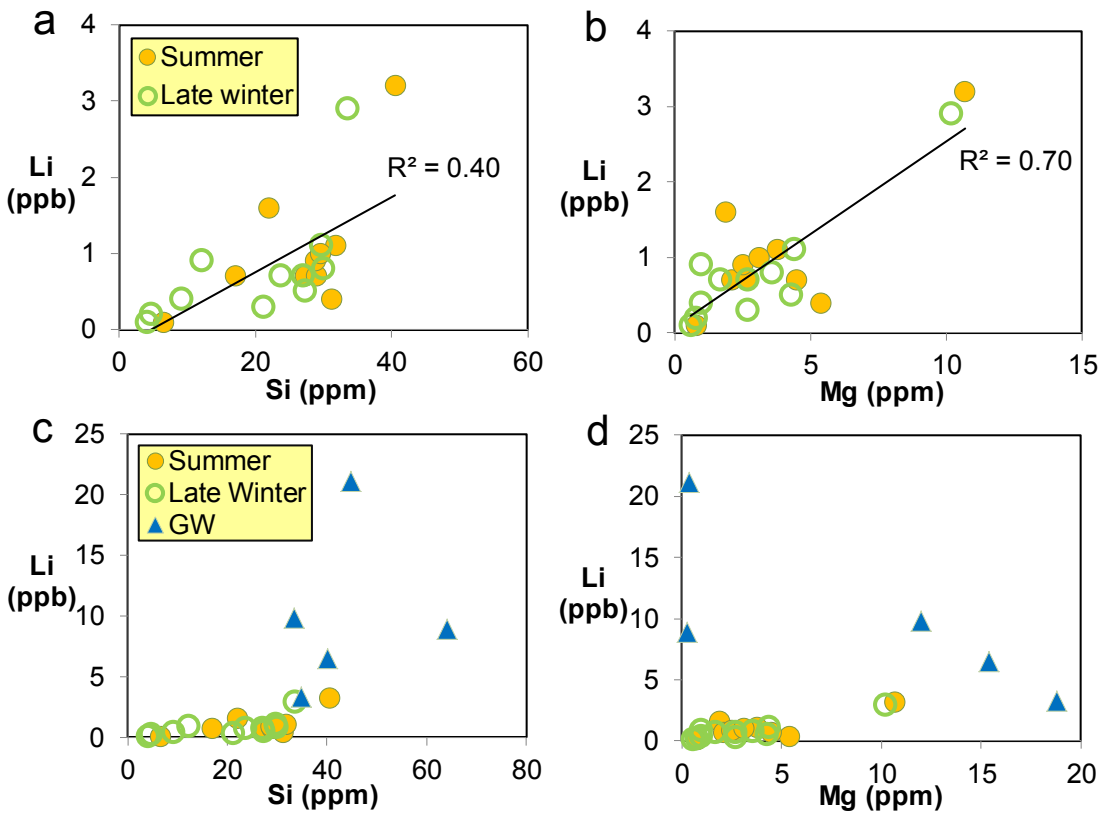

Figure 13. Plots of [Li] versus [Si] and [Mg] in streams and groundwaters. Summer and spring stream waters are shown in yellow and green circles, respectively. Ground waters are in blue triangles.

difference in [Li] between the summer and late winter streams (Table 6, Figure A2 in appendix). The δ^7Li of the dissolved load ranges from 10 to 30 in the streams sampled during the summer, and shows a similar range in the streams sampled in the late winter (9 to 22). In streams east of the Cascades, the dissolved load δ^7Li does not change with season, except for the one sample (Silva Creek, δ^7Li = 30) that may show anthropogenic contamination. By contrast, the streams to the west of the Cascades show consistently lower δ^7Li values in the summer compared to the winter (Figure 14).

[Li] in the suspended loads varies from 7 to 24 μg/g in the streams sampled during the summer, and shows a greater range in the streams sampled during the late winter (from 13 to 66 μg/g). The δ^7Li of the suspended load varies from season to season. In the streams sampled during the summer, δ^7Li of the suspended load ranges from -5.6 to 4.2, while in the same streams sampled during the late winter, the δ^7Li of the suspended load ranges from -5.9 to -0.2. All suspended loads, except for the summer Deschutes River sample, have lower δ^7Li compared to the average fresh CRBs (δ^7Li = 1.1, Liu et al., (2010)). This sample is also the only one to show a seasonal change in the δ^7Li of the suspended load, from 4.2 in summer to -0.3 in late winter. The light δ^7Li in the suspended loads of the streams are comparable to the low δ^7Li regolith on the upper continental crust (δ^7Li = 0 on average, Teng et al., (2004)).

6. Discussion

6.1 Mineral saturation status in streams and groundwaters

Primary mineral dissolution during the weathering of basalts is one of the most important processes that transfers soluble elements, such as Li, into rivers and

groundwaters. In addition, formation of secondary minerals may exert significant control on the elemental and isotopic compositions of metals, such as Li, in water. We therefore seek to determine the mineral saturation of the stream and groundwaters in order to assess the possible mineralogical control on Li elemental and isotopic behavior. Saturation index (SI) modeling using the PHREEQC program (Parkhurst and Appelo, 1999) was conducted in order to understand the stability of secondary minerals in the waters. The SI indicates the mineral equilibrium status in water: if SI > 0, the mineral is oversaturated in water and precipitates out; if SI < 0, the mineral is undersaturated and will dissolve in water. The saturation indices of major primary and secondary minerals that are commonly seen in rivers draining basalts are plotted in Figure 15.

Similar to other basaltic weathering systems, streams and groundwaters that drain the CRBs are undersaturated with respect to primary minerals (Si < 0) such as plagioclase, pyroxene, and olivine, which approach saturation as the pH increases (Figure 15a). Similarly, some secondary sheet silicates, such as chlorite, chrysotile, and talc are undersaturation at low pH and become oversaturated at higher pH (Figure 15b). By contrast, secondary minerals such as kaolinite, montmorillonite, gibbsite, and hematite are mostly oversaturated and become less saturated as pH increases (Figure 15c).

The calculation of mineral saturation is important because Li should be released with little isotopic fractionation by congruent weathering of primary minerals (Pistiner and Henderson, 2003). However, the saturation with respect to most secondary minerals implies that there should be Li isotopic fractionation due to

the oversaturation (formation) of secondary minerals, such as kaolinite and hematite, in most streams and some groundwaters. This is consistent with the observed Li isotopic compositions in streams draining only the CRBs, where dissolved and suspended loads of these streams have heavier (δ^7Li = +9 to +30) and lighter (δ^7Li = -6 to 0) values, respectively, compared to the average fresh CRBs (δ^7Li = 1.1, Liu et al., (2012), Chapter 2).

6.2 Seasonal variations and climate controls

There are large variations in δ^7Li in the dissolved loads of the streams draining only basalts, with more than 20‰ in summer and more than 10‰ in late winter, almost covering the entire range of δ^7Li (+6 to +32) reported in major world rivers (Huh et al., 1998). It is clear that δ^7Li can vary significantly even in the absence of lithological differences within drainage basins. Therefore, other factors may control the Li isotopic behavior of streams. We then investigate the possible influences on the observed large δ^7Li variation in streams and the degree of seasonal and climate contributions to the δ^7Li variation.

There does not appear to be any distinction in δ^7Li values between western and eastern streams, suggesting that climate does not have a clear influence on δ^7Li. This lack of climatic influence is consistent with the results of Millot et al. (2010), who suggest that neither mean annual precipitation nor distance to the coast

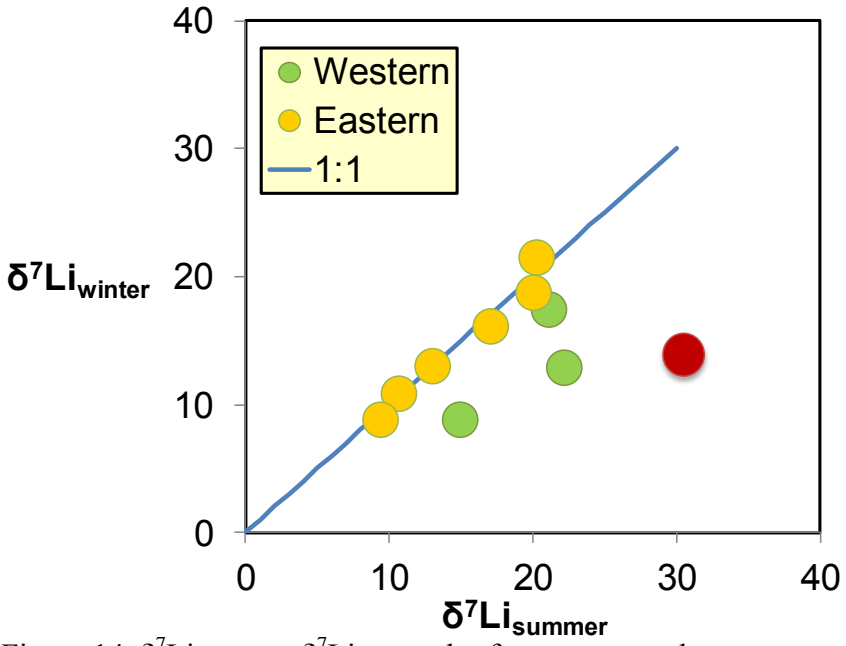

Figure 14. δ^7Li_{winter} vs. δ^7Li_{summer} plot for western and eastern streams. The sample showing suspected contamination (Silva, eastern) is plotted as a red circle.

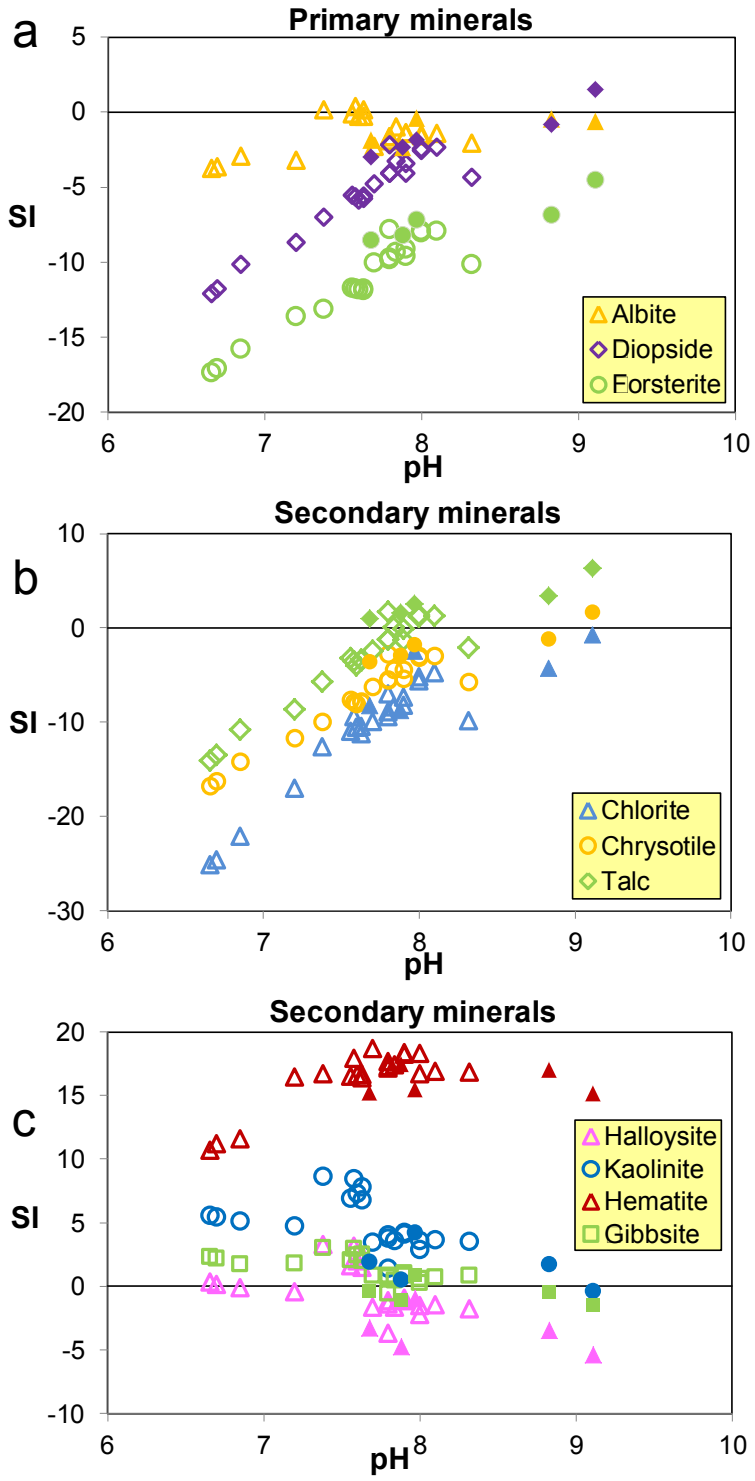

Figure 15. Saturation Index (SI, see text for details) of primary and secondary minerals plotted against pH in streams (open symbol) and groundwaters (closed symbol).
SI > 0 indicates oversaturation and SI < 0 indicates understaturation of a mineral in a given water sample.

have an influence on δ^7Li in waters from the Mackenzie River basin. Interestingly, for the streams on the east side of the Cascades, we have shown that $\delta^7Li_{late\ winter}$ vs. δ^7Li_{summer} plot follows a 1:1 line, except for the one locality (Silva Creek) that may have anthropogenic contamination in the summer (high $[Cl^-]$ and $[SO_4^{2-}]$). By contrast, in the streams located to the west of the Cascades, $\delta^7Li_{late\ winter}$ shows much lower values compared to δ^7Li_{summer} (plotting to the right of the 1:1 line, see Figure 14). It is clear that there is a seasonal control on δ^7Li in the dissolved loads of these western streams.

To explore the reason for the seasonal control, I plot the difference in δ^7Li between summer and winter ($\Delta^7Li_{summer\text{-}winter}$) against elevation of the sampled streams (Figure 16). Interestingly, $\Delta^7Li_{summer\text{-}winter}$ decreases with increasing elevation, and then shows no change after reaching a certain elevation (~200 m) in the streams only draining basalts. It is possible that there is an anthropogenic influence on the summer δ^7Li, such as fertilizer, as shown in Silva Creek. However, fertilizer would be more prominent in the eastern wheat fields than in the west, where there is less agriculture. Another possibility is that the groundwater sources that feed the streams at low elevations changes seasonally due to changes of water table levels, causing the seasonal δ^7Li variation in the lower streams (mostly western) but probably not in the higher eastern streams.

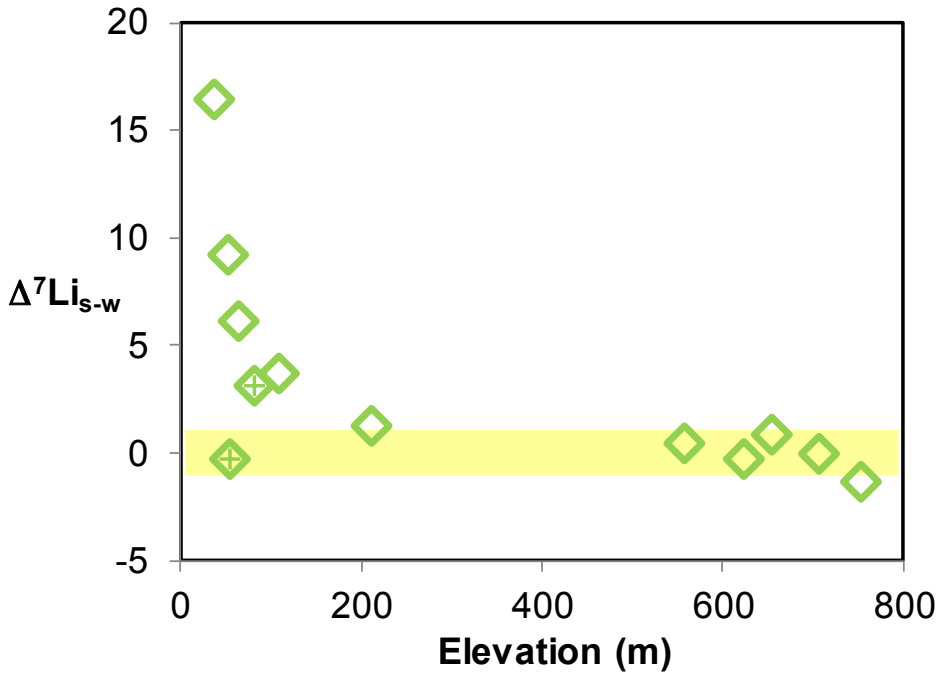

Figure 16. $\Delta^7Li_{s\text{-}w}$ (δ^7Li_{summer} - δ^7Li_{winter}) vs. elevation of the sampled streams. Streams draining only basalts are shown as open green diamonds, and the Deschutes and John Day Rivers are shown as diamonds with crosses. The yellow rectangular field indicates 2σ uncertainties of δ^7Li measurements (±1‰).

6.3 δ^7Li in streams as a tracer of chemical weathering intensity

In river water studies, chemical weathering intensity usually reflects the degree of chemical weathering in the river catchments, and multiple proxies, such as Si content and normalized Si content (e.g., Huh et al., 2001; 1998; 2006), have been used to constrain silicate weathering intensity. Li isotopic compositions of dissolved loads of rivers have been shown to be potentially good tracers of chemical weathering intensity of river systems (e.g., Huh et al., 2001; 1998; Pogge von Strandmann et al., 2010; 2006). To explore potentially superior weathering intensity tracers, we plot δ^7Li in dissolved stream waters and ground waters against various possible weathering intensity tracers (Figure 17). [Si] is a potential tracer of weathering intensity, especially in regions of limited biological activity, such as Iceland (Pogge von Strandmann et al., 2006). However, δ^7Li does not correlate with [Si] in this study (Figure 17a), which may be due to biogeochemical processes influencing [Si]. Normalized Si content (Si/TZ^+), which has the advantage of removing the different evapotranspiration influences on elemental concentrations in rivers, was used as weathering intensity tracer by Huh et al. (2001; 1998). δ^7Li correlates with Si/TZ^+ in stream waters, but shows no correlation in groundwaters (Figure 17b). When plotting δ^7Li versus Li/TZ^+ ([Li] is normalized to TZ^+ in order to correct for differences due to difference in evapotranspiration among streams) (Figure 17c), a negative correlation between δ^7Li and Li/TZ^+ is observed. Millot et al. (2010) have suggested coupled weathering intensity tracers, δ^7Li and Li/Na ratios in dissolved large river waters, from a systematic study of Li isotopes in the Mackenzie River, Canada. When plotting δ^7Li vs. 1000×Li/Na in dissolved loads of streams and groundwaters, we can

see there is a clear negative correlation (Figure 17d). Since δ^7Li is a good weathering intensity tracer, as suggested by previous studies (e.g., Huh et al., 2001; Huh et al., 1998; Kisakürek et al., 2005; Pogge von Strandmann et al., 2006), the combined δ^7Li vs. 1000×Li/Na plot may indicate chemical weathering intensity in the stream catchments and groundwater reservoirs. Then, we plot δ^7Li vs. 1000×Li/Na in global river waters that drain only or mainly basalts (Figure 18), where the combined δ^7Li vs. 1000×Li/Na plot still shows a negative correlation, indicating that the great potential of the paired weathering intensity tracers.

6.4 Processes controlling Li isotopes in rivers

Li isotopic compositions of dissolved loads of rivers (δ^7Li_{dis}) have been suggested to be the result of isotopic fractionation between solution and secondary minerals (e.g., Huh et al., 2001; 1998; Pogge von Strandmann et al., 2010; 2006). However, δ^7Li_{dis} is not simply controlled by one fractionation process for secondary minerals, as there is no correlation between δ^7Li_{dis} and SI of the oversaturated secondary minerals, such as hematite and kaolinite.

To explain the large δ^7Li_{dis} variations in different river systems, most previous studies suggest that δ^7Li in dissolved loads reflects chemical weathering intensity of the corresponding river catchments (Huh et al. 2001; 1998; Pogge von Strandmann et al., 2006; Millot et al. 2010). One possible explanation is that Li isotopic fractionation between secondary minerals (such as hematite and kaolinite) and water is significant during the initial stage of chemical weathering (low weathering intensity). As

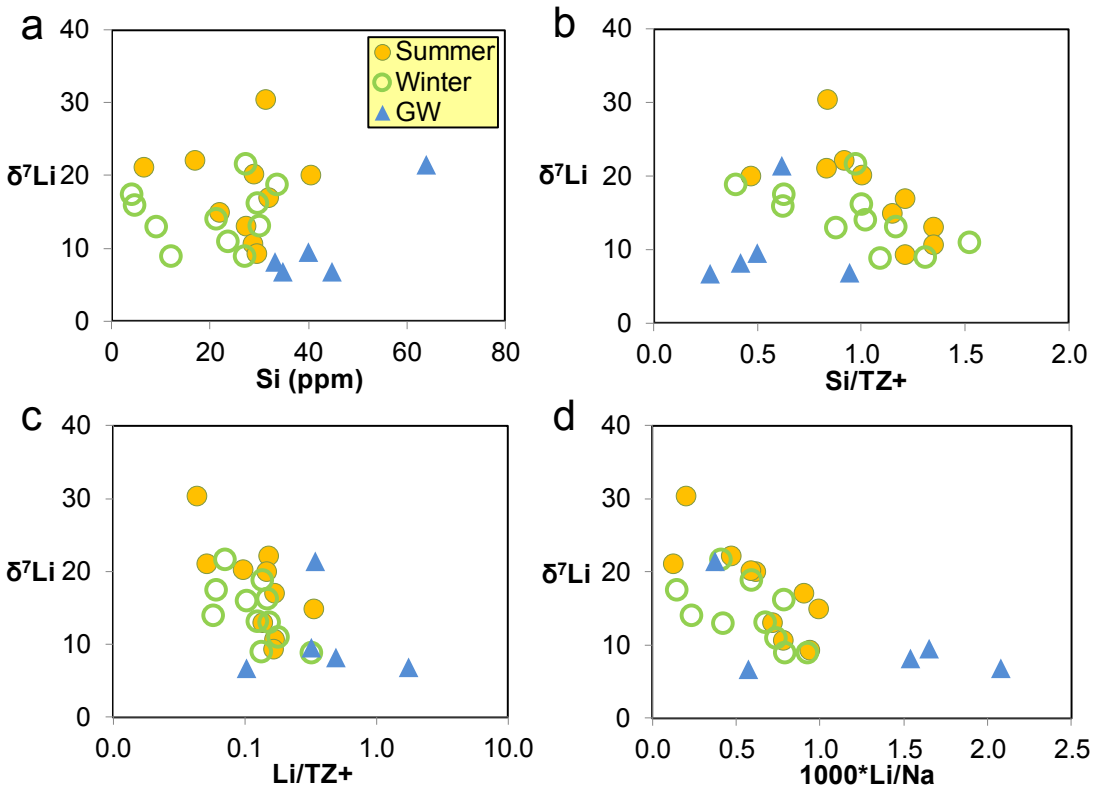

Figure 17. δ^7Li versus Si concentrations, Si/TZ^+, Li/TZ^+, and 1000×Li/Na in dissolved stream waters and groundwaters.
Summer and late winter stream waters are shown in yellow and green circles, respectively. Groundwaters are in blue triangles. The total cation charge (TZ^+) is defined as $TZ^+ = Na^+ + 2Mg^{2+} + K^+ + 2Ca^{2+}$ in 10^{-3} equivalents per liter, mEq/L.

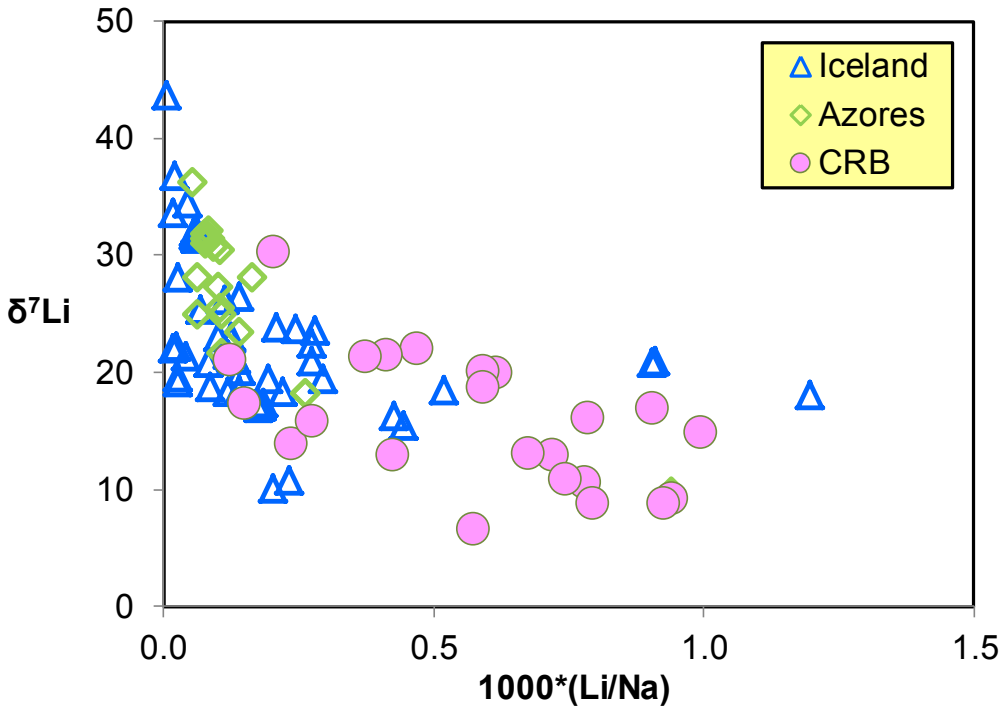

Figure 18. δ^7Li versus 1000×Li/Na in dissolved loads of streams and rivers draining basalts.
Data are from this study, Pogge von Strandmann et al. (2006; 2010), and Vigier et al. (2006; 2009).

chemical weathering becomes more intense, secondary minerals in weathered regolith may become unstable and are dissolved in river waters, releasing the Li they previously incorporated/sorbed back into the rivers. The Li they release is isotopically light, driving the river waters to be isotopically lighter at the advanced weathering stage (high weathering intensity). This interpretation is also supported by high [Li] and low δ^7Li in suspended loads (δ^7Li_{sus}), where the breakdown of suspended sediments can raise the [Li] and lower δ^7Li in dissolved river waters.

7. Conclusions

The main conclusions from this study are:

1. We have observed large δ^7Li variations (up to 20‰) in streams that only drain basalts, suggesting that Li isotopic compositions in streams are not controlled solely by the lithology of their catchments.

2. δ^7Li and Li/Na in dissolved loads of rivers are not sensitive to distance from the coast or the climate, but reflect the local weathering intensity. The chemical weathering intensity tracers, δ^7Li and Li/Na, seem to have global significance, at least in streams that only drain basalts.

3. Elevation may be responsible for seasonal variation of δ^7Li in dissolved stream waters.

4. Li isotopic fractionation in streams is likely controlled by the formation and destruction of secondary minerals. In addition, the variation of δ^7Li in different streams may reflect their maturity (weathering intensity), with low δ^7Li corresponding to high weathering intensity of the catchments.

Appendices

Table A.1. Accuracy of the major cation analyses based on repeat analyses of river water standard, SLRS-5.

	Na	Mg	Al	Si	K	Ca	Fe
analyses	mg/l	mg/l	µg/l	mg/l	mg/l	mg/l	µg/l
SLRS-5 (cert)	5.38	2.54	49.5		0.84	10.5	91.2
SLRS-5	5.5	2.4	48.5	2.9	0.88	9.4	92.9
SLRS-5	5.3	2.4	48.4	2.8	0.88	9.2	91.3
SLRS-5	5.5	2.4	44.9	2.7	0.87	9.5	92.7
SLRS-5	6.1	2.5	50.6	2.5	1.01	10.4	94.1
SLRS-5	6.0	2.5	44.0	2.4	0.97	10.4	94.3
SLRS-5	5.8	2.8	54.5		1.07	13.3	110
SLRS-5	4.9	2.4	50.1		0.82	9.4	94
SLRS-5	6.0	2.9	58.5		0.98		86.9
SLRS-5	5.2	2.5	52.5		0.85		86.8
SLRS-5	5.8	2.8	57.7		0.97		89.5
SLRS-5	5.2	2.5	52.1		0.84		89.6
ave	**5.6**	**2.55**	**51.1**	**2.7**	**0.92**	**10.3**	**92.9**
accuracy (%)	**3.4**	**0.3**	**3.2**		**9.9**	**2.4**	**1.9**
precision (%RSD)	7.2	7.4	9.1	7.6	8.8	13.9	6.7

Table A.2. Accuracy of the major anion analyses.

	Name	**floride**	**chloride**	**nitrate**	**sulfate**
	unit	**mg/l**	**mg/l**	**mg/l**	**mg/l**
	std1	**0.25**	**5.0**	**0.50**	**2.5**
	std1	0.2646	4.8677	0.5056	2.7443
	std1	0.2552	4.6757	0.506	2.5215
ave		0.26	4.77	0.51	2.63
% accuracy		4.0	-4.6	1.2	5.3
	std2	**2.0**	**10.0**	**10.0**	**10.0**
	std2	2.0885	10.2177	10.6397	10.7019
	std2	1.9387	9.0413	9.3258	9.3926
ave		2.01	9.63	9.98	10.05
% accuracy		0.7	-3.7	-0.2	0.5

Note: % accuracy is calculated using deviation of averaged measured values from the standard values in solutions (in blue).

Table A.3. [Li] and δ^7Li in several USGS rock standards.

Standard Name	Date Run	[Li] (ppm)	δ^7Li	Source
Basalt, Hawaii				
BHVO-1	2010 12 11	4.5	4.1	this study
BHVO-1	2011 09 02	3.8	4.1	this study
BHVO-1	2011 08 05	3.8	5.2	this study
BHVO-1	2012 06 21	4.1	4.9	this study
BHVO-1	2012 07 05	4.4	4.5	this study
Average		4.1	4.6	
2σ			1.0	
BHVO-1		4 ~ 5	4.0 ~ 5.6	GEOREM database
Basalt, Oregon				
BCR-2	2011 09 02	9.6	3.4	this study
BCR-2	2011 03 04	9.1	2.1	this study
BCR-2	2012 07 05	7.6	3.4	this study
Average		8.7	2.9	
2σ			1.5	
BCR-2		8 ~ 10	2.6 ~ 4.6	GEOREM database
Andesite, Oregon				
AGV-1	2010 12 11	9.2	4.9	this study
AGV-1	2012 07 04	9.0	5.4	this study
AGV-1	2012 07 05	11.0	5.4	this study
Average		9.7	5.2	
2σ			0.6	
AGV-1		10 ~ 12	4.6 ~ 6.7	GEOREM database

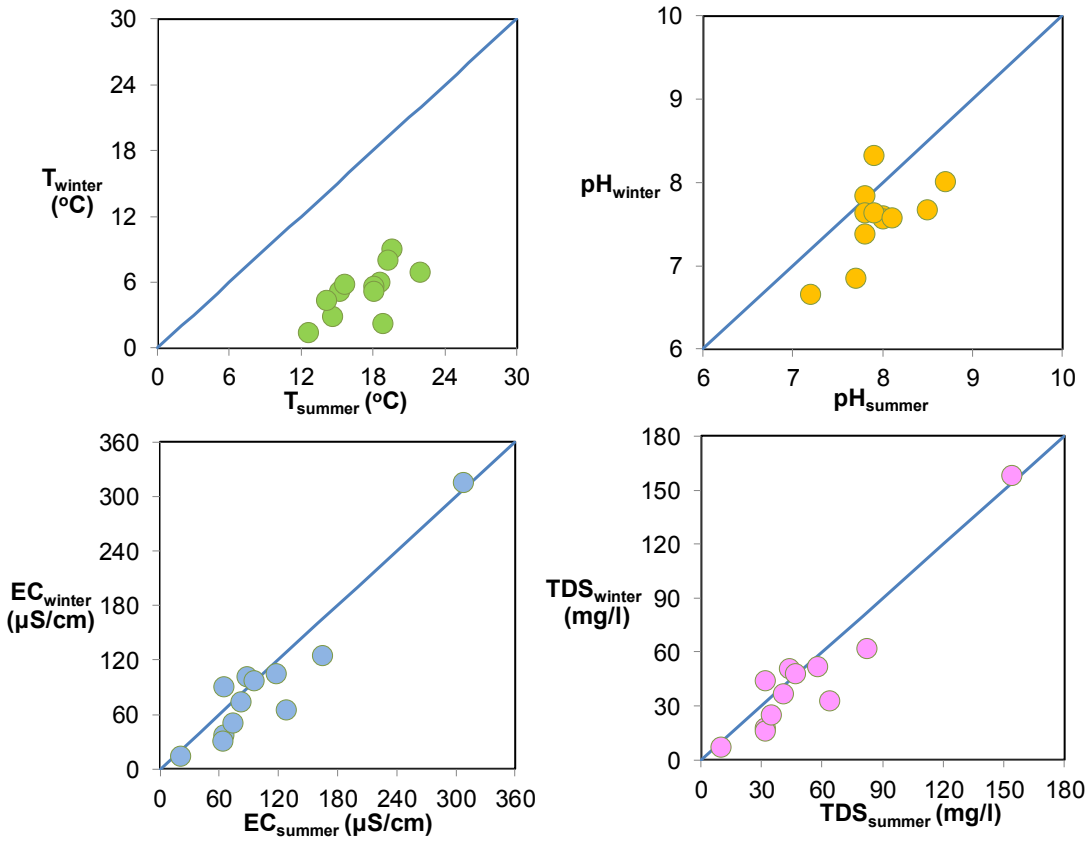

Figure A1. Seasonal variations in steams between summer and late winter.

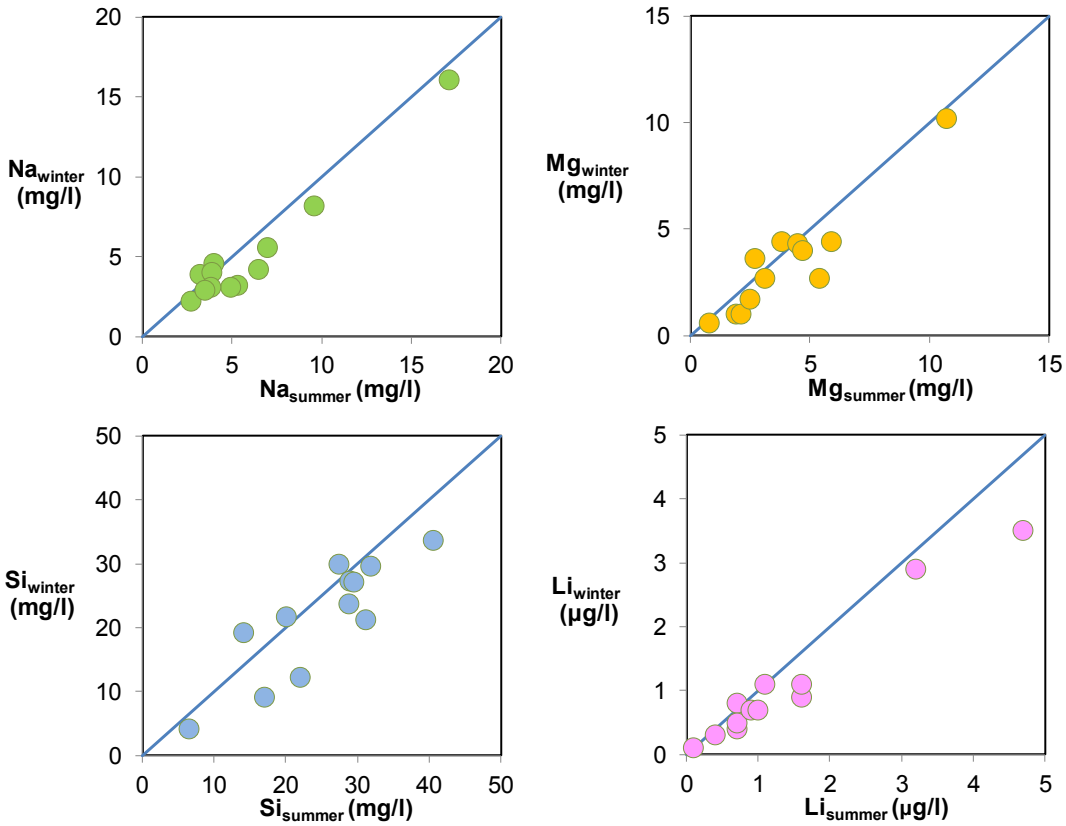

Figure A2. Seasonal variations in selected cation concentrations (Na, Mg, Si and Li) in steams between summer and late winter.

Chapter 5: Constraints on continental crustal mass loss via chemical weathering

Abstract

Chemical weathering as well as physical erosion changes the composition and shapes the surface of the continental crust. However, the amount of continental material that has been lost over Earth's history due to chemical weathering is poorly constrained. Using a mass balance model for lithium inputs and outputs from the continental crust, we find that the mass of continental crust that has been lost due to chemical weathering is at least 15% of the original mass of the juvenile continental crust, and may be as high as 60%, with a best estimate of ~45%. Our results suggest that chemical weathering and subsequent subduction of soluble elements have major impacts on both the mass and the compositional evolution of the continental crust.

1. Introduction

It is well established that the average composition of the continental crust is intermediate or "andesitic", if described in terms of an igneous rock type (SiO_2 = 57 ~ 64 wt. %) (Rudnick and Gao, 2003b and references therein). However, the magmas that generate the present-day continental crust are dominantly basalt (Rudnick, 1995 and references therein). This discrepancy has been referred to as the "Crust Composition Paradox" (Rollinson, 2008). Various hypotheses have been proposed to solve this paradox, including stripping of Mg through chemical weathering (Albarède, 1998; Anderson, 1982; Lee et al., 2008), removal of mafic/ultramafic lower crust through foundering/delamination (Arndt and Goldstein, 1989; Jull and Kelemen,

2001; Kay and Kay, 1993), subduction of continental crust followed by "relamination" of buoyant, felsic crust (Hacker et al., 2011), or direct addition of tonalites to the crust through slab melting in a hotter Archean Earth (e.g., Martin, 1986; Rollinson, 2008; Rudnick, 1995).

During chemical weathering of the continents, soluble elements (e.g., Na, Ca, Mg and Li) are dissolved and transported to the oceans via rivers and/or groundwater, while insoluble elements, such as Si and Al, remain in the continental regolith. Ultimately, these soluble components may be recycled into the mantle by subduction (e.g., Mg and Ca) or may re-enter continental crust via arc magmatism (e.g., Na). Therefore, chemical weathering may be an important process that controls the mass, the composition and the evolution of the continental crust. However, only one attempt has previously been made to quantify the influence of chemical weathering on the mass and composition of the continental crust (Lee et al., 2008).

Using a mass balance model coupled with the correlation observed between lithium and magnesium in modern river waters and assumptions regarding the mass lost from the continental crust due to lower crustal recycling, Lee et al. (2008) argued that ~20% of the juvenile continental crustal mass has been lost from the continental crust due to chemical weathering. However, the Li concentration they used for primitive island arc basalts (15 ppm) is about a factor of two higher than average compositions of arc basalts or other oceanic basalts (e.g., mid-ocean ridge basalts (MORB) or ocean island basalts (OIB) see below). When using a more accurate concentration (7 ppm), the Mg/Li mass balance becomes untenable, as the proportion of bulk continental crust exceeds one, implying mass addition due to chemical

weathering. A fundamental problem is that Li is a moderately incompatible trace element, whose concentration in crustal rocks varies by several orders of magnitude, while Mg, a major element, may vary in concentration by only a factor of two to three. Thus, the Li/Mg ratio is sensitive to the more variable Li concentration. In addition, Li is a trace element whose partitioning may not always follow Mg, and, with newer data (see *SI dataset1*), it is clear that the Mg/Li ratio in river waters is quite variable, reflecting the influence of factors such as watershed lithology, that influence riverine Mg/Li, in addition to continental weathering.

Here, we explore the utility of using a single soluble element, Li, and its isotopes (^{6}Li and ^{7}Li), to constrain the mass of continental crust lost to weathering, employing a mass balance approach similar to that of Lee et al. (2008). While there are a number of assumptions that go into this calculation, giving rise to a family of outcomes, our aim here is not so much to provide "the answer" regarding the mass of continental crust lost to chemical weathering, but rather, to place limits on this mass.

Lithium Isotopes

Lithium has two stable isotopes: ^{6}Li ~7.5% and ^{7}Li ~92.5%. Because the mass difference between these two isotopes is relatively large (~16%), they show significant mass dependent fractionation in nature (> 50‰) (Tomascak, 2004), expressed in δ^{7}Li notation: $\delta^{7}Li(‰) = ([^{7}Li/^{6}Li]_{sample}/ [^{7}Li/^{6}Li]_{standard}-1)\times1000$, where the standard used is a synthetic Li carbonate, L-SVEC (Flesch et al., 1973). During chemical weathering, secondary minerals, such as clays, take ^{6}Li preferentially into their structure, resulting in heavier Li isotopic composition in rivers and lighter isotopic composition in the regolith (e.g., Huh et al., 2001; Huh et al., 1998;

Kisakürek et al., 2004; Millot et al., 2010; Pistiner and Henderson, 2003; Vigier et al., 2009). The lithium concentration and isotopic composition of the continental crust, as well as river waters, are well documented by various authors (Teng et al. 2004; 2008; Millot et al. 2010; Pogge von Strandmann et al. 2006; 2008; 2010). In addition, Li concentration and isotopic composition of potential building blocks of the continental crust, namely, basaltic arc lavas (Chan et al., 2002; Martin and Moyen, 2002; Moriguti and Nakamura, 1998a; Moriguti et al., 2004; Tomascak et al., 2002) and Archean tonalites, trondhjemites and granodiorites (TTG, (Ryan and Kyle, 2004; Teng et al., 2004)) are known. Collectively, these studies demonstrate that the δ^7Li of present-day bulk continental crust is 2-3‰ lower than that of its potential building blocks (i.e., mantle-derived basalts), which likely reflects the influence of chemical weathering on the bulk crust composition (Teng et al. 2004; 2008). Therefore, Li and its isotopes may be useful in quantifying the amount of continental crust lost through chemical weathering.

2. Mass balance model

The conceptual model of continental crust recycling is illustrated in Figure 19, where juvenile arc basalts or felsic slab melts form the input to the crust, and there are three outputs: recycled lower crust (lower crust that is lost from the continents by foundering, subduction or other processes), subducted terrigenous sediments (net output from the continent to the ocean in solid form, transported as the suspended

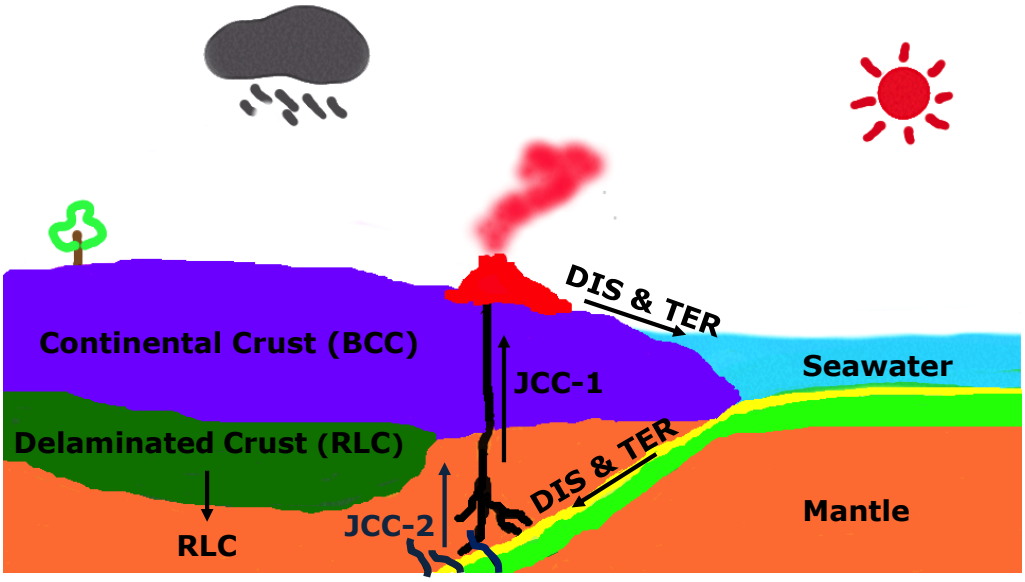

Figure 19. Cartoon illustrating the mass balance approach used for solving the weathering flux from the continents (DIS).
Juvenile crust is created via a JCC magmatic flux from the mantle that produces either a basalt (JCC-1) or felsic slab melts (e.g., in a hotter, Archean Earth) (JCC-2). There are three outputs fluxes from this juvenile crust: recycled lower crust (RLC), soluble components dissolved during weathering (DIS), which wash into the ocean and may be removed by uptake in sea floor sediments and altered basalt, and sediments derived from the continents and removed via subduction (TER). The net result of these input and outputs to the continental crust is the present-day bulk continental crust (BCC).

sediments and bed load of rivers), and the crust dissolved and removed from the continents by weathering. The net effect of these processes is a change of the composition of the continental crust, leading to the current bulk continental crust composition.

The following assumptions and definitions are applied (all variables used in this model are defined in Table 8):

The continental crust is ultimately derived from juvenile continental crust (JCC), X_i is the mass fraction of each reservoir, BCC is the present-day bulk continental crust, RLC is recycled lower crust, DIS is the mass of crust dissolved during weathering and removed via rivers, TER is terrigenous sediments removed via subduction, and the sum of the mass fraction of each reservoir is one ($X_{BCC}+X_{RLC} + X_{DIS} +X_{TER} =1$). The ^{6}Li and ^{7}Li removed from the continents due to chemical weathering is approximated by their concentration ratios in modern rivers; that is $f^i_{DIS} = f^i_{RIV}$ (f is defined below).

The mass balance model is:

$$C^i_{JCC} = X_{BCC}C^i_{BCC} + X_{RLC}C^i_{RLC} + X_{DIS}C^i_{DIS} + X_{TER}C^i_{TER} \qquad [1],$$

where, for an isotope i, the concentration of i in JCC, BCC, RLC, DIS, and TER are C^i_{JCC}, C^i_{BCC}, C^i_{RLC}, C^i_{DIS}, and C^i_{TER}. And X_{BCC}, X_{RLC}, X_{DIS} and X_{TER} are the mass fractions of BCC, RLC, DIS and TER relative to JCC, respectively. The fraction of i lost by dissolution is f^i_{DIS}, where $f^i_{DIS} = X_{DIS}\frac{C^i_{DIS}}{C^i_{JCC}}$. For example, we have $f^{^7Li}_{DIS} = X_{DIS}\frac{C^{^7Li}_{DIS}}{C^{^7Li}_{JCC}}$

Table 9. Variables used and their definitions.

Variable	Definition
X_{BCC}	mass fraction of the present-day bulk continental crust relative to JCC
X_{RLC}	mass fraction of the recycled lower crust relative to JCC
X_{DIS}	mass fraction of the dissolved crust during weathering removed via rivers relative to JCC
X_{TER}	mass fraction of the terrigenous sediments removed via subduction relative to JCC
i	an isotope (either ^{6}Li or ^{7}Li in this study)
C_{JCC}	concentration of i in JCC
C_{BCC}	concentration of i in BCC
C_{RLC}	concentration of i in DLC
C_{DIS}	concentration of i in DIS
C_{RIV}	concentration of i in river
C_{TER}	concentration of i in TER
f_{BCC}	fraction of i in BCC relative to JCC
f_{RLC}	fraction of i in RLC relative to JCC
f_{DIS}	fraction of i in DIS relative to JCC
f_{RIV}	fraction of i in river relative to JCC
f_{TER}	fraction of i in TER relative to JCC
$R_{RLC/BCC}$	ratio of mass removed by crustal recylce (X_{RLC}) compare to BCC (X_{BCC})
$R_{TER/BCC}$	ratio of mass of sediments removed by subduction (X_{TER}) compare to BCC (X_{BCC})

and $f_{DIS}^{^6Li} = X_{DIS}\frac{C_{DIS}^{^6Li}}{C_{JCC}^{^6Li}}$ for ^{7}Li and ^{6}Li, respectively. Similar definitions are applied for the fraction of *i* in the present-day bulk continental crust (BCC) and recycled lower crust (RLC). Thus, equation [1] becomes

$$f_{BCC}^{i} + f_{RLC}^{i} + f_{DIS}^{i} + f_{TER}^{i} = 1 \qquad [2].$$

Rearranging equations [1] and [2], and substituting ^{7}Li and ^{6}Li for *i* we have

$$f_{DIS}^{^7Li} = 1 - X_{BCC}\frac{C_{BCC}^{^7Li} + R_{RLC/BCC}C_{RLC}^{^7Li} + R_{TER/BCC}C_{TER}^{^7Li}}{C_{JCC}^{^7Li}}$$
$$f_{DIS}^{^6Li} = 1 - X_{BCC}\frac{C_{BCC}^{^6Li} + R_{RLC/BCC}C_{RLC}^{^6Li} + R_{TER/BCC}C_{TER}^{^6Li}}{C_{JCC}^{^6Li}} \qquad [3],$$

where $R_{RLC/BCC}$ =X_{RLC}/X_{BCC} and $R_{TER/BCC}$ =X_{TER}/X_{BCC}. Lithium concentrations and isotopic compositions in different reservoirs, such as those in JCC, BCC, RLC and TER can be estimated, along with uncertainties, from published data. Therefore, the concentration of ^{7}Li and ^{6}Li in JCC, BCC, RLC and TER can be calculated based on Li concentration and δ^7Li (correction is made for the difference in molecular weight of ^{7}Li and ^{6}Li). Inputs to the mass balance model are discussed in detail below and summarized in Table 9.

Lithium concentration and isotopic composition in JCC (juvenile continental crust) are discussed in terms of two end-member scenarios: (1) the JCC has the same Li concentration and isotopic composition as present-day arc basalts; (2) JCC is a 70:30 mixture of arc basalts and Archean TTG, which have been suggested to result from melting of subducted slabs (Qiu, 2011).

Table 10. Input parameters for mass balance model with sensitivity analysis results for scenarios one and two, and associated change in the amount of crust lost due to weathering (X_{DIS}).

Scenario 1: JCC (present arc basalt)

	[Li] (ppm)	Range††	*SI*§§	X_{DIS} range (%)	δ^7Li (‰)	Range††	*SI*§§	X_{DIS} range (%)
JCC*	6.9	4.5 - 10.6	0.48	38 - 74	3.6	2.4 - 4.8	0.08	57 - 62
BCC†	18	11 - 20	0.20	50 - 62	1.2	0 - 4	0.07	57 - 61
RLC§	3.5	1.5 - 8	0.10	58 - 64	3.6	-7.5 - 11.5	0.06	58 - 62
TER#	48	32 - 73	0.20	53 - 67	3	-1.6 - 5	0.08	58 - 63
DIS/RIV**	$1.5x10^{-3}$	--	--	--	23.4	14 - 28	0.04	59 - 62

	Best est.	Range††	*SI*§§	X_{DIS} range (%)
$R_{RLC/BCC}$	1	1.5-4.5	0.57	23 - 53
$R_{TER/BCC}$	0.3	0.2-1.1	0.27	53 - 72

Scenario 2: JCC (Archean TTG and present arc basalt)

	[Li] (ppm)	Range††	*SI*§§	X_{DIS} range (%)	δ^7Li (‰)	Range††	*SI*§§	X_{DIS} range (%)
JCC*	10.2	8 – 14	0.60	22 - 56	4	3.4 - 4.5	0.07	42 - 45
BCC†	18	11 - 20	0.34	31 - 47	1.2	0 - 4	0.12	40 - 45
RLC§	5.1	1.5 - 8	0.19	38 - 47	3.6	-7.5 - 11.5	0.14	41 - 47
TER#	48	32 - 73	0.35	35 - 53	3	-1.6 - 5	0.15	41 - 48
DIS/RIV**	$1.5x10^{-3}$	--	--	--	23.4	14 - 28	0.10	43 - 47

	Best est.	Range††	*SI*§§	X_{DIS} range (%)
$R_{RLC/BCC}$	1	1.1-3.1	0.67	14 - 42
$R_{TER/BCC}$	0.3	0.2-1.1	0.43	34 - 60

Note: * From the compilation of current arc basalt and Archean TTG data (see Figure 20). † From Teng et al. (2008) and references therein. § The optimal value of [Li] is assumed to be half that of the original crust (JCC), with the same δ^7Li. # From Teng et al. (2004) and references therein. ** World river average from Huh et al., (1998). †† All ranges are discussed in text, compilation of [Li] and δ^7Li in JCC for scenario one are shown in Figure 20A and 20B; and [Li] and δ^7Li in JCC for scenario two were calculated based on weighted distribution of Archean TTG (Figure 20C and 20D) and mean of arc basalts. §§ Sensitivity analyses are performed to evaluate the uncertainty on the mass balance model. Sensitivity index, defined as $SI = [X_{max}-X_{min}]/X_{max}$, was calculated for each parameter.

In scenario one, we assume that present-day arc basalts are representative of JCC through time. The lithium concentration and isotopic composition in JCC are compiled from literature data for arc basalts (SiO_2=45~55% wt.) (Chan et al., 2002; Magna et al., 2006; Moriguti and Nakamura, 1998a; Moriguti et al., 2004a; Ryan and Kyle, 2004b; Tomascak et al., 2002) and the GEOROC database. Overall, 552 Li concentrations and 75 δ^7Li values are available, worldwide. Data are compiled in *SI dataset2* and histograms of Li concentration and δ^7Li are plotted in Figures 20A and 20B. Lithium concentrations in arc basalts follow a log-normal distribution, having a mean of 6.9 ppm, with a one sigma lower and upper limit of 4.5 ppm and 10.6 ppm, respectively. The δ^7Li of arc basalts follow a normal distribution, with a mean δ^7Li of +3.6‰ and a standard deviation of 1.2. Because arc basalts may contain enhanced Li from subducted terrigeneous sediments or altered oceanic crust, and this Li ultimately derives from weathering of continental crust (e.g., Chan et al. 2002), alternative juvenile basaltic additions to the crust that lack such potential crustal input (e.g., MORB and OIB, rather than island arc basalt), and the resulting influence on the mass balance outcome, are discussed below.

In scenario two, we assume that 30% of the JCC is composed of Archean tonalite-trondhjemite-granodiorite (TTG), which may have formed as slab melts, and the remaining 70% is present-day arc basalts (assuming Archean basalts have the same Li compositions as present-day arc basalts). This proportion of TTG derives from estimates of Taylor and McLennan (2009), who suggest that 60% of the continental crust formed in the Archean and that this Archean crust is half basalt and half TTG, yielding 30% total TTG in the bulk crust, with the remainder assumed to

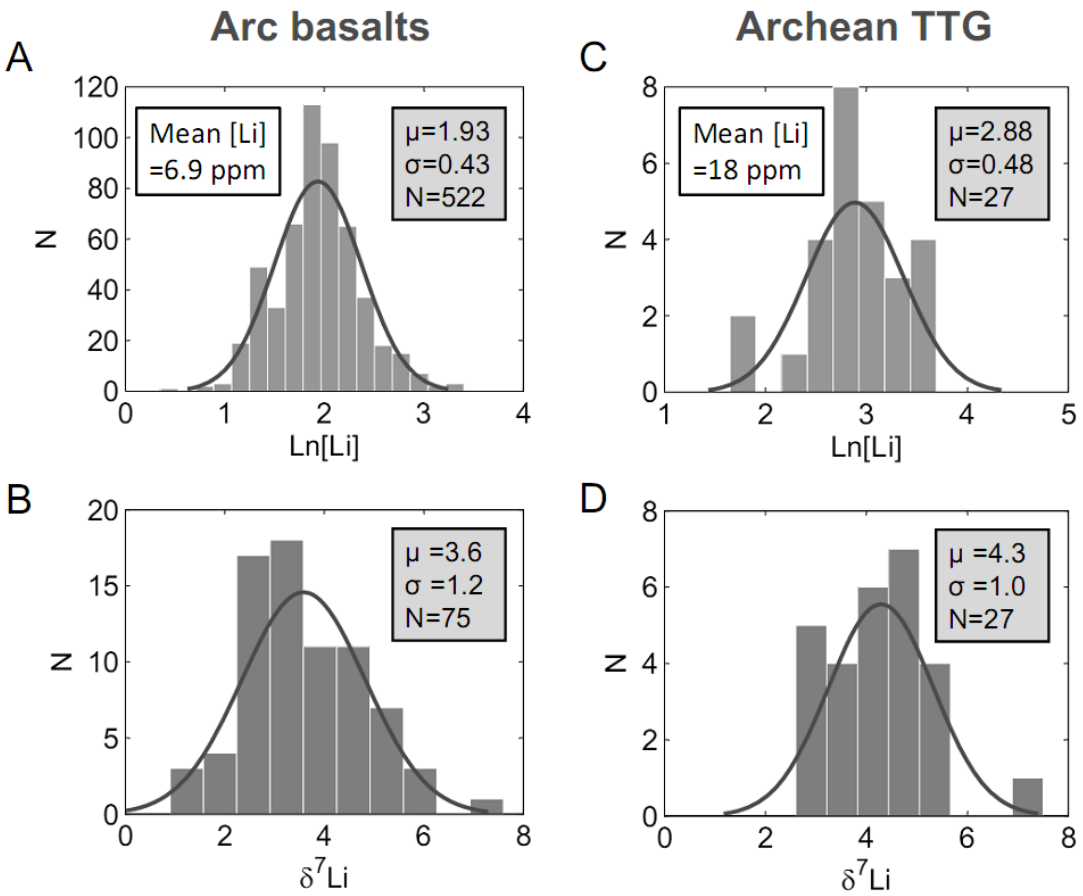

Figure 20. Histogram of lithium concentrations and isotopic compositions in basaltic arc lavas and Archean TTGs.

μ, σ, and N represent mean, standard deviation, and number of the sample population. (A) In arc basalts, Li concentration follows a log-normal (natural log) distribution with a mean of 6.9 ppm and upper and lower limits of 10.6 ppm and 4.5 ppm, respectively. (B) δ^7Li in arc basalts matches a normal distribution curve, with a mean of +3.6 and a standard deviation of 1.2. (C) In Archean TTGs, Li concentration follows a log-normal (natural log) distribution with a mean of 18 ppm and upper and lower limits of 30 ppm and 11 ppm, respectively. (D) δ^7Li in Archean TTGs matches a normal distribution curve, with a mean of +4.3 and a standard deviation of 1.0.

be arc basalts. This proportion of continental crust formed in the Archean is in agreement with crust preservation curves based on detrital zircon Hf model ages (Kemp and Hawkesworth, 2012 and references therein). Limits on the proportion of TTG in JCC, and its influence on the mass balance outcome, are discussed in the following section.

There are two sources of Li isotopic data for TTG (Teng et al. 2004; Qiu 2011). Teng et al. (2008) report lithium data for composite Archean TTG from the North China Craton. Qiu (2011) reports Li concentration and isotopic compositions for a variety of Archean TTG, which range from inferred juvenile melts (e.g., the "Sanukatoids" of the Superior Craton, (Shirey and Hanson, 1984)) to melts of thickened basaltic crust (e.g., TTG of Barberton Mountain Land, South Africa, (Clemens et al., 2006)). Because granulite-facies TTG of the Scourian Complex have unusually low Li concentration (3.0 to 12.5 ppm) and highly variable δ^7Li (+0.2‰ to +11.7‰), suggesting that Li was lost and possibly fractionated by deep crustal processes (Teng et al. 2008), we confine our compilation to TTG that have experienced amphibolite-facies or lower grades of metamorphism. These data are compiled in the *SI dataset2,* and histograms of Li concentration and δ^7Li of these Archean TTGs are plotted in Figures 20C and 20D. Li concentrations of juvenile Archean TTGs follow a log-normal distribution, having a mean of 18 ppm, with an upper limit of 30 ppm and a lower limit of 11 ppm. The δ^7Li of the Archean TTGs are fit to a normal distribution with a mean of +4.3‰ and a standard derivation of 1.0.

Using the average Li concentration of 18 ppm, along with its upper and lower limits, we calculate the average Li concentration in the JCC for scenario two is 10

ppm, with a lower and upper limit of 8 ppm and 14 ppm, respectively. Since δ^7Li in Archean TTG show mantle-like values of +4.3‰ ± 1.0 (1σ) (Teng et al. 2008 and Qiu 2011), we calculate a weighted average δ^7Li of +4.0 for scenario two JCC, with a lower limit of +3.4‰ and an upper limit of +4.5‰.

Li concentration and isotopic composition of the current bulk continental crust (BCC) is 18 ppm and +1.2‰, respectively (Teng et al. 2008). Because Li is a moderately incompatible element, recycled lower crust, which forms as cumulates or residues, should have a lower concentration than its juvenile parent (JCC). Thus, we assume a Li concentration of either 3.5 ppm or 5.1 ppm for RLC, which is half that of the juvenile continental crust value for scenario one and two, respectively. Such concentrations are similar to or lower than the average Li concentration of the present lower continental crust (8 ppm; (Teng et al., 2008; Qiu et al., 2011)). It is assumed that the Li isotopic composition in RLC is the same as that of JCC, since there is no significant isotopic fractionation during basalt differentiation (Albarède, 1989). Li concentration and isotopic composition in TER can be approximated from the average [Li] and δ^7Li of terrigenous sediments of 48 ppm and +3‰, respectively (*SI dataset1 and* Chan et al., 2006).

Adopting the above values leaves four unknowns in equation [3]: f^i_{DIS}, $R_{RLC/BCC}$, $R_{TER/BCC}$ and X_{BCC}. In addition, we have

$$\frac{f^{^7Li}_{DIS}}{f^{^6Li}_{DIS}} = \frac{X_{DIS}\dfrac{C^{^7Li}_{DIS}}{C^{^7Li}_{JCC}}}{X_{DIS}\dfrac{C^{^6Li}_{DIS}}{C^{^6Li}_{JCC}}} = \frac{\dfrac{C^{^7Li}_{RIV}}{C^{^7Li}_{JCC}}}{\dfrac{C^{^6Li}_{RIV}}{C^{^6Li}_{JCC}}} = \frac{\dfrac{C^{^7Li}_{RIV}}{C^{^6Li}_{RIV}}}{\dfrac{C^{^7Li}_{JCC}}{C^{^6Li}_{JCC}}} \qquad [4],$$

Equation [3] can now be expressed in terms of both ^{7}Li and ^{6}Li and, according to assumption two, the ratio of these two equations should be related to the lithium isotopic composition of modern rivers (RIV), so we have

$$\frac{\frac{C^{7}_{RIV}}{C^{6}_{RIV}}}{\frac{C^{7}_{JCC}}{C^{6}_{JCC}}} = \frac{1 - X_{BCC}\dfrac{C^{7}_{BCC} + R_{RLC/BCC}C^{7}_{RLC} + R_{TER/BCC}C^{7}_{TER}}{C^{7}_{JCC}}}{1 - X_{BCC}\dfrac{C^{6}_{BCC} + R_{RLC/BCC}C^{6}_{RLC} + R_{TER/BCC}C^{6}_{TER}}{C^{6}_{JCC}}} \qquad [5].$$

We use the world river data compilation of Huh et al. (1998), who report that the discharge-weighted average Li concentration is 1.5 ppb and $\delta^{7}Li$ is +23.4‰. These values are adopted for the soluble component that is removed from the continents during chemical weathering (DIS) over the course of Earth history. Then the only remaining unknown, X_{BCC}, can be solved using data from Table 9, providing that the ratio by mass of recycled lower crust compared to the mass of BCC ($R_{RLC/BCC}$) and the ratio by mass of terrigenous sediment removed by subduction compared to the mass of BCC ($R_{TER/BCC}$) are assumed. Based on studies from the Sierra Nevada Batholith, which represents a Cretaceous continental arc in California, USA (Lee et al., 2006; 2007), $R_{RLC/BCC} = X_{RLC}/X_{BCC} = 1$. $R_{TER/BCC}$ can be calculated from the average modern subducted sediment flux. Global subducted sediment flux has been estimated by various methods, including O and Nd isotopes, and sedimentary records from Deep Sea Drilling Projects (Albarède, 1989; Clift et al., 2009; Depaolo, 1983; Plank and Langmuir, 1998; Rea and Ruff, 1996; Simon and Lecuyer, 2005), and varies from 1.1×10^{12} to 4.4×10^{12} kg/yr, assuming the average density of the subducted sediments is 2.65 g/cm^{3} (Rea and Ruff, 1996). Thus, $R_{TER/BCC} = 0.33$, assuming that the average subducted sediment flux is constant through time at

2.1×10^{12} kg/yr and continental crust formed since 3.5 Ga, approximately the start of the geologic record (see Kemp and Hawkesworth 2012, and references therein). Below, we evaluate how changing the input parameters affects the outcome of the model.

3. Results and uncertainties

Using the above assumptions and inputs for scenario one, the calculated X_{BCC} is 0.17. Therefore, the mass fraction of BCC and RLC are both 17%, and the mass fraction lost to chemical weathering (X_{DIS}) is 60%. For scenario two, the mass fraction of BCC and RLC are both 24%, and the mass fraction lost to chemical weathering (X_{DIS}) is 43%. Both results are displayed in Figure 21.

We performed sensitivity analyses to evaluate which of the input parameters have the greatest influence on the results and whether it is possible for X_{DIS} to equal zero. The simplest form of sensitivity analysis is the One-At-A-Time measure (Hamby, 1994), which repeatedly varies one parameter at a time while keeping others constant. A simple way to quantitatively determine the sensitivity of different parameters is to calculate the relative difference of output between maximum and minimum values of the varying parameters (Hamby, 1994). The sensitivity index, defined as $SI=\frac{X_{max} - X_{min}}{X_{max}}$, was calculated for each series of the input parameters. The results are provided in Table 9 (see *SI calculation spreadsheet* for details) and are discussed below.

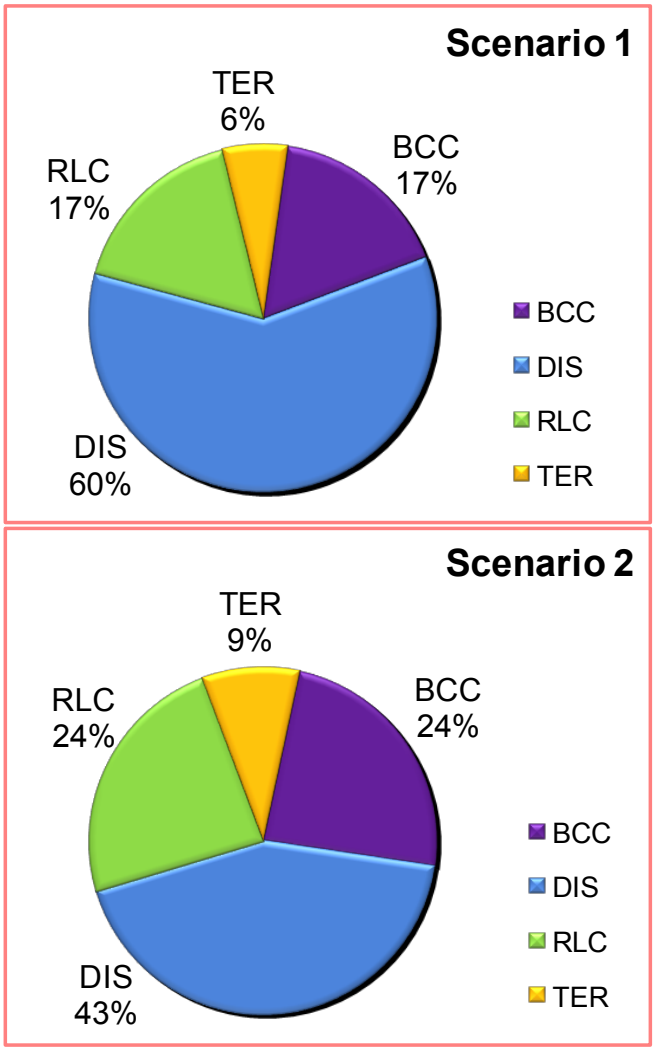

Figure 21. Pie diagrams of the optimal model results for two end-member scenarios, illustrating different portions of crustal types that must be added together to equal the juvenile continental crust.

For the crustal input, for scenario one was allowed to vary from 4.5 to 10.6 ppm and δ7Li values from +2.4‰ to +4.8‰ (the one sigma seen in arc basalts) during the parameter sensitivity analysis. For scenario two, JCC concentration was allowed to vary from 8 to 14 ppm and δ^7Li values from +3.4‰ to +4.5‰ (see above discussion); an in-depth discussion of the constraints on the proportion of primary TTG in the continental crust, which strongly influences the Li concentration in scenario two, is provided in the next sections, along with consideration of the influence of using other types of primary basalt for the basaltic component of JCC. For BCC, Li concentration was allowed to range from 11 to 20 ppm, based on the range of published values (Rudnick and Gao 2003 and references therein). The optimal δ^7Li of the BCC (+1.2‰) was calculated based on weighted δ^7Li of the upper, middle and lower crust, with their corresponding weight proportions of 0.32:0.29:0.39 (Rudnick and Fountain, 1995; Rudnick and Gao, 2003b). However, there are uncertainties associated with Li concentrations and δ^7Li of each crustal layer. Keeping the optimal Li concentration estimates for each crustal layer from Teng et al. (2004; 2008) and using their estimated δ^7Li uncertainty, we can propagate the uncertainty for δ^7Li in each layer and calculate the weighted δ^7Li of the BCC, which is +1.2‰ ± 5 (1σ). However, the δ^7Li of BCC is unlikely to be lower than that of the upper continental crust (UCC) or higher than that of the mantle. Therefore, we allowed δ^7Li of the BCC to vary from 0‰ (UCC average) (17) to +4‰ (mantle average) (Tomascak et al., 2008 and references therein).

Li concentration of RLC was allowed to vary between the concentration of the mantle (1.5 ppm, (McDonough and Sun, 1995)) and the lower continental crust (8

ppm) (Qiu et al., 2011b; Teng et al., 2008). δ^7Li of RLC was estimated from analyses of eight granulite xenoliths reported in Teng et al. (2008), with a concentration weighted average value of +2.5‰ and a simple average of +1.6‰ ± 8.9 (1σ).

Although δ^7Li values vary from -14‰ to +14.3‰ in granulite xenoliths, the isotopic heterogeneity of many of these samples was interpreted by Teng et al. (2008) to reflect the combined effects of isotopic fractionation during prograde metamorphism and kinetic Li isotopic fractionation associated with basaltic intrusions. Recent results for granulite-facies metapelites and metabasites from the Ivrea-Verbano Zone, Italy, suggest a concentration-weighted average δ^7Li of the lower crust in this region of 1.0‰ (Qiu et al., 2011b). Nonetheless, the average δ^7Li value of RLC is allowed to vary from -7.5‰ to +11.5‰ for the sensitivity analysis, based on the one-sigma variation in δ^7Li from the eight granulite xenoliths studied by Teng et al. (2008) (i.e., +2.5‰ ± 9).

A new estimate of global subducting sediment (GLOSS-II) reports Li concentration of 45 ± 3 ppm (Plank, 2012); δ^7Li of terrigenous turbidities and pelagic clays vary from -1.6‰ to +5‰ (Chan et al. 2006). However, GLOSS includes chemical and biogenic sediments, such as porcellanite, chert, ooze, radiolarite, and chalk, and it may therefore not reflect pure terrigenous Li values. Compiled Li concentrations of terrigenous sediments using recent ICP-MS data yield an average Li concentration of 48 ppm in TER, with lower and upper limits of 32 ppm and 73 ppm (1σ), respectively (*SI dataset 1*). Therefore, we adopt values for TER ranging from 32 to 73 ppm and -1.6‰ to +5‰ in the sensitivity analysis. The δ^7Li values for individual rivers range from +6.0‰ (Huh et al. 1998) to +43.7‰ (Pogge von

Strandmann et al. 2006). Our compilation of Li isotopic compositions in rivers (*SI dataset 1*) shows an average δ^7Li of +21‰ ± 7 (1σ). Thus, δ^7Li values varying from +14‰ to +28‰ were used for the parameter sensitivity analysis.

Of all the input parameters tested, X_{DIS} is most sensitive to the Li concentration adopted for JCC and BCC. For example, in scenario two, allowing Li concentration in JCC to vary within the one-sigma limits results in the largest range in X_{DIS}, from 22% to 56%. Similarly, allowing the Li concentration in BCC to vary within different authors' estimates (see Rudnick and Gao 2003, and references therein), results in a relatively large range in X_{DIS}, from 31% to 47% (see Table 9 and *SI calculation spreadsheet* for details).

Only one mass fraction ratio of RLC to BCC ($R_{RLC/BCC}$ =1), is considered in the mass balance model. In the limiting case of no lower crustal recycling, $R_{RLC/BCC}$ = 0, we obtain X_{DIS} = 75% and 63%, for scenarios one and two, respectively. However, we consider this case to be unlikely, based on evidence from a variety of Phanerozoic settings for such recycling (2012). Furthermore, according to Plank (2005), 25-60% of the JCC (X_{RLC} = 25-60%) is lost due to foundering of mafic cumulates and restites, which corresponds to a range of $R_{RLC/BCC}$ from 1 to 4 and X_{DIS} of 23 to 53% and 14 to 43% for scenarios one and two, respectively. The latter provides the minimum estimate of X_{DIS} for any of the various outcomes (Table 9).

Proportion of tonalite-trondhjemite-granodiorite in juvenile continental crust

The above exercise evaluates the uncertainties in the mass balance calculation and identifies the most important parameters (i.e., Li concentration in JCC and BCC) that control the calculated continental crustal mass loss due to weathering, assuming

that ≤30% of JCC comprises Archean TTG. Here we evaluate the bounds that can be placed on the proportion of TTG in JCC and how these bounds influence the weathering outcome. Since the mass lost due to weathering decreases with increasing proportion of TTG in juvenile crust, it is important to obtain a robust estimate of the maximum proportion of TTG in the crust in order to determine the minimum mass lost due to weathering.

We assume that addition of juvenile TTG is primarily confined to the Archean (e.g., Martin 1986), so a first step in placing bounds on the juvenile TTG component is to estimate the amount of present-day continental crust that formed in the Archean. Based on global geological maps, Goodwin (1996) estimated that Archean crust comprises 7% of total crust. Such an estimate is certainly a minimum, as Archean crust is often reworked by later events. A recent compilation of Lu-Hf model ages in detrital zircon suggests that Archean crust may constitute up to 60% of the present continental crust (Belousova et al., 2010 and references therein), an estimate that coincides with the previous estimate of Taylor and McLennan (2009). Given that Archean cratons are generally regions of low surface heat flow (Jaupart and Mareschal, 2012), these data, coupled with heat production for typical TTG and arc basalt, can be used to estimate the proportion of Archean crust that is TTG. A 40 km thick crust (Christensen and Mooney, 1995) composed of average Archean TTG of Condie (2005) would produce a surface heat flow of 44.3 mW/m^2, whereas 40 km of average arc basalt (Kelemen et al., 2003) generates a surface heat flow of 12.4 mW/m^2. Given that the average heat flow in Archean crust is 41 mW/m^2 (Nyblade and Pollack, 1993) and the minimum Moho heat flux is estimated to be

11 mW/m^2 (Jaupart and Mareschal, 2012), the maximum surface heat flux generated in average Archean crust is 29 mW/m^2, which places an upper limit on the proportion of TTG in Archean continental crust of ~55%. Combined with the limits discussed above, we estimate that the percentage of TTG in the entire juvenile crust can range from 4% to 33%. Therefore, even in the extreme case, where 33% of the JCC is composed of Archean TTG, yielding a Li concentration of 15 ppm for JCC, the weathering mass loss is still ~25% of total juvenile continental crust. The proportion of Archean TTG would need to rise to 59% of the mass of the JCC in order for the weathering mass flux to drop to zero. However, such a large mass fraction of TTG is unlikely, given geological constraints.

The Juvenile Basaltic Crust

We have chosen average modern arc basalt as the juvenile basaltic end member. How might the picture change if other types of basalts are considered instead, since subducted terrigenous sediments may influence the Li composition of arc basalt (Plank 2012)? Data for Li in MORB compiled from PetDB, supplemented with data from recent Li isotope studies (Elliott et al., 2006; Tomascak et al., 2008) and Li in OIB from the GEOROC database, are reported in the *SI dataset2* and shown in Figure 22. Like arc basalts, Li concentrations in both MORB and OIB follow log-normal distributions, having means of 5.9 and 5.6 ppm, respectively, which are slightly lower compared to the mean of arc basalts, 6.9 ppm. The slight enrichment of Li seen in arc basalts is likely due to incorporation of Li from subducted sediments (Plank 2012). In this sense, Li lost from the continental crust in TER, partially re-enters the crust in arc basalts. Thus, using arc basalt for the JCC rather than MORB or

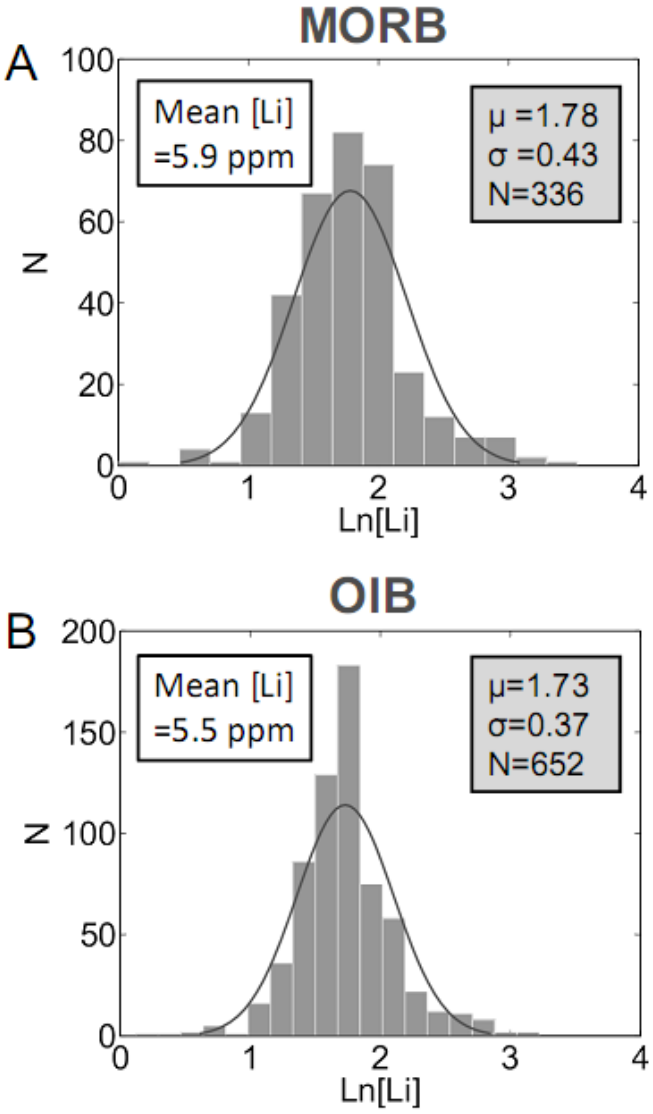

Figure 22. Histogram of lithium concentrations in MORB and OIB.
μ, σ, and N represent mean, standard deviation, and number of the sample population.
(A) In MORB, Li concentration follows a log-normal (natural log) distribution with a mean of 5.9 ppm and upper and lower limits of 9.1 ppm and 3.9 ppm, respectively.
(B) In OIB, Li concentration follows a log-normal (natural log) distribution with a mean of 5.6 ppm and upper and lower limits of 8.2 ppm and 3.9 ppm, respectively.

OIB accounts for this Li "short circuit". Perhaps more importantly, during the sensitivity test discussed above, Li concentration in JCC was allowed to be as low as 4.5 ppm, which encompasses the mean Li concentrations of MORB and OIB. Therefore, the choice of basaltic source does not significantly influence the mass balance model.

In summary, the global uncertainty (accounting for variations in all parameters) in the mass balance model is large. However, even with these uncertainties, we show that a considerable mass (at least 15%, with a best estimate of ~45%) of the juvenile continental crust was lost via incongruent chemical weathering, given the best available constraints on the input parameters in this first-order mass balance model.

4. Model prediction and discussion

We show that zero mass loss due to chemical weathering is not a possible outcome, which agrees with observations from other stable isotope systems, such as oxygen (Simon and Lecuyer, 2005), that the bulk continental crust is isotopically distinct from the mantle due to the cumulative effects of chemical weathering over Earth history. Chemical weathering is one of the mechanisms that preferentially removes soluble elements, such as magnesium–abundant in easily weathered mafic minerals (e.g., olivine and pyroxene), and leaves silicon- and aluminium-rich, weathering-resistant minerals (e.g., quartz and clays). Therefore, the mass balance model and its accompanying uncertainty estimates indicate that chemical weathering plays an important role in shifting the continental crust composition from basaltic (SiO_2 =45 ~ 55 wt. %) to andesitic (SiO_2 = 57 ~ 64 wt. %). This quantification of the

amount of chemical weathering mass loss (> 15%) over geological history, is consistent with the 20% of chemical weathering mass loss suggested by Lee et al. (2008), and provides a first-order constraint for further investigation of the "Crust Composition Paradox".

Important predictions from this study also include total mass of dissolved continental crust, total mass of subducted continental crust and total mass of continental crust formed over Earth's history, all of which are shown in Table 10 for scenarios one and two. We calculate the mass ratio of different components relative to the BCC. The mass of dissolved continental crust is three and two times that of the mass of BCC for scenarios one and two, respectively, while the total mass of the juvenile continental crust (JCC) is six and four times that of BCC for scenarios one and two, respectively. Interestingly, both the mass of dissolved continental crust and total mass of juvenile continental crust in scenario two are twice as much as those in scenario one, although the mass of subducted continental crust (TER) is about 30% of the mass of BCC in both scenarios.

The results from this study can also be used to estimate the global average chemical weathering rate over Earth history. The minimum current chemical weathering rate estimated from dissolved material originating from rock weathering in the 60 largest rivers on Earth is about 2.1×10^9 t/yr (Gaillardet et al., 1999). This estimate does not incorporate weathering of basalts in arcs, where the chemical weathering rate is higher compared to the average continental silicate weathering rate

Table 11. Important predictions from this study.

	Scenario 1	Scenario 2		Scenario 1	Scenario 2
M_{DIS} (kg)	$7.8x10^{22}$	$3.9x10^{22}$	M_{DIS}/M_{BCC}	4	2
M_{TER} (kg)	$7.8x10^{21}$	$8.3x10^{21}$	M_{TER}/M_{BCC}	0.4	0.4
M_{JCC} (kg)	$1.3x10^{23}$	$9.2x10^{22}$	M_{JCC}/M_{BCC}	6	4
CWR (kg/yr)	$2.2x10^{13}$	$1.1x10^{13}$			

Note: $M_{BCC} = M_{RLC} = 2.2x10^{22}$kg is used for the above calculations. M_{DIS} is total mass of dissolved continental crust, M_{TER} is total mass of subducted continental crust, M_{JCC} is total mass of continental crust formed over geologic time and CWR is predicted average chemical weathering rates over time.

(e.g., Dessert et al., 2001; Louvat and Allègre, 1997); it also does not include the dissolved continental material lost via groundwater flow into the oceans, which may be as much as 50% of that contributed by rivers (Zektser and Loaiciga, 1993), although the overall flow of groundwater into the ocean is not likely to be more than 6% of the total continental runoff (Burnett et al., 2003). Thus, this chemical weathering rate estimate is considered a minimum estimate. The mass of the current bulk continental crust, M_{BCC}, is ~2.2×10^{22} kg (Peterson and Depaolo, 2007). The optimal X_{DIS} varies between 43% (X_{BCC} = 24%) and 60% (X_{BCC} = 17%) for scenario two and one, respectively; the mass lost during chemical weathering, M_{DIS}, can be estimated from X_{DIS}/X_{BCC}. If we assume that the continental crust has mainly formed since 3.5 Ga, then the average global chemical weathering rate (CWR) can be calculated as ~1.1×10^{10} to ~2.2×10^{10} t/yr, for scenarios two and one, respectively.

The choice of age of the continental crust does not significantly influence this outcome. For example, if we assume crust formed mainly since 4.5 Ga or 2.7 Ga, the average CWR will change to ~0.9×10^{10} and ~1.5×10^{10} t/yr, respectively, for the optimal values in scenario two. This range is up to an order of magnitude higher than the estimate of the minimum present-day weathering rate from Gaillardet et al. (1999) and may reflect the greater weathering rate in basaltic arcs, continental dissolved mass transported by groundwater and/or an increased weathering rate in the past.

Finally, the assumption that the Li isotopic composition of material removed from the continent due to chemical weathering can be represented by modern rivers may not be valid. Li weathering fluxes from rivers may have changed over the Cenozoic, according to Li isotope studies on forams (Misra and Froelich, 2012).

However, the influence of δ^7Li_{DIS} on the model output is relatively small, and so large changes in the riverine isotopic composition are unlikely to significantly affect the outcome (e.g., in scenario two, if δ^7Li_{DIS} is lower by 9‰, the average river water δ^7Li_{DIS} decreases from the current day average 23‰ to 14‰, and X_{DIS} increases from 43% to 47%).

5. Conclusions

Using Li concentration and isotope data in a mass balance model, a significant percentage (at least 15%, with best estimates of ~45%) of the juvenile continental crustal mass is found to be lost from the continents due to chemical weathering. The mass balance model is particularly sensitive to the composition of primary crustal additions. The accumulated percentage of mass loss due to chemical weathering leads to an average global chemical weathering rate (CWR) of ~ 9×10^9 to 2×10^{10} t/yr since 3.5 Ga, which is about an order of magnitude higher than the current (minimum) estimates based on modern rivers. While we cannot constrain the exact portion of crustal mass loss via chemical weathering, given the uncertainties of the calculation, we can demonstrate that the weathering flux is non-zero. Therefore, chemical weathering must play a role in the evolution of the composition and mass of the continental crust.

Appendices

This chapter contains supporting materials (SI dataset 1, 2 and 3) online at www.pnas.org/lookup/suppl/doi:10.1073/pnas.1115671108/-/DCSupplemental.

Chapter 6: Summary and future work

With the advent of MC-ICP-MS, many studies have focused on non-traditional stable isotopes (e.g., Li, Mg, Ca, Fe, Cu, Zn, Mo and Hg). Due to their large mass difference and significant isotope fractionation potential, Li isotopes have been used as a tracer of various geological processes, including fluid-rock interactions in subduction zones, seafloor alteration, metamorphic dehydration, and continental weathering. Compared to Li isotopes, magnesium isotopes are less well studied, but have increasingly been used for tracing continental weathering. Chemical weathering, in particular, is important in changing the mass and composition of the continental crust, as well as regulating the global CO_2 cycle. Therefore, this dissertation focuses on understanding Li and Mg isotopic behavior during chemical weathering, and exploring Li and Mg isotopes as tracers of continental weathering. The main conclusions drawn from this dissertation include:

1. This study demonstrates the open and dynamic characteristics of chemical weathering of basalt. Leaching, secondary mineral formation, and eolian addition are the main processes controlling lithium concentration and isotopic composition in bauxites developed on basalts.
2. The $\delta^{26}Mg$ values in bauxites correlate with the abundance of gibbsite. The heaviest samples have the greatest gibbsite abundance, demonstrating that Mg partitioning between water and gibbsite leads to large isotopic fractionation. The results show that chemical weathering produces

isotopically light Mg in water, leaving an isotopically heavy regolith within the continental crust.

3. The Li isotopic compositions of dissolved loads in streams draining only basalts are quite variable and show seasonal variation, but are not sensitive to distance from the coast or climate; the δ^7Li may reflect chemical weathering intensity, with lower δ^7Li corresponding to higher weathering intensity.
4. The quantification of continental mass loss due to chemical weathering indicates that at least 15% of the original mass of the juvenile continental crust may have been lost in this way, and perhaps as much as 60%, with a best estimate of approximately 45% over the Earth's history.
5. The study demonstrates that both Li and Mg isotopes have the potential to be useful in tracing continental chemical weathering, especially for extreme weathering conditions, where strong depletion of elements occurs. Moreover, this study corroborates previous suggestions that significant mass loss due to chemical weathering is one of the possible mechanisms that drove the bulk continental crustal composition from basaltic to andesitic.

The work done in this dissertation provides some advances in understanding Li and Mg isotopic behavior during chemical weathering of basalts and constraints on quantifying the mass loss of juvenile continental crust due to chemical weathering. Nevertheless, there is still much to be learned. The following paragraphs describe

future study directions that will serve to enhance our understanding of continental weathering.

Although Li isotopic fractionation factors between water and secondary minerals, such as gibbsite, kaolinite, and smectite, have been determined experimentally, few studies have focused on determining Mg isotopic fractionation factors between aqueous phases and different silicate minerals, especially those commonly produced during chemical weathering (such as kaolinite, gibbsite, and goethite). This is important because we only know the direction and magnitude of Mg isotopic fractionation in natural environments and the fractionation during weathering is controlled by secondary minerals. But how exactly Mg isotopes fractionate is still unknown. For example, is it by adsorption onto the surface of minerals or absorption into the secondary minerals? Therefore, experimental investigations of Mg isotopic fractionation factors between aqueous phases and minerals are in great need.

The continental mass loss due to chemical weathering is currently not well constrained. Better quantification of mass loss via chemical weathering on the mass and compositional evolution of the continental crust is needed, especially using multi-proxy approaches, such as Sr isotopes. Sr isotopes have a few advantages for this purpose: 1) Large amounts of Sr data are available in the literature, including Sr isotopes in rivers, soils, sediments, as well as igneous rocks; 2) Sr is relative abundant in silicate rocks and waters; 3) Sr is soluble and can be easily transported during continental weathering.

Other non-traditional stable isotopes, such as Fe, Zr, and Ti, behave differently (insoluble and/or multiple oxidation states) than Li and Mg (soluble and

single oxidation state) during geological processes. Therefore, coupled study of these isotopes with Li and Mg systems in the weathering regime will give a more complete picture of processes.

Bibliography

Albarède, F., 1989. Sm-Nd Constraints on the growth rate of continental crust. Tectonophysics 161, 299-305.

Albarède, F., 1998. The growth of continental crust. Tectonophysics 296, 1-14.

Anderson, A.T., 1982. Parental basalts in subduction zones - implications for continental evolution. Journal of Geophysical Research 87, 7047-7060.

Arndt, N.T., Goldstein, S.L., 1989. An open boundary between lower continental crust and mantle: its role in crust formation and crustal recycling. Tectonophysics 161, 201-212.

Aulbach, S., Rudnick, R.L., McDonough, W.F., 2008. Li-Sr-Nd isotope signatures of the plume and cratonic lithospheric mantle beneath the margin of the rifted Tanzanian craton (Labait). Contributions to Mineralogy and Petrology 155, 79-92.

Balistrieri, L.S., Borrok, D.M., Wanty, R.B., Ridley, W.I., 2008. Fractionation of Cu and Zn isotopes during adsorption onto amorphous Fe(III) oxyhydroxide: Experimental mixing of acid rock drainage and ambient river water. Geochimica et Cosmochimica Acta 72, 311-328.

Barth, M.G., McDonough, W.F., Rudnick, R.L., 2000. Tracking the budget of Nb and Ta in the continental crust. Chemical Geology 165, 197-213.

Belousova, E.A., Kostitsyn, Y.A., Griffin, W.L., Begg, G.C., O'Reilly, S.Y., Pearson, N.J., 2010. The growth of the continental crust: Constraints from zircon Hf-isotope data. Lithos 119, 457-466.

Bergquist, B.A., Boyle, E.A., 2006. Iron isotopes in the Amazon River system: Weathering and transport signatures. Earth and Planetary Science Letters 248, 54-68.

Berner, R.A., 1990. Atmospheric carbon-dioxide levels over phanerozoic time. Science 249, 1382-1386.

Berner, R.A., Lasaga, A.C., Garrels, R.M., 1983. The carbonate-silicate geochemical cycle and its effect on atmospheric carbon-dioxide over the past 100 million years. American Journal of Science 283, 641-683.

Black, J.R., Yin, Q.Z., Casey, W.H., 2006. An experimental study of magnesium-isotope fractionation in chlorophyll-a photosynthesis. Geochimica et Cosmochimica Acta 70, 4072-4079.

Bogatyrev, B.A., Zhukov, V.V., Tsekhovsky, Y.G., 2009. Formation conditions and regularities of the distribution of large and superlarge bauxite deposits. Lithology and Mineral Resources 44, 135-151.

Bolou-Bi, E.B., Poszwa, A., Leyval, C., Vigier, N., 2010. Experimental determination of magnesium isotope fractionation during higher plant growth. Geochimica et Cosmochimica Acta 74, 2523-2537.

Brenot, A., Cloquet, C., Vigier, N., Carignan, J., France-Lanord, C., 2008. Magnesium isotope systematics of the lithologically varied Moselle river basin, France. Geochimica et Cosmochimica Acta 72, 5070-5089.

Brimhall, G.H., Dietrich, W.E., 1987. Constitutive mass balance relations between chemical composition, volume, density, porosity, and strain in metasomatic

hydrochemical systems – results on weathering and pedogenesis. Geochimica et Cosmochimica Acta 51, 567-587.
Burnett, W.C., Bokuniewicz, H., Huettel, M., Moore, W.S., Taniguchi, M., 2003. Groundwater and pore water inputs to the coastal zone. Biogeochemistry 66, 3-33.
Busacca, A.J., 1989. Long quaternary record in eastern Washington, U.S.A, Interpreted from multiple buried paleosols in loess. Geoderma 45, 105-122.
Calvet, R., Prost, R., 1971. Cation migration into empty octahedral sites and surface properties of clays. Clays and Clay Minerals 19, 175-186.
Carlson, R.W., Lugmair, G.W., Macdougall, J.D., 1981. Columbia River volcanism: the question of mantle heterogeneity or crustal contamination. Geochimica et Cosmochimica Acta 45, 2483-2499.
Chan, L.-H., Leeman, W.P., Plank, T., 2006a. Lithium isotopic composition of marine sediments. Geochemistry Geophysics Geosystems 7, Q06005.
Chan, L.H., Edmond, J.M., Thompson, G., Gillis, K., 1992. Lithium isotopic composition of submarine basalts-implication for the lithium cycle in the oceans. Earth and Planetary Science Letters 108, 151-160.
Chan, L.H., Leeman, W.P., Plank, T., 2006b. Lithium isotopic composition of marine sediments. Geochemistry Geophysics Geosystems 7.
Chan, L.H., Leeman, W.P., You, C.F., 2002. Lithium isotopic composition of Central American volcanic arc lavas: implications for modification of subarc mantle by slab-derived fluids: correction. Chemical Geology 182, 293-300.
Christensen, N.I., Mooney, W.D., 1995. Seismic velocity structure and composition of the continental crust: A global view. J. Geophys. Res. 100, 9761-9788.
Clemens, J.D., Yearron, L.M., Stevens, G., 2006. Barberton (South Africa) TTG magmas: Geochemical and experimental constraints on source-rock petrology, pressure of formation and tectonic setting. Precambrian Research 151, 53-78.
Clift, P.D., Vannucchi, P., Morgan, J.P., 2009. Crustal redistribution, crust-mantle recycling and Phanerozoic evolution of the continental crust. Earth-Science Reviews 97, 80-104.
Coplen, T., Böhlke, J., De Bievre, P., Ding, T., Holden, N., Hopple, J., Krouse, H., Lamberty, A., Peiser, H., Revesz, K., 2002. Isotope-abundance variations of selected elements:(IUPAC technical report). Pure and Applied Chemistry 74, 1987-2017.
Das, A., Krishnaswami, S., Kumar, A., 2006. Sr and $^{87}Sr/^{86}Sr$ in rivers draining the Deccan Traps (India): Implications to weathering, Sr fluxes, and the marine $^{87}Sr/^{86}Sr$ record around K/T. Geochemistry Geophysics Geosystems 7, Q06014, doi:06010.01029/02005GC001081.
Depaolo, D.J., 1983. The mean life of continents - Esimates of continent recycling rates from Nd and Hf isotopic data and implications for mantle structure. Geophysical Research Letters 10, 705-708.
Dessert, C., Dupré, B., Francois, L.M., Schott, J., Gaillardet, J., Chakrapani, G., Bajpai, S., 2001. Erosion of Deccan Traps determined by river geochemistry: impact on the global climate and the $^{87}Sr/^{86}Sr$ ratio of seawater. Earth and Planetary Science Letters 188, 459-474.

Dessert, C., Dupré, B., Gaillardet, J., Francois, L.M., Allègre, C.J., 2003. Basalt weathering laws and the impact of basalt weathering on the global carbon cycle. Chemical Geology 202, 257-273.

Elliott, T., Thomas, A., Jeffcoate, A., Niu, Y.L., 2006. Lithium isotope evidence for subduction-enriched mantle in the source of mid-ocean-ridge basalts. Nature 443, 565-568.

Fantle, M.S., DePaolo, D.J., 2004. Iron isotopic fractionation during continental weathering. Earth and Planetary Science Letters 228, 547-562.

Fassio, J.M., 1990. Geochemical evolution of ferrginous bauxite deposits in northwestern Oregon and southwestern Washington. MS Thesis. Portland State University, p. 103.

Flesch, G., Anderson, A., Svec, H., 1973. A secondary isotopic standard for $^{6}Li/^{7}Li$ determinations. International Journal of Mass Spectrometry and Ion Physics 12, 265-272.

Gaillardet, J., Dupré, B., Louvat, P., Allègre, C.J., 1999. Global silicate weathering and CO_2 consumption rates deduced from the chemistry of large rivers. Chemical Geology 159, 3-30.

Galy, A., Yoffe, O., Janney, P.E., Williams, R.W., Cloquet, C., Alard, O., Halicz, L., Wadhwa, M., Hutcheon, I.D., Ramon, E., Carignan, J., 2003. Magnesium isotope heterogeneity of the isotopic standard SRM980 and new reference materials for magnesium-isotope-ratio measurements. Journal of Analytical Atomic Spectrometry 18, 1352-1356.

Georg, R.B., Reynolds, B.C., West, A.J., Burton, K.W., Halliday, A.N., 2007. Silicon isotope variations accompanying basalt weathering in Iceland. Earth and Planetary Science Letters 261, 476-490.

Gomes, P.C., Fontes, M.P.F., da Silva, A.G., Mendonca, E.D., Netto, A.R., 2001. Selectivity sequence and competitive adsorption of heavy metals by Brazilian soils. Soil Science Society of America Journal 65, 1115-1121.

Hacker, B.R., Kelemen, P.B., Behn, M.D., 2011. Differentiation of the continental crust by relamination. Earth and Planetary Science Letters 307, 501-516.

Hamby, D.M., 1994. A Review of Techniques of Parameter Sensitivity Analysis of Environmental Models. Environmental Monitoring and Assessment 32, 135-154.

Hawkesworth, C.J., Kemp, A.I.S., 2006. Evolution of the continental crust. Nature 443, 811-817.

Hooper, P.R., 1997. The Columbia River flood basalt provinces; current status, in: Mahoney, J.J., Coffin, M.F. (Eds.), Large igneous provinces; continental, oceanic, and planetary flood volcanism. American Geophysical Union : Washington, DC, United States, United States, pp. 1-27.

Huang, F., Glessner, J., Ianno, A., Lundstrom, C., Zhang, Z.F., 2009. Magnesium isotopic composition of igneous rock standards measured by MC-ICP-MS. Chemical Geology 268, 15-23.

Huang, K.-J., Teng, F.-Z., Wei, G.-J., Ma, J.-L., Bao, Z.-Y., 2012. Adsorption- and desorption-controlled magnesium isotope fractionation during extreme weathering of basalt in Hainan Island, China. Earth and Planetary Science Letters 359–360, 73-83.

Huh, Y., Chan, L.-H., Chadwick, O.A., 2004. Behavior of lithium and its isotopes during weathering of Hawaiian basalt. Geochemistry Geophysics Geosystems 5, Q09002.
Huh, Y., Chan, L.H., Chadwick, O., 2002. Lithium isotopes as a probe of weathering processes: Hawaiian soil climosequence. Geochimica et Cosmochimica Acta 66, A346-A346.
Huh, Y., Chan, L.H., Edmond, J.M., 2001. Lithium isotopes as a probe of weathering processes: Orinoco River. Earth and Planetary Science Letters 194, 189-199.
Huh, Y., Chan, L.H., Zhang, L., Edmond, J.M., 1998. Lithium and its isotopes in major world rivers: Implications for weathering and the oceanic budget. Geochimica et Cosmochimica Acta 62, 2039-2051.
Jackson, M.L., Gibbons, F.R., Syers, J.K., Mokma, D.L., 1972. Eolian influence on soils developed in a chronosequence of basalts of Victoria, Australia. Geoderma 8, 147-163.
Jackson, R.L., 1974. A mineralogical and geochemical study of the ferruginous bauxite deposits in Columbia County, Oregon and Wahkiakum County, Washington. MS Thesis. Portland State University, p. 87.
Jagoutz, O., Schmidt, M.W., 2012. The formation and bulk composition of modern juvenile continental crust: The Kohistan arc. Chemical Geology 298, 79-96.
Jaupart, C., Mareschal, J.C., 2012. Constraints on crustal heat production from heat flow data, Treatise on Geochemistry, 2nd edition. Pergamon, Oxford, p. XX in press.
Juillot, F., Marechal, C., Ponthieu, M., Cacaly, S., Morin, G., Benedetti, M., Hazemann, J.L., Proux, O., Guyot, F., 2008. Zn isotopic fractionation caused by sorption on goethite and 2-Lines ferrihydrite. Geochimica et Cosmochimica Acta 72, 4886-4900.
Jull, M., Kelemen, P.B., 2001. On the conditions for lower crustal convective instability. Journal of Geophysical Research-Solid Earth 106, 6423-6446.
Kay, R.W., Kay, S.M., 1993. Delamination and delamination magmatism. Tectonophysics 219, 177-189.
Kelemen, P.B., Hanghøj, K., Greene, A.R., 2003. One View of the Geochemistry of Subduction-Related Magmatic Arcs, with an Emphasis on Primitive Andesite and Lower Crust, in: Heinrich, D.H., Karl, K.T. (Eds.), Treatise on Geochemistry. Pergamon, Oxford, pp. 1-70.
Kemp, A.I.S., Hawkesworth, C.J., 2012. Growth and differentiation of the continental crust from isotope studies of accessory minerals Treatise on Geochemistry, 2nd edition. Pergamon, Oxford, p. XX in press.
Kinniburgh, D.G., Jackson, M.L., Syers, J.K., 1976. Adsorption of alkaline earth, transition, and heavy metal cations by hydrous oxide gels of rion and aluminum. Soil Science Society of America Journal 40, 796-799.
Kisakürek, B., James, R.H., Harris, N.B.W., 2005. Li and delta Li-7 in Himalayan rivers: Proxies for silicate weathering? Earth and Planetary Science Letters 237, 387-401.
Kisakürek, B., Widdowson, M., James, R.H., 2004. Behaviour of Li isotopes during continental weathering: the Bidar laterite profile, India. Chemical Geology 212, 27-44.

Kohn, M.J., Miselis, J.L., Fremd, T.J., 2002. Oxygen isotope evidence for progressive uplift of the Cascade Range, Oregon. Earth and Planetary Science Letters 204, 151-165.
Kump, L.R., Brantley, S.L., Arthur, M.A., 2000. Chemical, weathering, atmospheric CO2, and climate. Annual Review of Earth and Planetary Sciences 28, 611-667.
Kurtz, A.C., Derry, L.A., Chadwick, O.A., 2001. Accretion of Asian dust to Hawaiian soils: Isotopic, elemental, and mineral mass balances. Geochimica et Cosmochimica Acta 65, 1971-1983.
Kurtz, A.C., Derry, L.A., Chadwick, O.A., Alfano, M.J., 2000. Refractory element mobility in volcanic soils. Geology 28, 683-686.
Lee, C.T.A., 2012. Physics and chemistry of deep continental crust recycling, Treatise on Geochemistry, 2nd edition. Pergamon, Oxford, p. XX in press.
Lee, C.T.A., Cheng, X., Horodyskyj, U., 2006. The development and refinement of continental arcs by primary basaltic magmatism, garnet pyroxenite accumulation, basaltic recharge and delamination: insights from the Sierra Nevada, California. Contributions to Mineralogy and Petrology 151, 222-242.
Lee, C.T.A., Morton, D.M., Kistler, R.W., Baird, A.K., 2007. Petrology and tectonics of Phanerozoic continent formation: From island arcs to accretion and continental arc magmatism. Earth and Planetary Science Letters 263, 370-387.
Lee, C.T.A., Morton, D.M., Little, M.G., Kistler, R., Horodyskyj, U.N., Leeman, W.P., Agranier, A., 2008. Regulating continent growth and composition by chemical weathering. Proceedings of the National Academy of Sciences of the United States of America 105, 4981-4986.
Li, W.Y., Teng, F.Z., Ke, S., Rudnick, R.L., Gao, S., Wu, F.Y., Chappell, B.W., 2010. Heterogeneous magnesium isotopic composition of the upper continental crust. Geochimica et Cosmochimica Acta 74, 6867-6884.
Ling, M.-X., Sedaghatpour, F., Teng, F.-Z., Hays, P.D., Strauss, J., Sun, W., 2011. Homogeneous magnesium isotopic composition of seawater: an excellent geostandard for Mg isotope analysis. Rapid Communications in Mass Spectrometry 25, 2828-2836.
Liu, S.A., Teng, F.Z., He, Y.S., Ke, S., Li, S.G., 2010a. Investigation of magnesium isotope fractionation during granite differentiation: Implication for Mg isotopic composition of the continental crust. Earth and Planetary Science Letters 297, 646-654.
Liu, X.-M., Rudnick, R.L., Hier-Majumder, S., Sirbescu, M.-L.C., 2010b. Processes controlling lithium isotopic distribution in contact aureoles: A case study of the Florence County pegmatites, Wisconsin. Geochemistry Geophysics Geosystems 11, Q08014, 08010.01029/02010gc003063.
Liu, X.-M., Rudnick, R.L., McDonough, W.F., Cummings, M., 2012. Tracing Chemical Weathering of Basalts Using Lithium Isotopes: A Case Study from the Columbia River Basalts. Geochimica et Cosmochimica Acta in prep?
Liu, X.M., Rudnick, R.L., 2011. Constraints on continental crustal mass loss via chemical weathering using lithium and its isotopes. Proceedings of the National Academy of Sciences of the United States of America 108, 20873-20880.

Louvat, P., Allègre, C.J., 1997. Present denudation rates on the island of Reunion determined by river geochemistry: Basalt weathering and mass budget between chemical and mechanical erosions. Geochimica et Cosmochimica Acta 61, 3645-3669.
Ma, C., Eggleton, R.A., 1999. Cation exchange capacity of kaolinite. Clays and Clay Minerals 47, 174-180.
Magna, T., Wiechert, U.H., Halliday, A.N., 2004. Low-blank isotope ratio measurement of small samples of lithium using multiple-collector ICPMS. International Journal of Mass Spectrometry 239, 67-76.
Marks, M.A.W., Rudnick, R.L., McCammon, C., Vennemann, T., Markl, G., 2007. Arrested kinetic Li isotope fractionation at the margin of the llimaussaq complex, South Greenland: Evidence for open-system processes during final cooling of peralkaline igneous rocks. Chemical Geology 246, 207-230.
Marschall, H.R., Pogge von Strandmann, P.A.E., Seitz, H.-M., Elliott, T., Niu, Y., 2007. The lithium isotopic composition of orogenic eclogites and deep subducted slabs. Earth and Planetary Science Letters 262, 563-580.
Martin, H., 1986. Effect of steeper archean geothermal gradient on geochemistry of subduction-zone magmas. Geology 14, 753-756.
Martin, H., Moyen, J.F., 2002. Secular changes in tonalite-trondhjemite-granodiorite composition as markers of the progressive cooling of Earth. Geology 30, 319-322.
McDonough, W.F., Sun, S.S., 1995. The composition of the earth. Chemical Geology 120, 223-253.
Mikutta, C., Wiederhold, J.G., Cirpka, O.A., Hofstetter, T.B., Bourdon, B., Von Gunten, U., 2009. Iron isotope fractionation and atom exchange during sorption of ferrous iron to mineral surfaces. Geochimica et Cosmochimica Acta 73, 1795-1812.
Millot, R., Vigier, N., Gaillardet, J., 2010. Behaviour of lithium and its isotopes during weathering in the Mackenzie Basin, Canada. Geochimica et Cosmochimica Acta 74, 3897-3912.
Misra, S., Froelich, P.N., 2012. Lithium Isotope History of Cenozoic Seawater: Changes in Silicate Weathering and Reverse Weathering. Science 335, 818-823.
Moriguti, T., Nakamura, E., 1998a. Across-arc variation of Li isotopes in lavas and implications for crust/mantle recycling at subduction zones. Earth and Planetary Science Letters 163, 167-174.
Moriguti, T., Nakamura, E., 1998b. High-yield lithium separation and the precise isotopic analysis for natural rock and aqueous samples. Chemical Geology 145, 91-104.
Moriguti, T., Shibata, T., Nakamura, E., 2004. Lithium, boron and lead isotope and trace element systematics of Quaternary basaltic volcanic rocks in northeastern Japan: mineralogical controls on slab-derived fluid composition. Chemical Geology 212, 81-100.
Nesbitt, H.W., Wilson, R.E., 1992. Recent chemical weathering of basalts. American Journal of Science 292, 740-777.

Nesbitt, H.W., Young, G.M., 1982. Early Proterozoic climates and plate motions inferred from major element chemistry of lutites. Nature 299, 715-717.
Nyblade, A.A., Pollack, H.N., 1993. A Global Analysis of Heat Flow From Precambrian Terrains: Implications for the Thermal Structure of Archean and Proterozoic Lithosphere. J. Geophys. Res. 98, 12207-12218.
Olsher, U., Izatt, R.M., Bradshaw, J.S., Dalley, N.K., 1991. Coordination chemistry of lithium ion: a crystal and molecular structure review. Chemical Reviews 91, 137-164.
Opfergelt, S., Georg, R.B., Delvaux, B., Cabidoche, Y.M., Burton, K.W., Halliday, A.N., 2012. Mechanisms of magnesium isotope fractionation in volcanic soil weathering sequences, Guadeloupe. Earth and Planetary Science Letters 341-344, 176-185.
Parkhurst, D., Appelo, C., 1999. User's Guide to Phreeqc (version 2), A Computer Program for Speciation, Batch-Reaction, One-Dimensional Transport, and Inverse Geochemical Calculations. US Department of the Interior. Us Geological survey Water-Resources Investigations, 99-4259.
Peterson, B.T., Depaolo, D.J., 2007. Mass and composition of the continental crust estimated using the CRUST2.0 model, American Geophysical Union, Fall Meeting 2007.
Pett-Ridge, J.C., Derry, L.A., Kurtz, A.C., 2009. Sr isotopes as a tracer of weathering processes and dust inputs in a tropical granitoid watershed, Luquillo Mountains, Puerto Rico. Geochimica et Cosmochimica Acta 73, 25-43.
Pistiner, J.S., Henderson, G.M., 2003. Lithium-isotope fractionation during continental weathering processes. Earth and Planetary Science Letters 214, 327-339.
Plank, T., 2005. Constraints from thorium/lanthanum on sediment recycling at subduction zones and the evolution of the continents. Journal of Petrology 46, 921-944.
Plank, T., 2012. The chemical composition of subducting sediments, Treatise on Geochemistry, 2nd edition. Pergamon, Oxford, p. XX in press.
Plank, T., Langmuir, C.H., 1998. The chemical composition of subducting sediment and its consequences for the crust and mantle. Chemical Geology 145, 325-394.
Pogge von Strandmann, P.A.E., Burton, K.W., James, R.H., van Calsteren, P., Gislason, S.R., 2010. Assessing the role of climate on uranium and lithium isotope behaviour in rivers draining a basaltic terrain. Chemical Geology 270, 227-239.
Pogge von Strandmann, P.A.E., Burton, K.W., James, R.H., van Calsteren, P., Gislason, S.R., Mokadem, F., 2006. Riverine behaviour of uranium and lithium isotopes in an actively glaciated basaltic terrain. Earth and Planetary Science Letters 251, 134-147.
Pogge von Strandmann, P.A.E., Burton, K.W., James, R.H., van Calsteren, P., Gislason, S.R., Sigfusson, B., 2008. The influence of weathering processes on riverine magnesium isotopes in a basaltic terrain. Earth and Planetary Science Letters 276, 187-197.

Pogge von Strandmann, P.A.E., Opfergelt, S., Lai, Y.-J., Sigfusson, B., Gislason, S.R., Burton, K.W., 2012. Lithium, magnesium and silicon isotope behaviour accompanying weathering in a basaltic soil and pore water profile in Iceland. Earth and Planetary Science Letters 339-340, 11-23.

Pokrovsky, O.S., Viers, J., Emnova, E.E., Kompantseva, E.I., Freydier, R., 2008. Copper isotope fractionation during its interaction with soil and aquatic microorganisms and metal oxy(hydr) oxides: Possible structural control. Geochimica et Cosmochimica Acta 72, 1742-1757.

Pokrovsky, O.S., Viers, J., Freydier, R., 2005. Zinc stable isotope fractionation during its adsorption on oxides and hydroxides. Journal of Colloid and Interface Science 291, 192-200.

Prytulak, J., Vervoort, J.D., Plank, T., Yu, C.J., 2006. Astoria Fan sediments, DSDP site 174, Cascadia Basin: Hf-Nd-Pb constraints on provenance and outburst flooding. Chemical Geology 233, 276-292.

Qi, H.P., Taylor, P.D.P., Berglund, M., De Bievre, P., 1997. Calibrated measurements of the isotopic composition and atomic weight of the natural Li isotopic reference material IRMM-016. International Journal of Mass Spectrometry 171, 263-268.

Qiu, L., 2011. Lithium and δ^7Li Behavior During Metamorphic Dehydration Processes and Crustal Evolution. University of Maryland, p. 186.

Qiu, L., Rudnick, R.L., Ague, J.J., McDonough, W.F., 2011a. A lithium isotopic study of sub-greenschist to greenschist facies metamorphism in an accretionary prism, New Zealand. Earth and Planetary Science Letters 301, 213-221.

Qiu, L., Rudnick, R.L., McDonough, W.F., Bea, F., 2011b. The behavior of lithium in amphibolite- to granulite-facies rocks of the Ivrea–Verbano Zone, NW Italy. Chemical Geology 289, 76-85.

Qiu, L., Rudnick, R.L., McDonough, W.F., Merriman, R.J., 2009. Li and δ^7Li in mudrocks from the British Caledonides: Metamorphism and source influences. Geochimica et Cosmochimica Acta 73, 7325-7340.

Ra, K., Kitagawa, H., 2007. Magnesium isotope analysis of different chlorophyll forms in marine phytoplankton using multi-collector ICP-MS. Journal of Analytical Atomic Spectrometry 22, 817-821.

Rea, D.K., Ruff, L.J., 1996. Composition and mass flux of sediment entering the world's subduction zones: Implications for global sediment budgets, great earthquakes, and volcanism. Earth and Planetary Science Letters 140, 1-12.

Reidel, S.P., Tolan, T.L., Hooper, P.R., Beeson, M.H., Fecht, K.R., Bentley, R.D., Anderson, J.L., 1989. The Grande Ronde Basalt, Columbia River Basalt Group; stratigraphic descriptions and correlations in Washington, Oregon, and Idaho, in: Reidel, S.P., Hooper, P.R. (Eds.), Volcanism and tectonism in the Columbia River flood-basalt province. Geological Society of America (GSA) : Boulder, CO, United States, United States, pp. 21-53.

Retallack, G.J., 2010. Lateritization and Bauxitization Events. Economic Geology 105, 655-667.

Rex, R.W., Syers, J.K., Jackson, M.L., Clayton, R.N., 1969. Eolian Origin of Quartz in Soils of Hawaiian Islands and in Pacific Pelagic Sediments. Science 163, 277-279.
Rollinson, H., 2008. Secular evolution of the continental crust: Implications for crust evolution models. Geochemistry Geophysics Geosystems 9, Q12010.
Rudnick, R.L., 1995. Making Continental Crust. Nature 378, 571-578.
Rudnick, R.L., Fountain, D.M., 1995. Nature and composition of the continental crust - A lower crustal perspective. Reviews of Geophysics 33, 267-309.
Rudnick, R.L., Gao, S., 2003a. Composition of the Continental Crust, in: Heinrich, D.H., Karl, K.T. (Eds.), Treatise on Geochemistry. Pergamon, Oxford, pp. 1-64.
Rudnick, R.L., Gao, S., 2003b. Composition of the Continental Crust, in: Holland, H.D., Turekian, K.K. (Eds.), Treatise on Geochemistry. Elsevier-Pergamon, Oxford, pp. 1-64.
Rudnick, R.L., Tomascak, P.B., Njo, H.B., Gardner, L.R., 2004. Extreme lithium isotopic fractionation during continental weathering revealed in saprolites from South Carolina. Chemical Geology 212, 45-57.
Ryan, J.G., Kyle, P.R., 2004. Lithium abundance and lithium isotope variations in mantle sources: insights from intraplate volcanic rocks from Ross Island and Marie Byrd Land (Antarctica) and other oceanic islands. Chemical Geology 212, 125-142.
Ryu, J.S., Jacobson, A.D., Holmden, C., Lundstrom, C., Zhang, Z.F., 2011. The major ion, $\delta^{44/40}$Ca, $\delta^{44/42}$Ca, and $\delta^{26/24}$Mg geochemistry of granite weathering at pH=1 and T=25^{o}C: power-law processes and the relative reactivity of minerals. Geochimica et Cosmochimica Acta 75, 6004-6026.
Sawhney, B.L., 1972. Selective sorption and fixation of cations by clay mienrals: A review. Clays and Clay Minerals 20, 93-100.
Schellmann, W., 1994. Geochemical differentiation in laterite and bauxite formation. Catena 21, 131-143.
Shen, B., Jacobsen, B., Lee, C.T.A., Yin, Q.Z., Morton, D.M., 2009. The Mg isotopic systematics of granitoids in continental arcs and implications for the role of chemical weathering in crust formation. Proceedings of the National Academy of Sciences of the United States of America 106, 20652-20657.
Shirey, S.B., Hanson, G.N., 1984. Mantle-derived Archean monozodiorites and trachyandesites. Nature 310, 222-224.
Simon, L., Lecuyer, C., 2005. Continental recycling: The oxygen isotope point of view. Geochemistry Geophysics Geosystems 6, 10.
Srivastava, P., Singh, B., Angove, M., 2005. Competitive adsorption behavior of heavy metals on kaolinite. Journal of Colloid and Interface Science 290, 28-38.
Sweeney, M.R., Gaylord, D.R., Busacca, A.J., 2007. Evolution of Eureka Flat: A dust-producing engine of the Palouse loess, USA. Quaternary International 162, 76-96.
Takeuchi, A., Hren, M.T., Smith, S.V., Chamberlain, C.P., Larson, P.B., 2010. Pedogenic carbonate carbon isotopic constraints on paleoprecipitation:

Evolution of desert in the Pacific Northwest, USA, in response to topographic development of the Cascade Range. Chemical Geology 277, 323-335.
Taylor, S.R., McLennan, S.M., 1995. The geochemical evolution of the continental crust. Reviews of Geophysics 33, 241-265.
Taylor, S.R., McLennan, S.M., 2009. Planetary crusts: their composition, origin and evolution. Cambridge University Press.
Teng, F.-Z., Li, W.-Y., Rudnick, R.L., Gardner, L.R., 2010a. Contrasting lithium and magnesium isotope fractionation during continental weathering. Earth and Planetary Science Letters 300, 63-71.
Teng, F.Z., Li, W.Y., Ke, S., Marty, B., Dauphas, N., Huang, S.C., Wu, F.Y., Pourmand, A., 2010b. Magnesium isotopic composition of the Earth and chondrites. Geochimica et Cosmochimica Acta 74, 4150-4166.
Teng, F.Z., McDonough, W.F., Rudnick, R.L., Dalpe, C., Tomascak, P.B., Chappell, B.W., Gao, S., 2004. Lithium isotopic composition and concentration of the upper continental crust. Geochimica et Cosmochimica Acta 68, 4167-4178.
Teng, F.Z., McDonough, W.F., Rudnick, R.L., Wing, B.A., 2007a. Limited lithium isotopic fractionation during progressive metamorphic dehydration in metapelites: A case study from the Onawa contact aureole, Maine. Chemical Geology 239, 1-12.
Teng, F.Z., Rudnick, R.L., McDonough, W.F., Gao, S., Tomascak, P.B., Liu, Y.S., 2008. Lithium isotopic composition and concentration of the deep continental crust. Chemical Geology 255, 47-59.
Teng, F.Z., Wadhwa, M., Helz, R.T., 2007b. Investigation of magnesium isotope fractionation during basalt differentiation: Implications for a chondritic composition of the terrestrial mantle. Earth and Planetary Science Letters 261, 84-92.
Tipper, E.T., Calmels, D., Gaillardet, J., Louvat, P., Capmas, F.ß., Dubacq, B., 2012a. Positive correlation between Li and Mg isotope ratios in the river waters of the Mackenzie Basin challenges the interpretation of apparent isotopic fractionation during weathering. Earth and Planetary Science Letters 333-334, 35-45.
Tipper, E.T., Galy, A., Bickle, M.J., 2006a. Riverine evidence for a fractionated reservoir of Ca and Mg on the continents: Implications for the oceanic Ca cycle. Earth and Planetary Science Letters 247, 267-279.
Tipper, E.T., Galy, A., Bickle, M.J., 2008. Calcium and magnesium isotope systematics in rivers draining the Himalaya-Tibetan-Plateau region: Lithological or fractionation control? Geochimica et Cosmochimica Acta 72, 1057-1075.
Tipper, E.T., Galy, A., Gaillardet, J., Bickle, M.J., Elderfield, H., Carder, E.A., 2006b. The magnesium isotope budget of the modem ocean: Constraints from riverine magnesium isotope ratios. Earth and Planetary Science Letters 250, 241-253.
Tipper, E.T., Lemarchand, E., Hindshaw, R.S., Reynolds, B.C., Bourdon, B., 2012b. Seasonal sensitivity of weathering processes: Hints from magnesium isotopes in a glacial stream. Chemical Geology 312-313, 80-92.

Tolan, T.L., Reidel, S.P., Beeson, M.H., Anderson, J.L., Fecht, K.R., Swanson, D.A., 1989. Revisions to the estimates of the areal extent and volume of the Columbia River Basalt Group. Volcanism and tectonism in the Columbia River flood-basalt province: Geological Society of America Special Paper 239, 1-20.

Tomascak, P.B., 2004. Developments in the understanding and application of lithium isotopes in the earth and planetary sciences, Geochemistry of Non-Traditional Stable Isotopes, pp. 153-195.

Tomascak, P.B., Langmuir, C.H., le Roux, P.J., Shirey, S.B., 2008. Lithium isotopes in global mid-ocean ridge basalts. Geochimica et Cosmochimica Acta 72, 1626-1637.

Tomascak, P.B., Widom, E., Benton, L.D., Goldstein, S.L., Ryan, J.G., 2002. The control of lithium budgets in island arcs. Earth and Planetary Science Letters 196, 227-238.

Velde, B., 1995. Origin and mineralogy of clays: clays and the environment. Springer-Verlag, pp. 14-29.

Viers, K., Wasserburg, G.J., 2004. Behavior of Sm and Nd in a lateritic soil profile. Geochimica et Cosmochimica Acta 68, 2043-2054.

Vigier, N., Decarreau, A., Millot, R., Carignan, J., Petit, S., France-Lanord, C., 2008. Quantifying Li isotope fractionation during smectite formation and implications for the Li cycle. Geochimica et Cosmochimica Acta 72, 780-792.

Vigier, N., Gislason, S.R., Burton, K.W., Millot, R., Mokadem, F., 2009. The relationship between riverine lithium isotope composition and silicate weathering rates in Iceland. Earth and Planetary Science Letters 287, 434-441.

White, A.F., Brantley, S.L., 1995. Chemical weathering rates of silicate minerals: An overview, Chemical Weathering Rates of Silicate Minerals, pp. 1-22.

Williams, L.B., Hervig, R.L., 2005. Lithium and boron isotopes in illite-smectite: The importance of crystal size. Geochimica et Cosmochimica Acta 69, 5705-5716.

Wimpenny, J., Burton, K.W., James, R.H., Gannoun, A., Mokadem, F., Gíslason, S.R., 2011. The behaviour of magnesium and its isotopes during glacial weathering in an ancient shield terrain in West Greenland. Earth and Planetary Science Letters 304, 260-269.

Wimpenny, J., Gislason, S.R., James, R.H., Gannoun, A., Pogge Von Strandmann, P.A.E., Burton, K.W., 2010a. The behaviour of Li and Mg isotopes during primary phase dissolution and secondary mineral formation in basalt. Geochimica et Cosmochimica Acta 74, 5259-5279.

Wimpenny, J., James, R.H., Burton, K.W., Gannoun, A., Mokadem, F., Gislason, S.R., 2010b. Glacial effects on weathering processes: New insights from the elemental and lithium isotopic composition of West Greenland rivers. Earth and Planetary Science Letters 290, 427-437.

Zektser, I.S., Loaiciga, H.A., 1993. Groundwater fluxes in the global hydrologic-cycle - past, present and future. Journal of Hydrology 144, 405-427.

Zhang, L.B., Chan, L.H., Gieskes, J.M., 1998. Lithium isotope geochemistry of pore waters from Ocean Drilling Program Sites 918 and 919, Irminger Basin. Geochimica et Cosmochimica Acta 62, 2437-2450.

Zhong, K., Xu, R.K., Zhao, A.Z., Jiang, J., Tiwari, D., Li, H., 2010. Adsorption and desorption of Cu(II) and Cd(II) in the tropical soils during pedogenesis in the basalt from Hainan, China. Carbonates and Evaporites 25, 27-34.